

# Geometric Form Finding Method for Prismatic Tensegrity Systems

by

**Andrew Arthur Dobson**

A Thesis submitted to  
the Faculty of Graduate Studies and Research  
in partial fulfilment of  
the requirements for the degree of  
**Master of Applied Science**

Ottawa-Carleton Institute for  
Mechanical and Aerospace Engineering  
and  
University of Ottawa  
Medical Devices Division  
Ottawa Heart Institute

Department of Mechanical and Aerospace Engineering  
Carleton University  
Ottawa, Ontario, Canada  
January 2010

Copyright ©

2010 - Andrew Arthur Dobson

The undersigned recommend to  
the Faculty of Graduate Studies and Research  
acceptance of this Thesis

**Geometric Form Finding Method for Prismatic Tensegrity Systems**

Submitted by **Andrew Arthur Dobson**  
in partial fulfilment of the requirements for the degree of  
**Master of Applied Science**

---

Dr. J. Hayes, Supervisor

---

Dr. T. Mussivand, Supervisor

---

M. Yaras, Department Chair

Carleton University

2010

# Abstract

Tensegrity systems are composed of high strength to weight mechanisms. They achieve this strength by replacing heavy elements in tension with lightweight cables. This property has led to the application of tensegrity theory to many fields, ranging from architecture to robotics. The greatest difficulty for those wishing to exploit the benefit of tensegrity systems, is the unintuitive way in which the subelements of a tensegrity are connected to form a stable configuration. In this thesis, a new method for determining these stable configurations is developed, thereby providing a more intuitive tool for designing tensegrity systems. This novel approach is called the geometric intersection method, and is based on determining the common intersection point between three constraint surfaces, each of which represent one of the element lengths in the tensegrity system. The geometric intersection method was found to be algebraically equivalent to an established form finding method by deriving the established method from the geometric intersection method. This result was further reinforced by evaluating the two methods using several different tensegrity systems. While the two methods are algebraically equivalent, the geometric intersection method is derived using geometry instead of vector analysis. This difference arguably makes the geometric intersection method more intuitive, because it provides a visual rationale for how the element lengths affect the final configuration of the tensegrity system, and when the combination of these parameters will result in a configuration that has no real physical significance. It was also found that the geometric intersection method is easier to adapt to new tensegrity configurations than either of the most closely related form finding methods.

To Prof. Hayes for taking a chance on me;  
To Dr. Mussivand for supporting me;  
and to Susan Logie for helping to make this thesis intelligible.



# Table of Contents

<b>List of Tables</b>	<b>viii</b>
<b>List of Figures</b>	<b>ix</b>
<b>Nomenclature</b>	<b>xi</b>
<b>1 Introduction</b>	<b>1</b>
1.1 Applications . . . . .	3
1.1.1 Civil Engineering Structures . . . . .	3
1.1.2 Medical Applications . . . . .	4
1.1.3 Space Structures . . . . .	7
1.1.4 Robotics . . . . .	11
1.2 Rigidity and Stability . . . . .	13
1.3 Form Finding Methods . . . . .	14
1.4 Research Problem . . . . .	15
1.5 Original Contributions to Knowledge . . . . .	16
1.6 Outline . . . . .	16
<b>2 Rigidity and Stability</b>	<b>17</b>
2.1 Prismatic Tensegrity Topologies . . . . .	18
2.2 Graph Theory . . . . .	19
2.3 Rigidity Definitions . . . . .	22
2.3.1 Determining Rigidity using Motion Analysis . . . . .	23

2.3.2	Determining Rigidity using Forces . . . . .	24
2.3.3	Determining Rigidity using Stresses or Force Densities . . . . .	25
2.3.4	Infinitesimal Rigidity . . . . .	26
2.3.5	Second Order Rigidity . . . . .	30
2.3.6	Pre-Stress Stability . . . . .	31
2.3.7	Unyielding . . . . .	32
2.3.8	Global Rigidity . . . . .	33
2.3.9	Universally Global Rigidity . . . . .	34
2.3.10	Super Stability . . . . .	34
2.4	Summary . . . . .	39
<b>3</b>	<b>Literature Review of the Form Finding Problem</b>	<b>42</b>
3.1	The Form Finding Problem . . . . .	42
3.2	Kinematic Form Finding Methods . . . . .	44
3.2.1	Analytical Method . . . . .	44
3.2.2	Non-Linear Constrained Minimization Method . . . . .	45
3.2.3	Dynamic Relaxation Method . . . . .	46
3.3	Static Form Finding Methods . . . . .	46
3.3.1	Analytical Method . . . . .	46
3.3.2	Force Density Method . . . . .	47
3.3.3	Modified Force Density Methods . . . . .	48
3.3.4	Energy Method . . . . .	50
3.3.5	Coordinate Reduction Method . . . . .	50
3.4	Simultaneous Methods . . . . .	51
3.4.1	Axial Force Compatibility Method . . . . .	51
3.4.2	Differential Equation Method . . . . .	52
3.4.3	Genetic Algorithm Methods . . . . .	53
3.4.4	Sequential Quadratic Programming Method . . . . .	54
3.4.5	Iterative Numerical Method . . . . .	55

3.4.6	Finite Element Method . . . . .	56
3.5	Form Finding Method Summary . . . . .	57
3.5.1	Class . . . . .	57
3.5.2	Type . . . . .	58
3.5.3	Element Length Control . . . . .	59
3.5.4	Employs Symmetry . . . . .	59
3.5.5	Constraint Surfaces . . . . .	60
3.5.6	Comp. Complexity . . . . .	60
3.5.7	Form Finding Insight . . . . .	61
3.6	Discussion . . . . .	61
<b>4</b>	<b>Geometric Intersection Method</b>	<b>62</b>
4.1	Assumptions . . . . .	63
4.2	Geometric Intersection Method Premise . . . . .	65
4.3	Symmetry in the Geometric Intersection Method . . . . .	68
4.4	Geometric Intersection Method . . . . .	69
4.4.1	Analytical Method and Derivation of the Analytic Kinematic Method From the Geometric Intersection Method . . . . .	72
4.5	Mathcad/ProEngineer Implementation . . . . .	76
4.5.1	Computational Complexity . . . . .	76
<b>5</b>	<b>Examples</b>	<b>77</b>
5.1	Implementation of the Geometric Intersection Method . . . . .	77
5.2	Equivalence of the Geometric Form Finding Method to Connelly's Method .	81
5.3	Form Finding Method Algorithm Comparison . . . . .	83
5.4	Optimization of a Known Configuration . . . . .	86
5.5	Determining Boundary Conditions Geometrically . . . . .	87
5.6	Using Alternate Control Surfaces . . . . .	90

<b>6</b>	<b>Conclusions</b>	<b>96</b>
6.1	Contributions . . . . .	99
6.2	Future Work . . . . .	99
<b>7</b>	<b>Glossary</b>	<b>101</b>
	<b>List of References</b>	<b>104</b>
	<b>Appendix A Mathcad Transcript</b>	<b>108</b>

## List of Tables

3.1	Characteristics of historical form finding methods . . . . .	57
5.1	Example: $l_c$ Variable 1 . . . . .	79
5.2	Example: $l_c$ Variable 2 . . . . .	80
5.3	Example: $l_s$ Variable 1 . . . . .	81
5.4	Example: $l_s$ Variable 2 . . . . .	82
5.5	Cone Prismatic Tensegrity Example . . . . .	93

## List of Figures

1.1	Harmony Tensegrity . . . . .	2
1.2	Civil Engineering Tensegrity Structures . . . . .	4
1.3	Kurilpa Bridge . . . . .	5
1.4	Structural Elements of a Cell . . . . .	6
1.5	Tensegrity Space Boom Collapsed . . . . .	8
1.6	Tensegrity Space Boom Deployed . . . . .	9
1.7	Tensegrity Reflector Antenna . . . . .	10
1.8	Tensegrity Antenna Deployment . . . . .	10
1.9	Tensegrity Robot . . . . .	12
2.1	$P_3(1,1)$ and $P_5(1,1)$ Prismatic tensegrities . . . . .	19
2.2	$P_5(2,1)$ prismatic tensegrity . . . . .	19
2.3	$P_5(3,2)$ prismatic tensegrity . . . . .	20
2.4	Numbered elements of the Harmony tensegrity topology . . . . .	21
2.5	2D non rigid structure . . . . .	23
2.6	3D non rigid structure . . . . .	23
2.7	2D infinitely flexible structure . . . . .	28
2.8	3D infinitely flexible structure . . . . .	28
2.9	Infinitesimally Flexible Tensegrity . . . . .	30
2.10	Twist angle . . . . .	36
2.11	Stress Equilibrium . . . . .	37
2.12	Rigidity and Stability Hierarchy . . . . .	40
2.13	Rigidity Hierarchy Examples . . . . .	40

4.1	Harmony . . . . .	64
4.2	Geometric Method: Cylinder . . . . .	66
4.3	Geometric Method: Coordinate system . . . . .	67
4.4	Geometric Method: Surfaces . . . . .	68
4.5	Geometric Method: Angles . . . . .	70
4.6	Geometric Method: Solutions . . . . .	72
4.7	Geometric Method: Solutions . . . . .	73
4.8	Geometric Method: y Values . . . . .	74
5.1	Harmony Example . . . . .	78
5.2	Cylinder Boundary Evaluation . . . . .	88
5.3	Sphere Boundary Evaluation . . . . .	89
5.4	Boundary Condition Comparison . . . . .	90
5.5	Cone Control Surface Parameters . . . . .	91
5.6	Cone Infeasible Geometry Example . . . . .	94

# Nomenclature

## Units

This thesis uses English units to keep with North American aerospace industry practice.

The following conversion factors are provided to convert to S.I. units:

Imperial Unit	S.I. Conversion
in	25.4 mm
lbf	4.45 N
ksi	6.89 MPa

## Definitions

**Tensegrity system** a tensegrity arrangement that can either be a static structure, or an actuated mechanism

**Tensegrity structure** a static tensegrity arrangement

**Tensegrity mechanism** a tensegrity arrangement that can change its edge lengths

**Tensegrity topology ( $X(\mathbf{p})$ )** refers to a specific way in which the elements in a tensegrity structure or mechanism are connected to each other (it encompasses all possible lengths and nodal placements of the tensegrity elements using these connections)

**Tensegrity configuration ( $G(\mathbf{p})$ )** A specific instance of a tensegrity topology (all elements have a fixed length and all nodes have fixed coordinates)



## Symbols

$B(\mathbf{p})$  A structure with the same configuration as  $G(\mathbf{p})$ , but with all struts and cables replaced by bar elements.

$E(\mathbf{p})$  is the equilibrium matrix, which is equal to the transpose of the rigidity matrix.

$G(\mathbf{p})$  The graph of a unique tensegrity configuration whose nodes are given by a vector of coordinates  $p$ .

$R(\mathbf{p})$  The rigidity matrix is similar to the graph  $G(\mathbf{p})$  of a tensegrity configuration, but it is made up of the element edge lengths of the tensegrity system.

$X(\mathbf{p})$  Represents all possible graphs of a specific tensegrity topology.

$\mathbf{p}$  or  $\mathbf{p}_n$  a vector that contains the coordinates of the  $n$  nodes in a tensegrity system.

$\mathbb{E}^d$  the  $d$  dimensional Euclidean workspace ( $\mathbb{E}^2$  is equivalent to a 2D space and  $\mathbb{E}^3$  is equivalent to a 3D space).

$\mathbf{F}_{ext}$  the external force(s) acting on a tensegrity system.

$\mathbf{H}$  Hessian matrix. It is the first derivative of the tensegrity energy equation.

$\mathbf{H}$  The group of isometries that maintain the Euclidian distance between the nodes of the prismatic tensegrity  $P_{n_s}(j, k)$ .

$P_{\frac{n}{2}}(j, k)$  or  $P_{n_s}(j, k)$  are the representations for the connectivity of a prismatic tensegrity structure by its parameters  $\frac{n}{2}$  or  $n_s$ ,  $j$ , and  $k$ .

$T$  an array of the forces (tension or compression) in each in each of the element of a tensegrity system.

$\underline{\mathbf{\Omega}}$  The reduced stress matrix made from the vector of element stresses ( $n \times n$ ).

$\mathbf{\Omega}$  the full stress matrix which has all element stresses broken down into their vectorial components ( $nd \times nd$ ).

$\theta$  the angle of twist between the upper and lower polygons of a prismatic tensegrity structure.

$\mathbf{d}$  is the dimension of the workspace (for the bulk of this thesis  $d=3$  and therefore the workspace is in  $\mathbb{E}^3$ ).

$d$  an array of the edge lengths in a given topology.

$\mathbf{d}_i$  the change in edge length generated by the velocities in  $\mathbf{p}'_i$ .

$e$  is the number of elements in a tensegrity system including all struts, cables, and bars.

$\phi$  is the side angle of a cone measured from its central axis to its outer surface.

$h$  is the distance between the upper node plane and the lower node plane.

$h_{cone}$  is the height of a cone.

$j$  is the number of nodes between the lower node of a strut and the upper node of the same strut, counted in the lower plane of a prismatic tensegrity structure.

$k$  is the number of nodes between two nodes in the upper or lower plane of a prismatic tensegrity topology.

$n$  is the number of nodes or vertexes in a tensegrity system, including constrained nodes.

$n_s$  is the number of struts in a prismatic tensegrity system.

$\mathbf{p}'$  a vector of nodal velocity vectors.

$q$  the force density defined as the force per unit length in a tensegrity element (identical to  $\omega$ ).

$r$  is the radius of the circle described by the nodes in the upper or lower plane.

$r_{cone}$  is the radius of the base of a cone.

$\omega$  the tensegrity stress (not the engineering stress) defined as the force per unit length in a tensegrity element (identical to the force density  $q$ ).

$p_i$  the node on the lower node plane of a prismatic tensegrity structure, which is used as a reference coordinate for all other nodes.

$p_a$  the node on the upper node plane of a prismatic tensegrity structure, which denotes one end of the lateral strut (the other end is at node  $p_i$ ).

$p_b$  the node on the upper node plane of a prismatic tensegrity structure, which denotes one end of the lateral cable (the other end is at node  $p_i$ ).

$p_c$  one of the nodes on the lower node plane of a prismatic tensegrity structure, which denotes one end of the clockwise, horizontal cable (the other end is at node  $p_i$ ).

$p_d$  one of the nodes on the lower node plane of a prismatic tensegrity structure, which denotes one end of the counter clockwise, horizontal cable (the other end is at node  $p_i$ ).

$l_s$  is the length of the lateral strut in a prismatic tensegrity system. It is equal to the distance between nodes  $p_i$  and  $p_a$ .

$l_c$  is the length of the lateral cable in a prismatic tensegrity system. It is equal to the distance between both nodes  $p_i$  and  $p_a$ , and nodes  $p_d$  and  $p_a$ .

$l_e$  is the length of the end or horizontal cables in a prismatic tensegrity system. It is equal to the distance between both nodes  $p_i$  and  $p_c$  and nodes  $p_i$  and  $p_d$ .

## Chapter 1

### Introduction

The term tensegrity was coined by Richard Buckminster Fuller in the 1960's to describe systems that have compressive elements kept in static equilibrium by a continuous network of tension elements. The term itself is a contraction of the words tension and integrity, which refers to the continuous tension elements that keep the compression elements in a state of static equilibrium [1]. Although there is still debate concerning what constitutes a tensegrity system, the following definition will be used:

Tensegrity systems are in a stable self-equilibrated state and comprise a discontinuous set of compressed components inside a continuum of tensioned components [1].

Figure 1.1 depicts a Harmony tensegrity topology, which is the simplest three dimensional tensegrity structure possible. This Harmony tensegrity topology has three compression elements (struts) that are indirectly connected to each other through nine tension elements (cables).

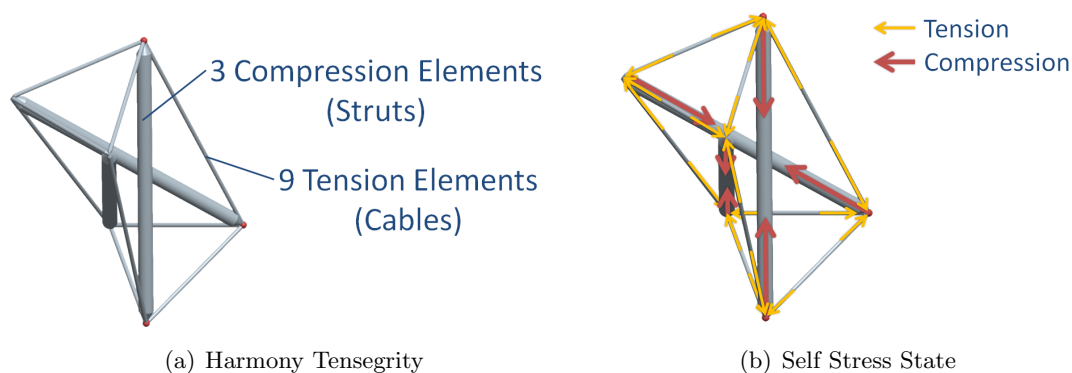


**Figure 1.1: *Harmony Compression and Tension*:** The simplest 3D tensegrity structure is the Harmony tensegrity structure (a), which has 9 elements in tension (cables) and 3 elements in compression (struts)(b).

Tensegrities can be classified according to their purpose, and whether they represent an individual instance or several instances of a particular way to connect the tensegrity elements (struts and cables). In this thesis the following nomenclature hierarchy will be used when discussing tensegrities (the terms are ordered based on decreasing generality):

Tensegrity system	a tensegrity topology that can either be a static structure, or an actuated mechanism
Tensegrity structure	a tensegrity topology in static equilibrium
Tensegrity mechanism	a tensegrity topology whose element lengths can be changed to produce a desired motion or redirection of energy
Tensegrity topology	refers to a unique set of connections between the elements in a tensegrity structure or mechanism (it encompasses all possible lengths and nodal placements of the tensegrity elements using this unique set of connections)
Tensegrity configuration	a specific instance of a tensegrity topology (all elements have a fixed length, all nodes have fixed coordinates, and all elements are connected by a unique set of connections)

There is an increasing amount of work being done on smart structures, and tensegrity based smart structures are especially interesting due to the ease with which these structures can be controlled [2]. Controlled tensegrity structures (or tensegrity mechanisms) are structures where the lengths of the struts and cables are controlled by actuators. If properly instrumented, tensegrity mechanisms can also function as strain sensors; thereby becoming part of their own control loop. Tensegrity systems have much higher strength to weight ratios compared to conventional structures [3]. These higher strength to weight ratios are due to the lighter cable elements that are used in tensegrity structures, as opposed to conventional structural elements which are designed to take both tension and compression loads. Once constructed, tensegrity systems are also relatively easy to analyze because all elements in the tensegrity system can be modelled as two force members. Furthermore, the isolation of the compression members results in the predictable, linear response of the joints of a tensegrity system under a wide range of external loads [2]. These advantages and others have allowed tensegrity systems to find wide applications in many different fields ranging from robotics [4], [5] to biological cell modeling [6].

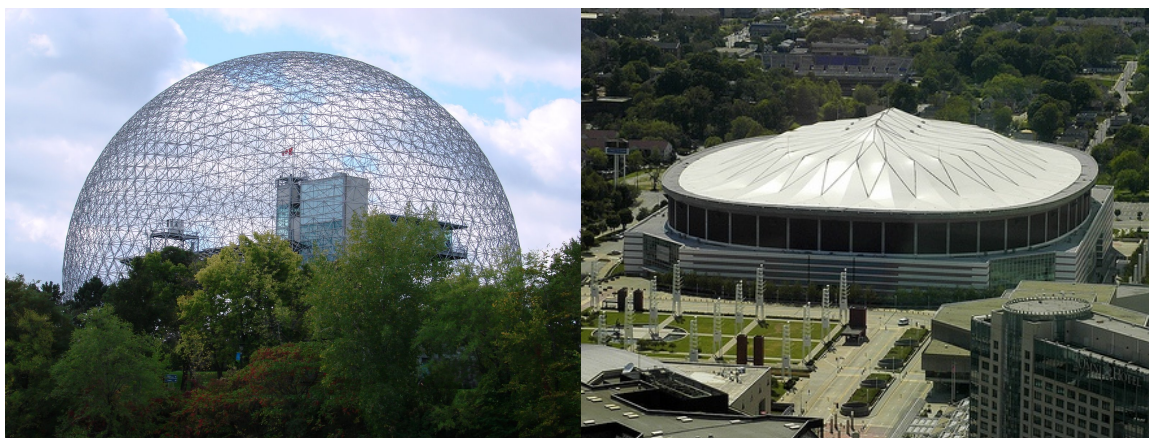
## 1.1 Applications

Tensegrity systems have been used successfully in a number of applications. Civil engineering was the first discipline to exploit the benefits of tensegrity structures in dome and grid structures [7].

### 1.1.1 Civil Engineering Structures

Tensegrity domes have been used to cover large structures, such as the United States Pavilion for Expo '67 (76 meters in diameter), and the Georgia Dome stadium (227 by 185 meters) in Atlanta Georgia (Figure 1.2). More recently, a tensegrity bridge with a 128 meter main span was commissioned by the city of Brisbane in Australia. The bridge was opened to pedestrians on October 4th, 2009 (Figure 1.3). These structures are able to span such large distances due to the high strength to weight ratio, scalability, and flexibility

inherent in tensegrity structures. The scalability of tensegrity structures results from the simplicity of the tensegrity elements (cables and struts), and the ability to combine smaller tensegrities or add more elements to an existing tensegrity, to achieve larger structures. The flexibility of tensegrity structures is the result of infinitesimal mechanisms at the joints of the tensegrity structure (nodes) which allow the structure to deform and rebound under loading cycles. These two properties of tensegrity systems led biology researchers to wonder if tensegrity systems could be used to model biological systems which also demonstrate these properties.



(a) US Pavilion Expo 67 [8]

(b) Georgia Dome [9]

**Figure 1.2: *Civil Engineering Tensegrity Structures:*** The American Pavilion was designed by Buckminster Fuller and Shoji Sadao for Expo '67, and the Georgia Dome was designed by Heery International *et al.* for the State of Georgia. Both are examples of tensegrity structures.

### 1.1.2 Medical Applications

Many biological systems can be modelled using tensegrity theory, most notably musculoskeletal systems and the structures of some cells. In the 1970's it was discovered that all cells that have nuclei also have a cytoskeleton. Dr. Ingber *et al.* [6] used this discovery to identify other elements of the cell which could function as anchor points (integrins and focal adhesions), tensile elements (primarily actin-containing microfilaments and the cell membrane), and compression elements (cytoskeleton microtubules) (Figure 1.4). Once



**Figure 1.3: *Tensegrity Bridge:*** The Kurilpa Bridge is a tensegrity structure that spans the Brisbane River in Brisbane, Australia [10].

the cellular analogues for the tensegrity elements were identified, it became possible to model the mechanical response of the cell under loads using a tensegrity model. Dr. Ingbar suggests that the tensegrity model is far superior to the previous cell models because it provides an explanation for how and why cells change their biochemistry and gene expression under mechanical loads [6].

This process is known as mechanotransduction, and prior to the application of the tensegrity model, the mechanism of signal transmission within the cell was unknown. The tensegrity model predicts that the forces acting anywhere on the cell are channeled through the tension and compression elements, into the extracellular matrix adhesion sites. Experimental results revealed that the load at the adhesion sites and the deformation of the cell caused deformation and reorientation of the molecules which regulate intracellular metabolism and gene expression (Figure 1.4). These reactions occurred on the millisecond time scale, allowing the cell to quickly respond to mechanical stimulus by altering its rate and direction of proliferation. These results may lead to therapies for heart conditions like cardiac hypertrophy [11].



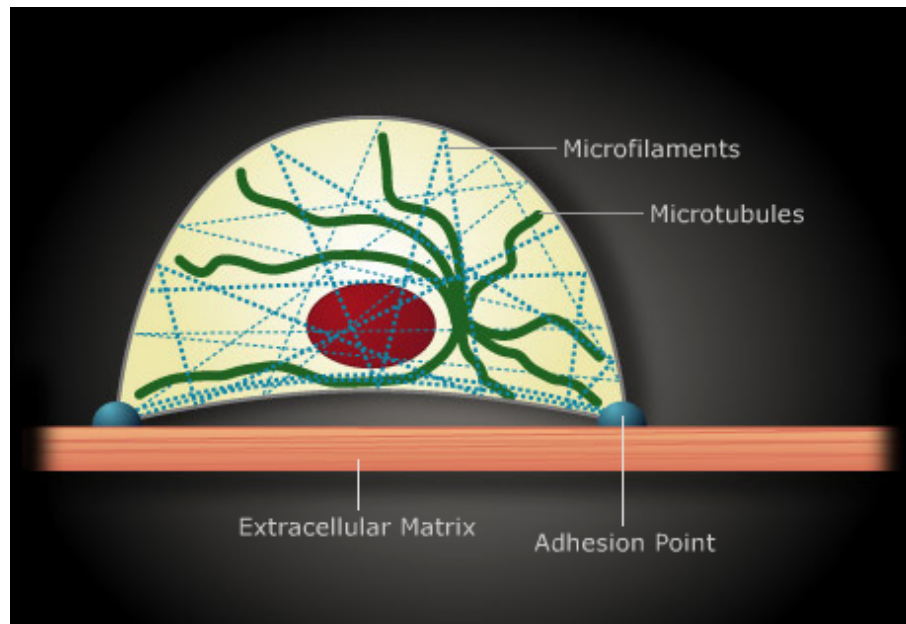


**Figure 1.4: *Tensegrity Structural Analogues in a Cell:*** This is a schematic representation of a cell created by Dr. Ingber et al. Microfilaments act as tension elements and microtubules act as compression elements. The cell is attached to the extracellular matrix via adhesion points. The tensegrity elements channel forces acting on the cell through these adhesion points and into the extracellular matrix [11].

Cardiac hypertrophy occurs when significant pressure builds on the cardiocyte cytoskeleton. This pressure buildup is caused by an increase in the number of microtubule compression elements, and it can interfere with the shortening of the cardiac tissue. This interference can lead to contractile dysfunction. The tensegrity model suggests that by changing the loading condition, either at the affected cells or at adjacent sites, the buildup of microtubules can theoretically be reversed [6]. Other applications for the tensegrity model include modeling the abnormal mechano-electrical coupling observed during the development of heart arrhythmias, and the structural modeling of viruses [1]. Tensegrity systems are also highly scalable providing an excellent model of mechanotransduction within the cell, and providing a model for larger biological systems such as the musculoskeletal system [12].

The mammalian skeleton functions as the compressive elements in a tensegrity system. The muscles, tendons, ligaments, fascia, and skin provide the tension elements that channel forces to the skeleton, holding the skeleton in place. Kassolik *et al.* [12] used this larger tensegrity model to predict how deep tissues might be massaged by manipulating surrounding or remote muscles. They concluded that by manipulating the brachioradialis and peroneal muscles they were able to stimulate the middle deltoid and tensor fasciae latae muscles respectively. This research indicates that physiotherapists can treat adverse muscle tension without directly manipulating the stressed area, amounting to less painful physiotherapy sessions for patients. Kassolik *et al.* also proposed that deep or inaccessible tissues could be stimulated remotely if a detailed tensegrity model of the human musculoskeletal system can be developed [12]. The scalability and flexibility of tensegrity systems also provides unique capabilities for weight and volume restricted space applications.

### 1.1.3 Space Structures

Space structures tend to be lightweight, strong, stiff, and foldable. These properties result from the desire to launch the space craft on the least expensive (smallest) launch vehicle possible, while providing a stable support for sensitive mission hardware like antennas and optical equipment. Furthermore, the effect of the launch loads on the structure and equipment can be reduced if the structure can be folded into a low volume, stowed configuration. Tensegrity systems tend to be lightweight structures that can be deployed and stiffened by tensioning their cable elements. They are especially attractive for space applications because the discontinuous nature of the compressive elements allow for large displacements of the tensegrity nodes when the tension elements are slackened. Consequently, greatly reduced storage volumes can be achieved. These properties have led several researchers to develop preliminary designs for tensegrity space booms, reflector antennas, and telescopes.

Tibert [13] developed a deployable tensegrity boom, which in some respects compared favourably with conventional booms used for space applications. The booms he designed

had excellent stowed/deployed volume ratios, high axial stiffnesses, fewer mechanical joints, and lower masses compared to conventional booms (Figures 1.5 and 1.6). However, the tensegrity booms had little resistance to bending loads, were prone to cable strut entanglements, and remained unstable until fully deployed. Tibert suggested methods for improving the tensegrity booms by using deployment canisters and selecting alternate tensegrity topologies. His later work dealt with tensegrity reflector antennas, which were better able to exploit the advantages of tensegrity systems.

The tensegrity reflector proposed by Tibert in [13] and [14] uses a tensegrity structure to

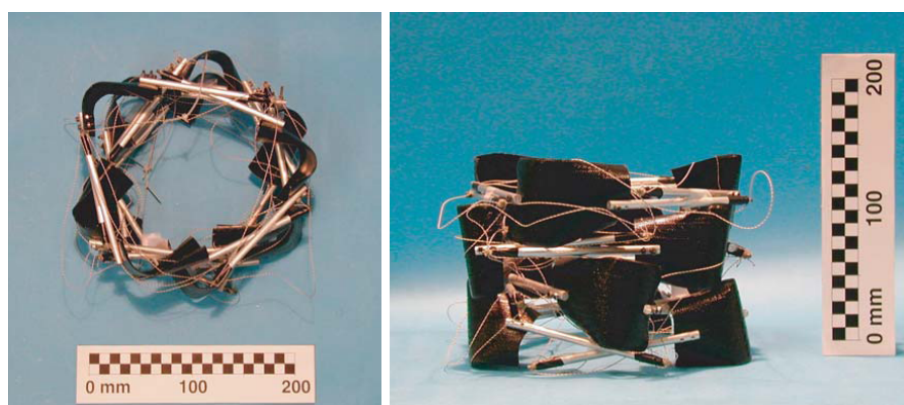


**Figure 1.5: *Collapsed Tensegrity Space Boom:*** The top and side views of the tensegrity boom in its collapsed state [13].

create a very stiff and lightweight structure, which also has an excellent stored/deployed ratio compared to conventional reflectors. One of the prime advantages of using a tensegrity structure for this application is the tunability of the final reflector. Reflector antennas must maintain their curvature within a specified range and have high natural frequencies in order to send and receive transmissions effectively. The stiffness of tensegrity structures can be adjusted by adjusting cable and strut lengths. This alters the level of prestress in the structure, which increases the stiffness and natural frequency of the structure. This tunability of the structure can help the tensegrity reflector adjust its shape to compensate for deployment defects, and stress relaxation within the elements over the life of the reflector.

The tensegrity reflector is made up of two nets that are suspended from the upper

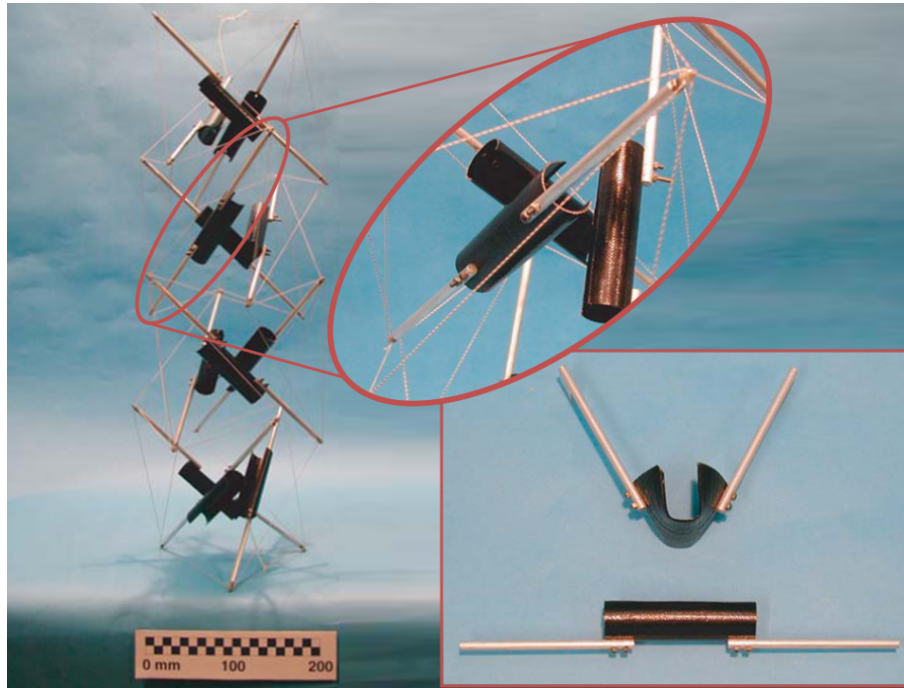


**Figure 1.6: Deployed Tensegrity Space Boom:** A general view of the tensegrity boom in its deployed state with details of the foldable compression members [13].

and lower faces of a regular tensegrity polygon. Additional members (springs) connect the upper and lower net knots, which force the nets to maintain their discrete parabolic shape (Figure 1.7). The compression members are telescoping tubes that extend (pulling against the net springs) during stowage, and retract to an equilibrium position under the action of the net springs (Figure 1.8). The remaining issues to be resolved with this design are minimizing compression and spring element interferences, and finding an optimum balance between the prestress levels and consequent mass of the compression elements. The high mass savings (partially due to the reduced number of mechanical joints and high stiffness) make the tensegrity reflector a promising technology for space applications. Other space structures that could exploit the high stiffness and controllability of tensegrity systems are solar arrays and space telescopes.

Sultan *et al.* [15] proposed using an actively controlled tensegrity structure to adjust the relative position of two mirrors in a space telescope. The control system for the proposed

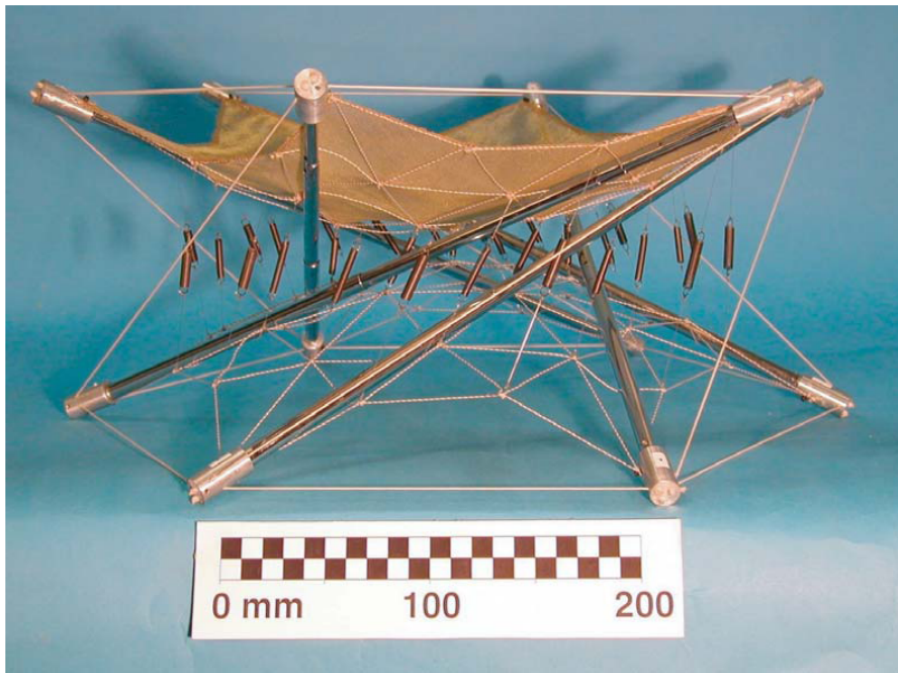


**Figure 1.7: *Tensegrity Reflector Antenna*:** A general view of the tensegrity reflector antenna in its deployed configuration [13].

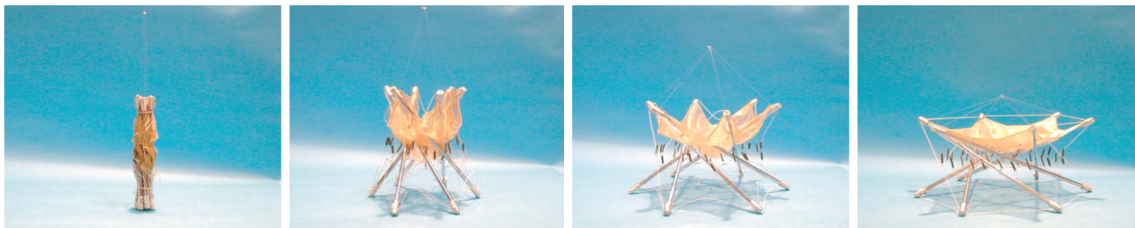


**Figure 1.8: *Tensegrity Antenna Deployment*:** The tensegrity antenna being deployed using the stored energy in the springs [13].

tensegrity telescope (and tensegrity mechanisms in general) tend to have a high level of precision because the model of the mechanical system is well characterized by rigid bars and two force elastic elements. Conventional rigid space telescopes (like the Hubble space telescope) must maneuver the entire, massive telescope into the desired position and then adjust the relative position of the mirrors inside the body of the telescope. The tensegrity telescope could use the reaction forces caused by the actuation of the tensegrity system to move the telescope into the correct orientation. The relative alignment of the two mirrors would then be fine tuned, while momentum wheels maintain the general orientation of the

telescope. This control method has the potential to be fuel efficient (and consequently mass efficient), which is always desirable for space applications due to the high cost per kilogram of launching hardware to orbit.

Sultan *et al.* also proposed using the tensegrity telescope structure itself as a sensor in [16]. This sensor would replace the tension cables with fibre optic sensors, which would continuously report their own length to the control system. The sensor controller would then use the length data to calculate the pose of the tensegrity structure, and the force in each of its elements. This system allows the structure to serve as its own integrated sensor, and can reduce the complexity and mass of the control system. This self sensing functionality has also come to the attention of roboticists, who would like to apply tensegrity theory to their robots.

#### 1.1.4 Robotics

Tensegrity robots tend to be light, fail safe, and more energy efficient than conventional robots. Their lightness comes from having the tension elements double as sensors, replacing more massive structural elements with lightweight cables, and being able to produce a desired output motion using different sets of actuators [7]. Tensegrity robots are usually controlled by varying the rest length of the cable elements. For every set of cable lengths there is a stable geometry where the stresses in the struts and cables are in equilibrium. This prestress can be exploited in tensegrity mechanisms by using this energy to help change the mechanisms pose. This energy storage relieves some of the workload on the actuators allowing tensegrity actuated robots to be more energy efficient. The interconnected nature of the tensegrity elements means that relatively few actuators are necessary to control the degrees of freedom of the robot. Furthermore, if one or more actuators fails the rest of the actuators can be actuated in such a way that the output motion remains almost the same [4]. In [4] and [5], Paul *et al.* developed two tensegrity robots, one of which was able to produce a usable gait despite one, and then two of its four actuators being taken off-line.



The tensegrity robots developed by Paul *et al.* in [4] and [5] were composed of three and four strut tensegrity topologies, named the TR-3 and TR-4 respectively (Figure 1.9). They created a simulation of the two configurations where three (TR-3) and four (TR-4) of the tension cable lengths were controlled using servo motors. They used a genetic algorithm to determine an actuation scheme that produced the fastest forward motion. The TR-4 produced a bounding gate with distinct take-off, flight, and stance motion phases. The TR-3's gate was more like that of an inchworm where two of its struts were dragged along by the third, which acted like a pickaxe. Another worm like mobile robot was developed by Masic and Skelton [17], which propelled itself by producing a longitudinal wave through its tensegrity structure.

These applications illustrate the wide potential of tensegrity systems from biological

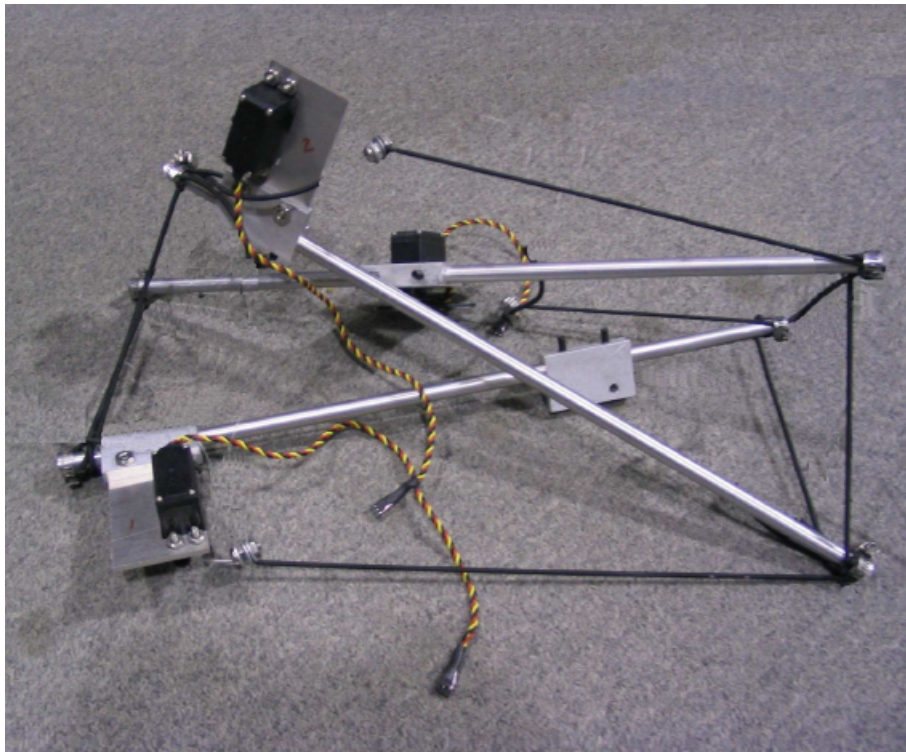


**Figure 1.9: Tensegrity Robot:** The TR-3 robot which was able to produce a worm like gate [4].

models to smart structures and robotics. The advantages of tensegrity systems are the

result of the unique way these systems balance compressive and tensile forces using a minimum of structural elements. However, most tensegrity systems are kinematically and statically indeterminate, meaning there are multiple solutions to the equilibrium equation, which defines the state of the tensegrity. This indeterminacy means that more relations or boundary conditions are necessary to define the stability of a unique configuration. This indeterminacy also results in several possible self stress states and mechanisms [18]. The stiffness of a tensegrity structure relies on constraining the motion of these mechanisms. These motions are constrained by specifying the tensegrity geometry in such a way that all cables are in tension and all struts are in compression. This initial loading or prestress is essential for the static stability and rigidity of the tensegrity system.

## 1.2 Rigidity and Stability

In [1], Motro discusses the importance of determining the stability of a given geometric tensegrity topology:

The stability of tensegrity systems can be satisfied only for geometry in which a situation of stable static self-equilibrium can be established: the study of tensegrity systems necessitates a “form finding process” which allows us to attain such geometric equilibrium [1].

Rigidity and stability can have several definitions depending on the context in which they are used. In the context of tensegrity systems rigidity implies that the only permissible motion of the tensegrity nodes are rigid body motions that preserve the length of the struts and cables. This definition of rigidity implies that a tensegrity is rigid if the only possible poses of the structure are congruent poses (poses that maintain the distance between the nodes in a tensegrity system). Stability indicates how close the structure is to physical collapse. A tensegrity structure is guaranteed to be both rigid and stable if it is super stable. Super stability and many other rigidity and stability criteria are more thoroughly presented in Chapter 2.



### 1.3 Form Finding Methods

There are several form finding methods that can be used to determine the geometry of tensegrity systems. A detailed description of form finding methods is presented in Chapter 3, building on work reported by Tibert and Pellegrino [2] and Tur and Juan [18]. The form finding methods have been categorized as either kinematic, static, or simultaneous methods.

The kinematic methods fix the length of the cables and then increase the length of the struts until a stable configuration is achieved. These methods provide some physical insight into the form finding problem, and some are relatively computationally simple. However, these methods become too cumbersome to use if the tensegrity topology is unsymmetric or has a variety of cable and strut lengths due to the number and interdependent nature of the variables necessary to describe the configuration. They also lack shape constraint surfaces, which can make the form finding process more intuitive. These methods have been largely surpassed by the static methods because the static methods can handle a wider range of tensegrity systems.

Unlike the kinematic methods that use the geometry of the elements, the static methods use the forces, stresses, or the energy within the tensegrity elements to determine a stable configuration. These methods are attractive because they can be used to analyze unsymmetric structures, and structures with more elements compared to the kinematic methods. This wider applicability comes at the cost of losing control over individual element lengths and more cumbersome calculations, which in general must rely on numerical methods. These methods are only concerned with finding stable configurations for the tensegrity structure and subsequent techniques must be used to determine other properties of the system.

The simultaneous methods solve for multiple properties of the tensegrity system as well as determining the stable configuration of the structure. These methods use genetic

algorithms, finite element analysis, and other numerical methods to arrive at one or multiple stable configurations. These methods can analyze unsymmetric tensegrity topologies and can generate completely new tensegrity topologies. Unfortunately they restrict the designers ability to specify element lengths and the shape of the final structure. They are also more cumbersome to implement, and would not be suitable for controlling a tensegrity mechanism as part of its control system. The disadvantages of the above form finding methods means there are many opportunities to develop new form finding methods that are better suited to the requirements of the designer.

## 1.4 Research Problem

The form finding methods discussed in Chapter 3 reveal that there is a need for a form finding method that is computationally simple and intuitive for designers to use. In smart structure applications, it is highly desirable for a form finding method to quickly calculate the change in pose of a tensegrity mechanism. Most of the current form finding methods either cannot handle multiple element lengths or are too computationally expensive to effectively implement in a real-time control system. Furthermore, many of these methods provide little insight into the solution space, or solution process of the form finding problem. They also fail to provide the designer with useful tools for manipulating the tensegrity system. These tools could include the use of shape constraint surfaces or the ability to either directly control the element lengths, or the overall shape parameters for the tensegrity. For example, the method could allow the designer to modify the radius and height of a cylindrical tensegrity structure instead of controlling the strut and cable lengths. Alternatively if the element lengths are important (as they would be for controlling a tensegrity mechanism) then the method could use the element lengths as inputs and produce the overall height and radius parameters as outputs. This thesis proposes a novel geometric form finding method that seeks to address the apparent lack of control and form finding insight missing in existing form finding methods.

## 1.5 Original Contributions to Knowledge

The objective of this thesis was to introduce and characterize a new geometric form finding method. The proposed method addresses some of the deficiencies of existing form finding methods. Specifically it:

1. allows direct control over the element lengths within symmetric tensegrities;
2. allows the shape of the tensegrity structure or mechanism to be parameterized with more intuitive parameters such as height and radius (as opposed to element angles and force densities);
3. uses the analytical geometry of surfaces to make the design process more intuitive;
4. provides more insight into the form finding solution space and process.

The new geometric method is compared with two of the most closely related form finding methods presented in Chapter 3 to validate the above claims.

## 1.6 Outline

Chapter 2 of this thesis provides a more rigorous mathematical definition of rigidity and stability as they relate to tensegrity systems. Chapter 3 contains a literature review of current form finding methods as well as a detailed comparison of their relative strengths and weaknesses. It also reinforces the rationale for developing the geometric form finding method proposed in this thesis. Chapter 4 discusses the new geometric intersection method. Chapter 5 provides a series of examples to illustrate the implementation, and unique characteristics of the geometric intersection method. Finally, Chapter 6 contains a short summary of the preceding chapters, and highlight the advantages of the geometric intersection method.

## Chapter 2

# Rigidity and Stability

Tensegrity systems have extremely minimal structures. Relatively few elements make up a tensegrity system's structure, and the majority of these elements are unable to support compressive loads. Additionally, the spherical joint like connections between tensegrity elements have many degrees of freedom due to the flexibility of the tension elements and the limited number of elements connected to each node. These properties naturally lead to the necessity of determining whether a given tensegrity arrangement (topology) is: a structure or a mechanism (rigidity), in static equilibrium (stability), and finally if that equilibrium is conditional. This chapter will define several forms of rigidity and stability that have been used to categorize tensegrity systems, and frameworks in general [18], [19]. The Harmony tensegrity topology (and by extension prismatic tensegrity structures) will be analyzed to prove that this topology is stable, regardless of the lengths of its elements, as long as it has a certain angle of twist between its upper and lower nodes. This chapter will begin with a description of prismatic tensegrity structures, followed by a description of graph theory, which is used to represent the edges, connections, and constraints of tensegrity topologies. Then the various rigidity and stability criteria will be presented in order of increasing inclusiveness, followed by a brief summary of how these methods pertain to the prismatic tensegrity topologies analyzed in this thesis.

## 2.1 Prismatic Tensegrity Topologies

The geometric form finding method presented in this thesis is formulated primarily for the analysis of prismatic tensegrity topologies, of which the Harmony tensegrity topology is a subset. A prismatic topology has two sets of nodes that lie on two separate, but parallel planes. These nodes form regular polygons on each plane such that a circle in each plane, passing through the nodes of that plane, share a common central axis. A prismatic topology can be completely parameterized using three parameters: half the number of nodes (denoted by  $\frac{n}{2}$ ) (which is equal to the number of struts denoted by  $n_s$ ); the number of nodes between the lower node of a strut and the upper node of the same strut (denoted by  $j$ ); and the number of nodes between two nodes connected by a cable in the nodal plane (denoted by  $k$ ) (Figures 2.1, 2.2, and 2.3) [20]. For example, the Harmony tensegrity topology is represented by  $P_{\frac{n}{2}}(j, k) \Rightarrow P_3(1, 1)$ . In Figure 2.3 one node from the upper node plane is selected as the reference node and the strut connected to this node is the reference strut.  $j$  is determined by projecting the reference node into the lower node plane and counting the number of nodes between the projected reference node and the node at the end of the reference strut (in this case there are three nodes so  $j = 3$ ).  $k$  is determined by counting the number of nodes between the reference node and the next node in the upper node plane that is connected to the reference node by a cable (in this case there are two nodes including the node connected to the reference node by the cable so  $k = 3$ ). These parameters define a family of prismatic tensegrity topologies, and a specific configuration within one of these topologies can be represented using graph theory.

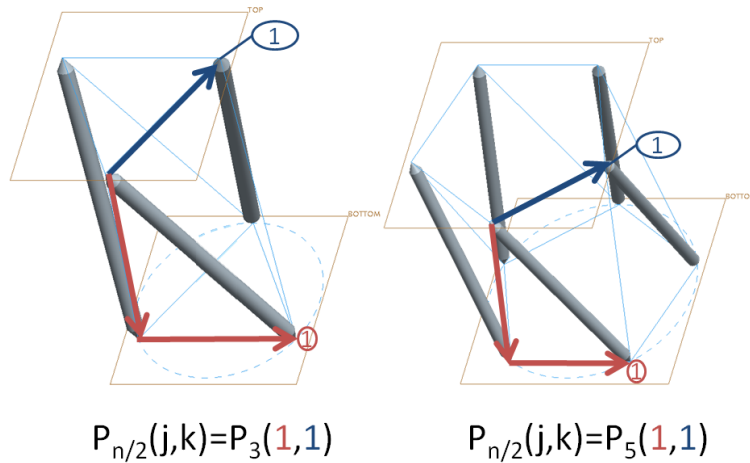


**Figure 2.1: Prismatic Tensegrity Notation:** The Harmony tensegrity topology ( $P_3(1,1)$ ) and the  $P_5(1,1)$  prismatic topology.

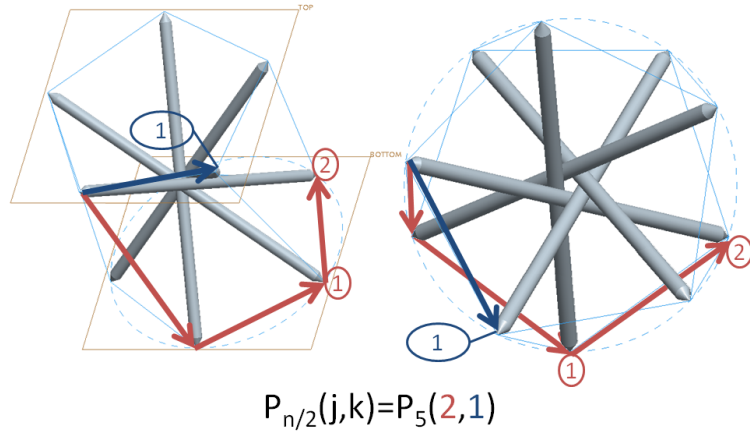


**Figure 2.2: Higher  $j$  Values:** The  $P_5(2,1)$  prismatic topology.

## 2.2 Graph Theory

Graph theory was originally used to describe cable net structures, but it was adapted to tensegrity structures by Roth and Whiteley [21]. A given tensegrity configuration can be described by a graph of its nodes  $G(\mathbf{p}_n)$ , where the nodal locations are given by their coordinates  $\mathbf{p}_n$ . Each node is connected to another node by an element in the tensegrity system (cable or strut). Each row of the graph represents one element by its two end node coordinates. The graph  $G(\mathbf{p})$  for the Harmony tensegrity topology in Figure 2.4 is:

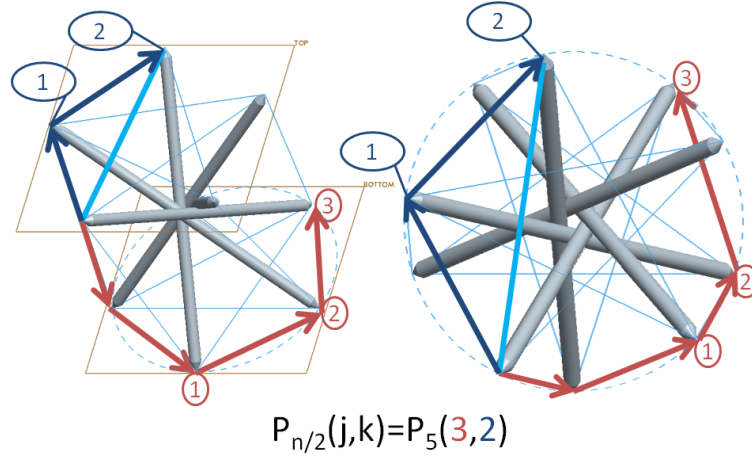


**Figure 2.3: Higher  $j$  and  $k$  Values:** The  $P_5(3,2)$  prismatic topology.

$$G(\mathbf{p}) = \begin{bmatrix} p_1 & p_2 & 0 & 0 & 0 & 0 \\ 0 & p_2 & p_3 & 0 & 0 & 0 \\ p_1 & 0 & p_3 & 0 & 0 & 0 \\ p_1 & 0 & 0 & 0 & p_5 & 0 \\ p_1 & 0 & 0 & 0 & 0 & p_6 \\ 0 & p_2 & 0 & 0 & 0 & p_6 \\ 0 & p_2 & 0 & p_4 & 0 & 0 \\ 0 & 0 & p_3 & p_4 & 0 & 0 \\ 0 & 0 & p_3 & 0 & p_5 & 0 \\ 0 & 0 & 0 & 0 & p_5 & p_6 \\ 0 & 0 & 0 & p_4 & 0 & p_6 \\ 0 & 0 & 0 & p_4 & p_5 & 0 \end{bmatrix}. \quad (2.1)$$

The graph of a tensegrity configuration presents a static image of the nodes of a tensegrity configuration, but most of the stability and rigidity criteria require the edge lengths of the elements to be monitored. The graph  $G(\mathbf{p})$  can be altered to include the edge length between nodes by subtracting the coordinates of the two nodes connected by an element. This new edge graph is known as the rigidity matrix  $R(\mathbf{p})$  [18]. The rigidity matrix is an

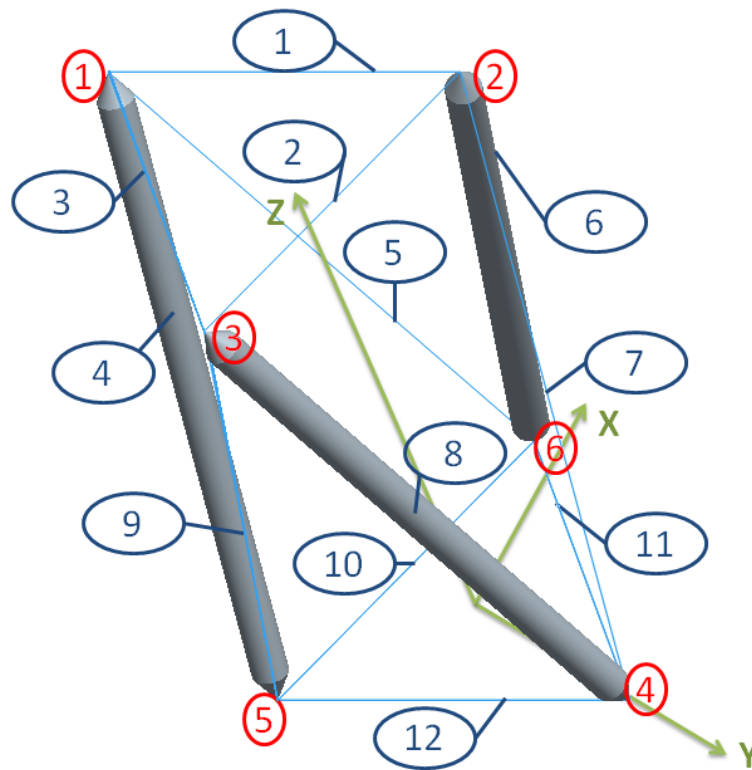


**Figure 2.4: Potential Numbering Scheme:** This is one possible numbering scheme and coordinate system for a Harmony tensegrity topology.

$e \times nd$  matrix where  $e$  is the number of elements in the tensegrity system,  $n$  is the number of nodes, and  $d$  is the dimension of workspace. The rigidity matrix is constructed such that there is a row for each element and  $d$  columns for each node; each node being located by  $d$  coordinates. The rigidity matrix entries are equal to the edge lengths at the nodes, and zero if the elements are not attached to a given node. The rigidity matrix for the harmony tensegrity topology is expressed by Equation (2.2).



$$R(\mathbf{p}) = \begin{bmatrix} p_1 - p_2 & p_2 - p_1 & 0 & 0 & 0 & 0 \\ 0 & p_2 - p_3 & p_3 - p_2 & 0 & 0 & 0 \\ p_1 - p_3 & 0 & p_3 - p_1 & 0 & 0 & 0 \\ p_1 - p_5 & 0 & 0 & 0 & p_5 - p_1 & 0 \\ p_1 - p_6 & 0 & 0 & 0 & 0 & p_6 - p_1 \\ 0 & p_2 - p_6 & 0 & 0 & 0 & p_6 - p_2 \\ 0 & p_2 - p_4 & 0 & p_4 - p_2 & 0 & 0 \\ 0 & 0 & p_3 - p_4 & p_4 - p_3 & 0 & 0 \\ 0 & 0 & p_3 - p_5 & 0 & p_5 - p_3 & 0 \\ 0 & 0 & 0 & 0 & p_5 - p_6 & p_6 - p_5 \\ 0 & 0 & 0 & p_4 - p_6 & 0 & p_6 - p_4 \\ 0 & 0 & 0 & p_4 - p_5 & p_5 - p_4 & 0 \end{bmatrix}. \quad (2.2)$$

The rigidity matrix, or its transpose the equilibrium matrix, can be used to monitor the element lengths of a tensegrity configuration, which has certain implications for the rigidity of the configuration.

### 2.3 Rigidity Definitions

One of the governing assumptions for tensegrity mathematical models and form finding methods is that all elements of a tensegrity system are connected using revolute ( $\mathbb{E}^2$  by nature) or spherical ( $\mathbb{E}^3$  by nature) joints. Since all connections have at least one degree of freedom, the framework may be either a structure or a mechanism depending on the lengths, locations, and interconnections of its elements. If the framework is a mechanism it has the ability to fold or skew into infinitely many discrete poses, and is thus termed flexible. A two dimensional example of a flexible structure (really a planar four bar mechanism) is depicted in Figure 2.5. The framework in Figure 2.5 can be made into a structure in  $\mathbb{E}^2$  by adding an additional link. This new framework is rigid, but only in  $\mathbb{E}^2$ . In  $\mathbb{E}^3$  the framework

can still be folded along the axis of the added link as illustrated in Figure 2.6. Therefore, determining rigidity can be thought of as determining whether or not a framework is a rigid structure or a flexible mechanism [22].



**Figure 2.5: 2D Flexible Structure:** This 2D structure has one degree of freedom. It can have infinitely many configurations and is therefore non-rigid or flexible [22].

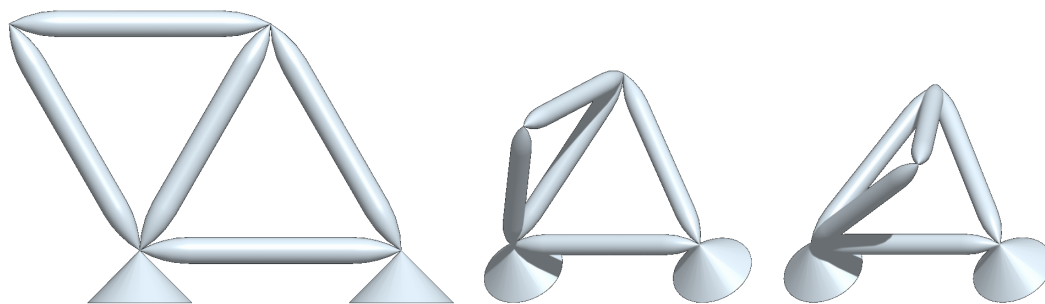


**Figure 2.6: 3D Flexible Structure:** This structure is rigid in 2D, but non-rigid in 3D because it can fold onto itself [22].

### 2.3.1 Determining Rigidity using Motion Analysis

The above definition of rigidity additionally requires that all the element lengths of the framework remain the same, and hence the rigidity matrix  $R(\mathbf{p})$  remains constant. This assumption can be stated mathematically by specifying that the distance between the two end nodes of an element,  $p_1(t)$  and  $p_2(t)$ , remain invariant for all values of time  $t$  [23]:

$$|p_1(t) - p_2(t)|^2 = [p_1(t) - p_2(t)] \cdot [p_1(t) - p_2(t)]. \quad (2.3)$$

Another way to determine rigidity is to prove that all possible configurations of the tensegrity framework are congruent configurations [18]. The graph of the tensegrity system is used to test for this condition. Let all tensegrity configurations  $G(\mathbf{p})$  that share common

element connection constraints (a specific topology) be represented by  $X(\mathbf{p})$ , where  $\mathbf{p}$  is the abstract map of all connections and nodal coordinates of the framework. Likewise, let all congruent configurations to a specific configuration  $G(\mathbf{p})$  be represented by  $M(\mathbf{p})$ . Then a tensegrity framework is rigid if the set  $X(\mathbf{p})$  is identical to the set  $M(\mathbf{p})$  [21]. In other words, if one configuration  $G(\mathbf{p})$  can only be transformed into new configurations by affine transformations<sup>1</sup> then the tensegrity framework is rigid. Physically, this amounts to proving that there is really only one possible configuration  $G(\mathbf{p})$ , and all other configurations are really just  $G(\mathbf{p})$ , but rotated, translated, or reflected to look like new configurations from the set  $X(\mathbf{p})$ . The key here is that under affine transformations or reflections the elements of  $G(\mathbf{p})$  cannot change their lengths. Therefore, if it is possible to move a portion of the framework  $G(\mathbf{p})$  without changing any of the element lengths, then there must be other, non-congruent configurations in the set  $X(\mathbf{p})$  and the framework is a mechanism (like the four bar mechanism depicted in Figure 2.5). The following discussion of stability will present mathematical methods for determining whether or not  $X(\mathbf{p})$  is equal to  $M(\mathbf{p})$ , and consequently if the elements in a particular tensegrity framework can change their lengths. The previous methods for determining rigidity have focused on the mechanical status of the tensegrity system, but another method is available that uses the forces in the tensegrity elements.

### 2.3.2 Determining Rigidity using Forces

If the nodal forces in the elements of a tensegrity topology are all in equilibrium, then the structure is statically rigid [18]. This can be represented by:

$$\sum_{ij} \frac{\mathbf{p}_i - \mathbf{p}_j}{\mathbf{d}} \mathbf{T} = \mathbf{F}_{ext}. \quad (2.4)$$

Equation (2.4) can be rewritten in terms of the rigidity matrix:

$$R(\mathbf{p})^T \frac{\mathbf{T}}{\mathbf{d}} = \mathbf{F}_{ext}. \quad (2.5)$$

---

<sup>1</sup>The group of affine transformations preserve distance, but not necessarily orientation. For example two points will always remain the same distance apart when an affine transformation is applied to them, but their location and orientation in space may be altered. The group of affine transformations include: rotations, translations, reflections, and glides (reflection and then translation or vice versa).

Equation (2.5) is non-linear because the element forces  $\mathbf{T}$  are dependent on the nodal coordinates  $\mathbf{p}_i$  and  $\mathbf{p}_j$  [18]. The transpose of the rigidity matrix  $R(\mathbf{p})^T$  is the equilibrium matrix  $E(\mathbf{p})$ . In the tensegrity community, the ratio between  $\mathbf{T}$  and the rest length of an element  $d$  is called a stress  $\omega$ , or a force density<sup>2</sup>  $q$  [19]. Using stresses, Equation (2.5) becomes:

$$R(\mathbf{p})\boldsymbol{\omega} = \mathbf{F}_{ext}. \quad (2.6)$$

The substitution of  $\boldsymbol{\omega}$  linearizes Equation (2.6), which makes certain form finding processes and stability analyses much easier (for example, see the force density method in Chapter 3).

### 2.3.3 Determining Rigidity using Stresses or Force Densities

When a tensegrity system is in equilibrium all struts must be in compression and all cables must be in tension. In terms of stress, a proper self stress occurs when the strut stresses are less than zero and the cable stresses are greater than zero (the proper stress is additionally termed strict if none of the stresses are identically equal to zero) [19]. The vector of stresses  $\boldsymbol{\omega}$  in the elements can be used to construct a reduced stress matrix  $\underline{\boldsymbol{\Omega}}$ . The reduced stress matrix has the form:

$$\underline{\boldsymbol{\Omega}} = \begin{cases} -\omega_{ij} & \text{if } i \neq j; \\ \sum_k \omega_{jk} & \text{if } i = j; \\ 0 & \text{if the nodes are not connected.} \end{cases} \quad (2.7)$$

and is similar to the rigidity matrix  $R(\mathbf{p})$  since it reveals the topology of the tensegrity system [18]. The reduced stress matrix for the Harmony tensegrity topology, using the arbitrary, strict, proper stress vector:

$$\boldsymbol{\omega} = \left[ 1 \ 1 \ 1 \ -1 \ 1 \ -1 \ 1 \ -1 \ 1 \ 1 \ 1 \ 1 \right]^T \quad (2.8)$$

---

<sup>2</sup>Stresses  $\omega$  and force densities  $q$  are equivalent terms and will be used interchangeably throughout this thesis. Stresses are used when the references work being discussed uses stresses and force densities are used when the references work uses force densities. In either case the reader is free to substitute stresses for force densities in any instance.

is:

$$\underline{\mathbf{\Omega}} = \begin{bmatrix} 2 & -1 & -1 & 0 & 1 & -1 \\ -1 & 2 & -1 & -1 & 0 & 1 \\ -1 & -1 & 2 & 1 & -1 & 0 \\ 0 & -1 & 1 & 2 & -1 & -1 \\ 1 & 0 & -1 & -1 & 2 & -1 \\ -1 & 1 & 0 & -1 & -1 & 2 \end{bmatrix}. \quad (2.9)$$

The full stress matrix  $\mathbf{\Omega}$  is an  $nd \times nd$  square matrix, where each stress  $\omega$  is given by its direction and magnitude (a vector of  $d$  elements). Since the stresses are generally used to set up a desired pre-stress within the tensegrity system, the direction of the pre-stress within the elements is usually arbitrary. For this reason it is generally easier to use the  $n \times n$  reduced stress matrix  $\underline{\mathbf{\Omega}}$ , since the important parts of the stresses are their signs and magnitudes, not their directions [24]. The equilibrium condition in Equation (2.6) can now be interpreted in terms of the stress matrix [18]:

$$\mathbf{p}^T \mathbf{\Omega} = \mathbf{F}_{ext}, \quad (2.10)$$

and a self stress is any  $\omega$  that satisfies the homogenous form of Equation (2.10):

$$\mathbf{p}^T \mathbf{\Omega} = 0. \quad (2.11)$$

### 2.3.4 Infinitesimal Rigidity

Another class of rigidity applies if the framework element lengths do not change with time. This class of rigidity is called infinitesimal rigidity, or first order rigidity, because it implies that the structure is rigid for an infinitesimally short time  $dt$ , starting from the initial time  $t = 0$ . This can be represented mathematically by evaluating the derivative of Equation (2.3) at  $t = 0$  [21]:

$$\left. \frac{d}{dt} |p_1(t) - p_2(t)|^2 \right|_{t=0} = [p_1(0) - p_2(0)] \cdot [p'_1(0) - p'_2(0)] \quad (2.12)$$

The tensegrity framework is then infinitesimally rigid (or first order rigid) if Equation (2.12) is equal to zero for bars, less than zero for cables, and greater than or equal to zero for

struts [21]:

$$[p_1 - p_2] \cdot [p'_1 - p'_2] = \begin{cases} = 0 & \text{for bars} \\ < 0 & \text{for cables} \\ > 0 & \text{for struts} \end{cases} . \quad (2.13)$$

Equation (2.13) is better understood by considering how cables, struts, and bars are allowed to deform. By definition bars are not allowed to change in length, cables are not allowed to reduce in length, and struts are not allowed to increase in length. Equation (2.13) can be restated in terms of the rigidity matrix:

$$R(\mathbf{p})\mathbf{p}'_i = \mathbf{d}_i, \quad (2.14)$$

where  $\mathbf{p}'_i$  is a vector of nodal velocities and  $\mathbf{d}_i$  is a vector of edge length changes due to  $\mathbf{p}'_i$ .

Without loss in generality, we can replace all the cables and struts of a given tensegrity framework with bars and examine the properties of Equation (2.13) [18]. The first term of Equation (2.13),  $[p_1 - p_2]$  can never be zero if the element between  $p_1$  and  $p_2$  has a non-zero length. It follows that there are only two cases in which Equation (2.13) can equal zero. The first is the trivial case where  $[p'_1 - p'_2]$  equals zero. This case amounts to either no motion of the nodes ( $p'_1 = 0$  and  $p'_2 = 0$ ) or both nodes having the same velocity vectors ( $p'_1 = p'_2$ ). If  $p'_1 = p'_2$  then the element between  $p_1$  and  $p_2$  is experiencing a rigid body motion. If all element lengths within the framework remain constant, then the entire structure must be moving in the same direction, with the same velocity. In other words, if  $p'_1 = p'_2$  then the whole structure is experiencing a rigid body motion, otherwise some elements would have to change their lengths. The second case occurs if a dissimilar, non-zero velocity can be applied to either  $p_1$  or  $p_2$ .

If  $p'_1$  and  $p'_2$  are non-zero and  $p'_1 \neq p'_2$ , then the velocity vector must be perpendicular to the element between  $p_1$  and  $p_2$ :

$$(p_1 - p_2) \cdot (p'_1 - p'_2) = |(p_1 - p_2)| |p'_1 - p'_2| \cos(\theta) = 0, \quad (2.15)$$

where:  $\theta$  is the angle between the direction of the velocity vector and the element. Equation (2.15) indicates that the only way a non-zero, dissimilar velocity can be assigned to  $p'_1$

and  $p'_2$  is when  $\theta = 90^\circ$  or  $270^\circ$ . In  $\mathbb{E}^2$  this occurs if the elements connected by point  $p$  are parallel (Figure 2.7). At  $t = 0$  velocity  $p'$  is orthogonal to the links, but a short time  $dt$  later the links have moved and  $p'$  is no longer perpendicular to both links. This short movement is called an infinitesimal flex and indicates that the structure is infinitesimally flexible. In  $\mathbb{E}^3$  there are a pencil of velocity vectors  $p'$  that are perpendicular to the base links for a infinitesimal time  $dt$  (Figure 2.8).

An alternate way to determine infinitesimal rigidity is to use the first order stress test

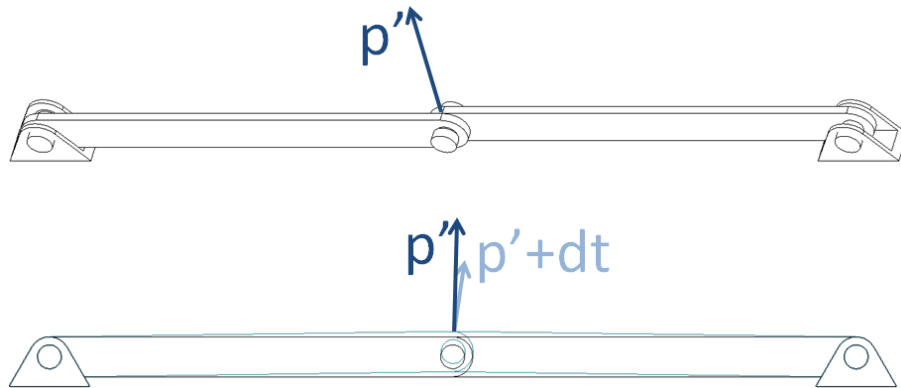


**Figure 2.7: 2D Infinitesimal Flex:** This structure is infinitely flexible in 2D, because the node velocity  $p'$  is perpendicular to the link for a brief moment ( $dt$ ) until the link rotates and the nodal velocity becomes  $p' + dt$  [21].

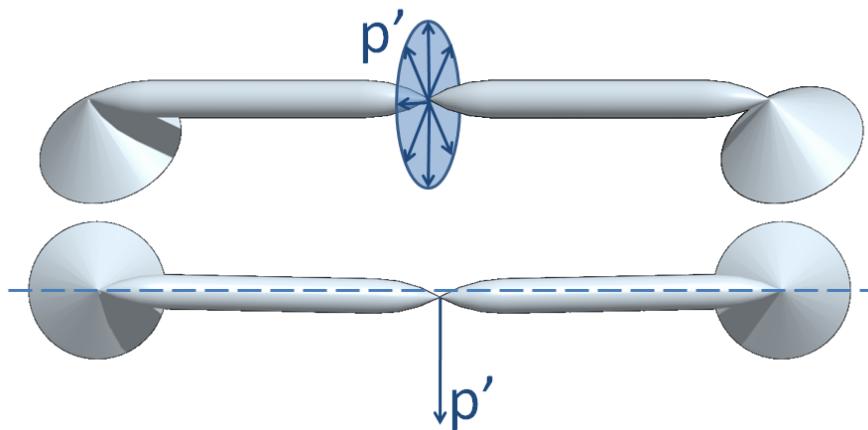


**Figure 2.8: 3D Infinitesimal Flex:** This structure is infinitely flexible in 3D, because there are several velocity vectors  $p'$  that are perpendicular to the links [21].

reported by Connelly and Whiteley [25]. The first order stress test exploits the fact that the only way an element in a tensegrity system can change its length is if the stress in that element is zero. If all the stresses in the tensegrity elements are selected to be strict proper stresses then no stress can be equal to zero. Moreover, if the equivalent bar framework  $B(\mathbf{p})$  ( $G(\mathbf{p})$  with all cables and struts replaced by bars) of the tensegrity configuration  $G(\mathbf{p})$  is infinitesimally rigid, then  $G(\mathbf{p})$  must also be infinitesimally rigid [25].

Roth and Whiteley [21] proved that if the equivalent bar framework  $B(\mathbf{p})$  has a certain rank then the configuration is potentially infinitesimally rigid. The principle of this proof is that the nodal coordinates form a dense open set in  $\mathbb{E}^d$ . This means that there is an infinitesimal distance between the nodes and the nodes can move an infinitesimal distance from their initial position and still be members of  $\mathbb{E}^d$ . If one instance of the configuration  $B(\mathbf{p})$  is infinitesimally rigid then the entire topology is also infinitesimally rigid [18]. The results of this proof can be stated as [26]:

$$\text{if } \text{rank}[R(\mathbf{p})] \geq nd - \frac{d(d+1)}{2} \Rightarrow G(\mathbf{p}) \text{ is infinitesimally rigid.} \quad (2.16)$$

The rank of the  $R(\mathbf{p})$  matrix for the equivalent bar framework of the Harmony tensegrity topology reveals that this topology will satisfy Equation (2.16), yielding:

$$\text{rank}[R(\mathbf{p})] = 12 = 6 \cdot 3 - \frac{3(3+1)}{2}. \quad (2.17)$$

However the Harmony topology can never be infinitesimally rigid because non-trivial flexes can be applied in the plane of the upper and lower nodes [26] (Figure 2.9). Therefore Equation (2.16) can only predict rigidity, it is not a sufficient condition to guarantee rigidity. Similarly, all prismatic tensegrity topologies will never be infinitesimally rigid because non-trivial velocities can be applied to their nodes in the planes of their upper and lower nodes. Most will also fail the rigidity predictor in Equation (2.16) due to their low node to element ratio [20]. These topologies can be made rigid by adding a pre-stress to the tensegrities elements. This pre-stress will stabilize the infinitesimal flexes in the tensegrity by ensuring that its nodes are always in equilibrium.



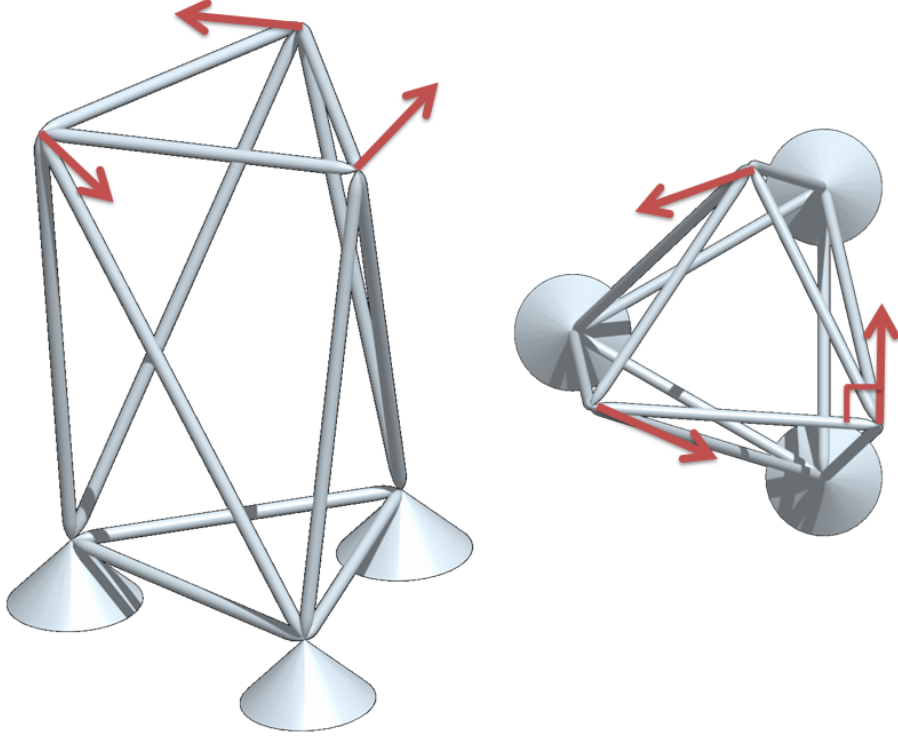


**Figure 2.9: Prismatic Tensegrity Infinitesimal Flex:** This bar framework has the same configuration as the Harmony tensegrity topology. It will always be infinitesimally flexible because non trivial velocities can be applied to its upper or lower nodes since the nodes share the same plane. This is true regardless of the length of the tensegrity elements.

### 2.3.5 Second Order Rigidity

Another class of rigidity is second order rigidity. Second order rigidity differs from infinitesimal, or first order rigidity, in that it is based on taking a higher derivative of the length function [18]:

$$\left. \frac{d^2}{dt^2} |p_1(t) - p_2(t)|^2 \right|_{t=0} = [p'_1(0) - p'_2(0)] \cdot [p'_1(0) - p'_2(0)] + (p_1 - p_2) \cdot [p''_1(t) - p''_2(t)]. \quad (2.18)$$

Similar to the infinitesimal rigidity equation (Equation (2.12)), Equation (2.18) reveals that in order for a tensegrity to be second order rigid its elements must not be capable of relative, second order motions (ie. accelerations) (Equation (2.13)). Connelly and Whiteley [25] proved that the only way Equation (2.18) can be satisfied is if all second order motions (accelerations,  $\mathbf{p}''$ ) have trivial first order motions (velocities  $\mathbf{p}' = 0$ ). It follows that if all accelerations have trivial velocities ( $\mathbf{p}' = 0$ ) then the structure must

be second order rigid. If the velocities associated with the accelerations are non-trivial then the framework is second order flexible. Connelly and Whiteley [25] proved that if a framework is second order rigid then the framework is also first order rigid. It follows that the framework must also be rigid since a first order rigid framework is rigid.

The second order stress test can also be used to determine if a given topology is second order rigid. The second order stress test states that if:

$$\mathbf{p}'^T \underline{\boldsymbol{\Omega}} \mathbf{p}' \leq 0, \quad (2.19)$$

for all proper self stresses, then  $\mathbf{p}'$  can be extended to  $\mathbf{p}''$  and the topology is not second order rigid [18]. Equation (2.19) will always be satisfied if the reduced stress matrix  $\underline{\boldsymbol{\Omega}}$  is positive semi-definite [25].

### 2.3.6 Pre-Stress Stability

The energy state of a given tensegrity configuration can be used to verify many of the above stability criteria, as well as the pre-stress stability of the structure. For instance, a tensegrity configuration  $G(\mathbf{p})$  is considered rigid when its energy is at a local minimum for  $\mathbf{p}$  (the vector of nodal coordinates) and all other congruent configurations share the same minimum [25]. The energy function is given by [18]:

$$E(\mathbf{p}) = \sum_{ij} \mathbf{f}_{ij} |\mathbf{p}_i - \mathbf{p}_j|^2. \quad (2.20)$$

The local minimum for the energy function in Equation (2.20) is found by evaluating the derivative of the energy function at  $t = 0$  [18]:

$$\left. \frac{dE(\mathbf{p})}{dt} \right|_{t=0} = \sum_{ij} \mathbf{f}'_{ij} (|\mathbf{p}_i - \mathbf{p}_j|^2) [2(\mathbf{p}_i - \mathbf{p}_j)(\mathbf{p}'_i - \mathbf{p}'_j)]. \quad (2.21)$$

$\mathbf{f}'_{ij} (|\mathbf{p}_i - \mathbf{p}_j|^2)$  is equivalent to the stress  $\boldsymbol{\omega}_{ij}$  and  $(\mathbf{p}_i - \mathbf{p}_j)$  can be replaced by the rigidity matrix  $R(\mathbf{p})$  to give the local minimum energy condition given in Equation (2.22) [18]:

$$\left. \frac{dE(\mathbf{p})}{dt} \right|_{t=0} = 2\boldsymbol{\omega}^T R(\mathbf{p}) \mathbf{p}' = 0. \quad (2.22)$$

Equation (2.22) guarantees that the tensegrity topology is a local minimum at  $\mathbf{p}$ , but the second derivative of the energy equation must be used to determine if the configuration is at a global minimum [18]:

$$\left. \frac{d^2 E(\mathbf{p})}{dt^2} \right|_{t=0} = \sum_{ij} \mathbf{f}_{ij}''(|\mathbf{p}_i - \mathbf{p}_j|^2) [2(\mathbf{p}_i - \mathbf{p}_j)(\mathbf{p}'_i - \mathbf{p}'_j)]^2 + \sum_{ij} \mathbf{f}_{ij}(|\mathbf{p}_i - \mathbf{p}_j|^2) 2(|\mathbf{p}'_i - \mathbf{p}'_j|^2). \quad (2.23)$$

Equation (2.23) can be rearranged into the Hessian matrix  $\mathbf{H}$  by substituting the element stiffness terms ( $\mathbf{c}_{ij}$ ) in a diagonal stiffness matrix  $\mathbf{C}$  for the  $\mathbf{f}_{ij}''(|\mathbf{p}_i - \mathbf{p}_j|^2)$  term [18]:

$$\left. \frac{d^2 E(\mathbf{p})}{dt^2} \right|_{t=0} = \mathbf{H} = \mathbf{p}'^T [2\underline{\mathbf{\Omega}} + 4R(\mathbf{p})^T \mathbf{C} R(\mathbf{p})] \mathbf{p}'. \quad (2.24)$$

The Hessian matrix equation (Equation (2.24)) can be used to determine if the tensegrity topology is pre-stress stable. If the Hessian matrix equation is satisfied then the stress matrix  $\underline{\mathbf{\Omega}}$  must be positive semi-definite. The stress matrix is positive semi-definite if its eigenvalues are positive, and the eigenvalues will only be positive if the stress vector  $\boldsymbol{\omega}$  contains strict, proper stresses [25]. Therefore, if  $\boldsymbol{\omega}$  contains strict, proper stresses then the tensegrity framework  $G(\mathbf{p})$  is pre-stress stable. Pre-stress stability is a key component of the following stability definitions.

### 2.3.7 Unyielding

A tensegrity topology can be classified as unyielding if all elements maintain their lengths in all possible non-congruent and congruent configurations [18]. If all congruent configurations are classified as  $G(\mathbf{p})$  and all non-congruent configurations of the same topology are  $G(\mathbf{q})$  then a topology is unyielding if:

$$\|\mathbf{q}_i - \mathbf{q}_j\| = \|\mathbf{p}_i - \mathbf{p}_j\|. \quad (2.25)$$

One way to verify Equation (2.25) is to examine the energy state of the desired tensegrity configuration. A tensegrity configuration  $G(\mathbf{p})$  is unyielding if it is pre-stress stable and the stress matrix  $\underline{\mathbf{\Omega}}$  is positive semi-definite [18]. These conditions ensure that the Hessian matrix is positive semi-definite, which means that the tensegrity configuration  $G(\mathbf{p})$  is at a

global minimum energy state. Any other configuration  $G(\mathbf{q})$  must then be close to  $G(\mathbf{p})$  to also be in a minimum energy state. If this is the case, then the lengths of the elements in  $G(\mathbf{q})$  must be approaching the lengths of the elements in  $G(\mathbf{p})$ , and they are in fact the same configuration (Equation (2.25)).

In terms of the Hessian matrix  $\mathbf{H}$  (Equation (2.24)), when a tensegrity configuration is unyielding the first term dominates the second term. This relationship ensures that  $\mathbf{H}$  is positive semi-definite [18]. Connelly [25] noted that even if a tensegrity configuration has a non positive semi-definite stress matrix and is therefore not unyielding, it may still be prestress stable. This state can occur if the physical characteristics of the topology (stiffness  $\mathbf{C}$  and placement  $R(\mathbf{p})$ ) are large enough to preserve the positive semi-definiteness of the Hessian matrix. In this case the second term in the Hessian matrix dominates the stress matrix term ensuring that  $\mathbf{H}$  is positive semi-definite, and consequently that the structure would only fail if its elements physically failed [18].

### 2.3.8 Global Rigidity

A tensegrity topology is globally rigid if all possible configurations are actually the same configurations or congruent configurations [19]. For a tensegrity topology to be globally rigid, the Hessian matrix must be greater than zero for all non-trivial flexes  $\mathbf{p}'$  (ie. be in a positive, energy storing state), and it must be equal to zero for trivial flexes. These conditions ensure that configuration  $G(\mathbf{p})$  is the global minimum energy configuration, because all configurations that have negative energy (returning energy to the environment), and configurations that result from trivial flexes are eliminated; leaving only the energy storing configurations that have proper stresses by definition [18]. The second term of the Hessian matrix represents the physical characteristics of the frameworks connections and its material properties. The second term will always be positive semi-definite because both the rigidity matrix  $R(\mathbf{p})$  and the stiffness matrix  $\mathbf{C}$  are selected to be positive semi-definite. The first term represents the internal and external loads on the tensegrity topology. Therefore the Hessian matrix equation (Equation (2.24)) will always be satisfied if the stresses

are strict proper stresses and are selected to make the stress matrix  $\underline{\Omega}$  positive semi-definite.

If the Hessian equation is satisfied, then the configuration  $G(\mathbf{p})$  is rigid because any other configuration close to  $G(\mathbf{p})$  must be at a higher energy state. Each local energy state corresponds to a specific configuration. If there is only one minimum energy state then the only other possible configurations are congruent configurations, and  $G(\mathbf{p})$  must be globally rigid [25]. Connelly and Terrell [20] proved that prismatic tensegrities, including the Harmony tensegrity, can only be globally rigid if  $k = 1$  or  $k = \frac{n}{2} - 1$ . This condition is true because the  $k = 1$  and  $k = \frac{n}{2} - 1$  topologies are equivalent (it just depends on the direction in which the nodes are counted) and the only other possible configuration is the congruent configuration  $(P_{\frac{n}{2}}(j, \frac{n}{2} - k))$ , where the vertical struts and cables are switched [20].

### 2.3.9 Universally Global Rigidity

A tensegrity topology is universally globally rigid if it is globally rigid in a higher dimensional space. That is, if  $G(\mathbf{p})$  is globally rigid in  $\mathbb{E}^o$  and is also rigid in  $\mathbb{E}^d$ , and  $o$  is less than or equal to  $d$  then the topology is universally globally rigid [19]. In other words, if more degrees of freedom are added to the tensegrity structure because the dimension of the workspace has increased, the tensegrity must maintain its shape to be considered universally globally rigid [18].

### 2.3.10 Super Stability

A tensegrity topology is super stable when it has a proper self stress, when all possible alternate configurations are congruent configurations or affine transformations of the topology configuration  $G(\mathbf{p})$ , and when the shape of the tensegrity topology does not change regardless of the dimension of the workspace [18]. Mathematically, a tensegrity topology is super stable if:

1. the stress matrix  $\underline{\Omega}$  is positive semi-definite;
2. the configuration  $G(\mathbf{p})$  contains all other possible configurations of the topology

( $G(\mathbf{p}) = X(\mathbf{p})$ ), hence there can be no affine image of  $\mathbf{p}$  such that  $G(\mathbf{q})$  is connected in the same way as  $G(\mathbf{p})$  [19].

The first condition in the above list occurs when the stresses in  $\mathbf{\Omega}$  are all strict proper stresses as discussed in the global rigidity criterion. In order for the second condition to be satisfied the stress matrix  $\mathbf{\Omega}$  must have a nullity of three in  $\mathbb{E}^2$ , four in  $\mathbb{E}^3$ , etc... [20]. Alternatively the rank of the stress matrix must be equal to the number of nodes minus the dimension of the workspace minus one [19]:

$$\text{rank}(\mathbf{\Omega}) = n - d - 1. \quad (2.26)$$

Equation (2.26) ensures that any alternate configuration  $G(\mathbf{q})$  resulting from affine transformations of  $G(\mathbf{p})$  are eliminated by the null space of  $\mathbf{\Omega}$ . This elimination means that the only possible alternate configurations  $G(\mathbf{q})$  are congruent configurations to  $G(\mathbf{p})$  [20]. These conditions also ensure that as long as the stresses in the elements are all adequately large the stress matrix will dominate in the energy equation  $\mathbf{H}$ , and keep the structure in static equilibrium [27].

Connelly [20] proved that prismatic tensegrity structures are only super stable when a certain angle of twist (Figure 2.10) between the upper and lower polygons creates a symmetric proper stress in the elements. The angle of twist is determined by [2]:

$$\theta = \pi \left( \frac{1}{2} - \frac{j}{\frac{n}{2}} \right). \quad (2.27)$$

A symmetric proper stress state occurs when all elements of the same type (horizontal cables, vertical cables, and struts) have the same stress. The derivation of Equation (2.27) is especially relevant to this thesis so it will be reproduced here (see Connelly [20] for the original derivation). Due to the symmetry of prismatic tensegrity structures it is only necessary to consider the equilibrium of one node in order to determine the equilibrium of the entire structure [20]. The equilibrium equation (Equation (2.6)) will be used to analyze the  $\mathbf{p}_i$  node in Figure 2.11. The equilibrium equation for the case where there are

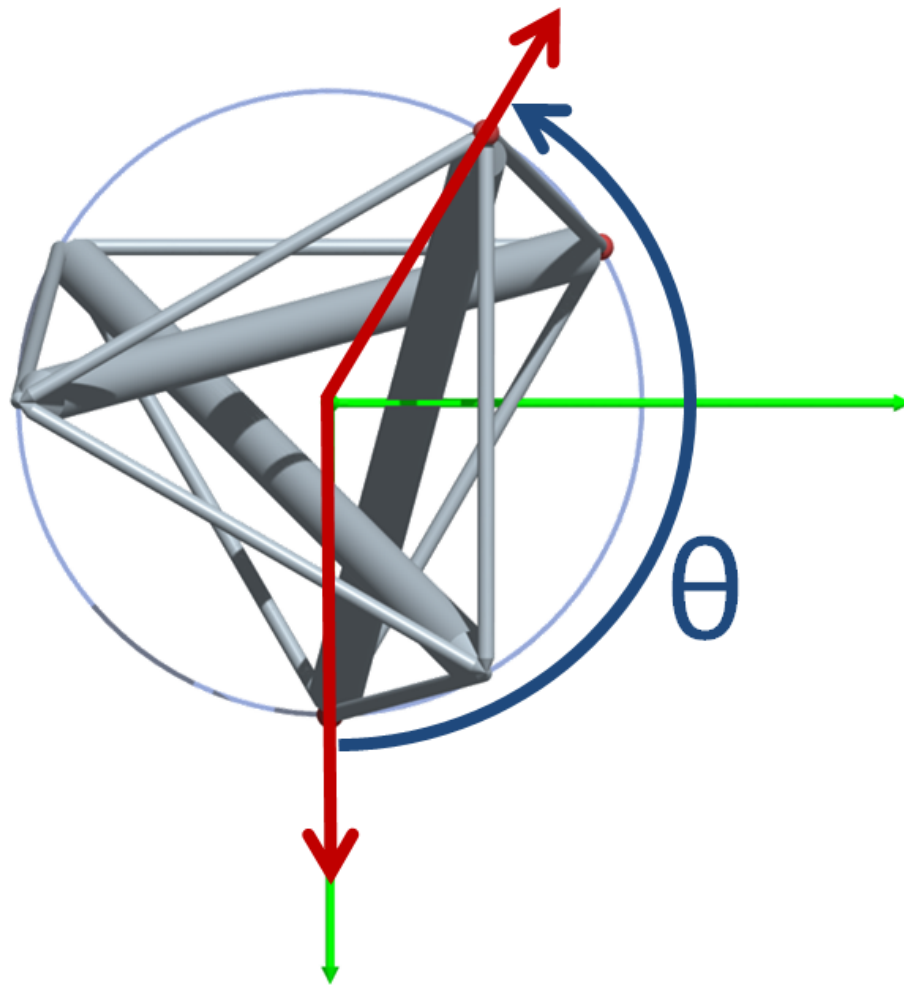


**Figure 2.10: *Angle of Twist*:** The angle of twist is the angle the top or bottom polygon must be rotated in order to line up with each other. For the Harmony topology this angle is  $150^\circ$  regardless of the lengths of the elements.

no external loads is [20]:

$$\sum_l \omega_{l,i}(\mathbf{p}_l - \mathbf{p}_i) = 0, \quad (2.28)$$

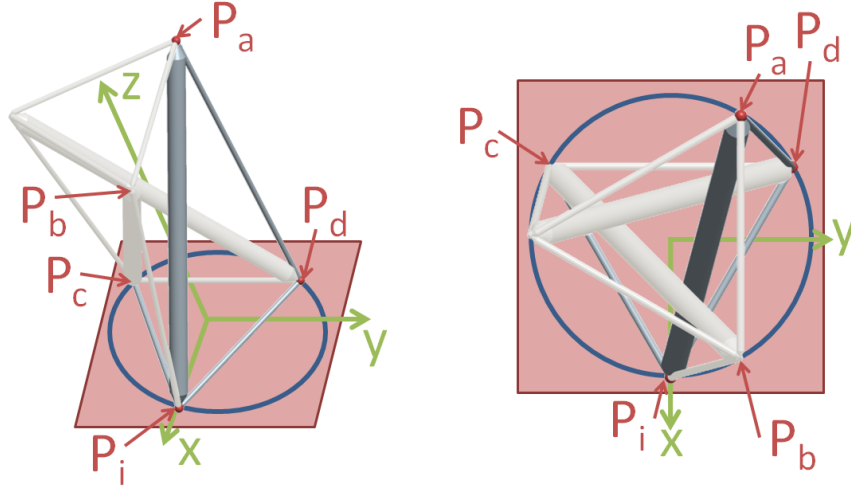


**Figure 2.11: Single Node Equilibrium:** The equilibrium of only one node must be analyzed due to the symmetry of prismatic tensegrity structures. Each node connected to the selected node  $\mathbf{p}_i$  is given an arbitrary label.

where  $l$  is equal to  $a$ ,  $b$ ,  $c$ , or  $d$  for prismatic tensegrity structures (Figure 2.11). The coordinates for the five nodes are [2]:

$$\begin{aligned}
 p_i &= [0, r, 0], \\
 p_a &= [r \sin(\theta), r \cos(\theta), h], \\
 p_b &= \left[ r \sin\left(\theta + \frac{2\pi j}{n}\right), r \cos\left(\theta + \frac{2\pi j}{n}\right), h \right], \\
 p_c &= \left[ r \sin\left(\frac{2\pi k}{n}\right), r \cos\left(\frac{2\pi k}{n}\right), 0 \right] \\
 p_d &= \left[ -r \sin\left(\frac{2\pi k}{n}\right), r \cos\left(\frac{2\pi k}{n}\right), 0 \right],
 \end{aligned} \tag{2.29}$$

where  $r$  is the radius of the circle passing through the nodes in the upper or lower plane and  $h$  is the distance between the upper and lower plane. Using the  $z$  coordinates and the equilibrium equation about node  $i$  [20]:

$$\begin{aligned}
 \omega_{i,a}(p_a - p_i) + \omega_{i,b}(p_b - p_i) + \omega_{i,c}(p_c - p_i) + \omega_{i,d}(p_d - p_i) &= 0, \\
 \omega_{i,a}(h - 0) + \omega_{i,b}(h - 0) + \omega_{i,c}(0 - 0) + \omega_{i,d}(0 - 0) &= 0, \\
 h\omega_{i,a} + h\omega_{i,b} &= 0.
 \end{aligned} \tag{2.30}$$



Since  $h$  cannot equal zero:

$$\omega_{i,a} + \omega_{i,b} = 0, \quad (2.31)$$

$$\omega_{i,a} = -\omega_{i,b}.$$

Finally, a similar analysis of the  $x$  and  $y$  coordinates reveals that  $\omega_{i,c} = \omega_{i,d}$ . Using the  $x$  coordinates of the nodes (Equation (2.29)) and Equation (2.31) the twist angle  $\theta$  can be determined [20]:

$$\begin{aligned} \omega_{i,a} [r \sin(\theta) - 0] + \omega_{i,b} \left[ r \sin\left(\theta + \frac{2\pi j}{2}\right) - 0 \right] + \omega_{i,c} \left[ r \sin\left(\frac{2\pi k}{2}\right) - 0 \right] + \omega_{i,d} \left[ -r \sin\left(\frac{2\pi k}{2}\right) - 0 \right] &= 0, \\ r\omega_{i,a} \sin(\theta) - r\omega_{i,a} \sin\left(\theta + \frac{2\pi j}{2}\right) &= 0, \\ r\omega_{i,a} \left[ \sin(\theta) - \sin\left(\theta + \frac{2\pi j}{2}\right) \right] &= 0. \end{aligned} \quad (2.32)$$

Both  $r$  and  $\omega_{i,a}$  cannot simultaneously equal zero because the resulting structure would be trivial, and unstable, respectively (ie. not a strict proper stress) allowing Equation (2.32) to be reduced to:

$$\sin(\theta) - \sin\left(\theta + \frac{2\pi j}{2}\right) = 0. \quad (2.33)$$

Assuming  $\theta$  is between 0 and  $2\pi$ :

$$\begin{aligned} \theta + \left(\theta + \frac{2\pi j}{2}\right) &= \pi, \\ 2\theta &= \pi - \left(\frac{2\pi j}{2}\right), \\ \theta &= \pi \left(\frac{1}{2} - \frac{j}{2}\right). \end{aligned} \quad (2.34)$$

By construction, Equation (2.34) forces the stresses in the tensegrity elements to be symmetric, strict, and proper self stresses. Connelly [20] has shown that for prismatic tensegrity structures, this stress state implies that the stress matrix  $\mathbf{\Omega}$  is positive semi-definite with a nullity of four. This positive semi-definiteness in turn implies that only  $\theta$  (expressed by Equation (2.34)) will result in a super stable structure. Equation (2.34) also proves that the angle of twist will be constant for prismatic tensegrity structures, regardless of the lengths of the elements, as long as the connectivity term  $j$  and the the number

of struts  $\frac{n}{2}$  are constant. Therefore, Equation (2.34) is a geometric constraint for this class of structure and will be used to reduce the solution space produced by the geometric intersection form finding method proposed in this thesis.

## 2.4 Summary

Figure 2.12 depicts the hierarchy of the rigidity and stability definitions presented in this chapter [18]. This diagram has been modified from the diagram presented in Tur [18], which was an expansion of the diagram presented by Connelly and Whiteley in [25]. In both these sources the diagram had the most restrictive definition for rigidity and stability at the bottom and the most inclusive definitions at the top. Reversing this order (as was done in Figure 2.12) is clearer because the larger boxes enclose the smaller boxes that contain the definitions that are implied by the definitions of the larger boxes. For example, several of the authors reported in this section [19], [21], [27], have shown that pre-stress stability implies that the configuration is also second-order rigid and generally rigid (Figure 2.13a). Super stability implies global rigidity and pre-stress stability. Hence the structure is also second-order rigid and generally rigid (Figure 2.13b) [18]. Finally an infinitesimally rigid structure is also pre-stress stable and consequently second-order and generally rigid [18] (Figure 2.13c). These relationships are not generally reversible therefore the rearrangement of Figure 2.12 is justified because a larger box cannot fit within a smaller box. For example, a super stable structure is not necessarily first-order rigid, but a first-order rigid structure is always super stable [18].

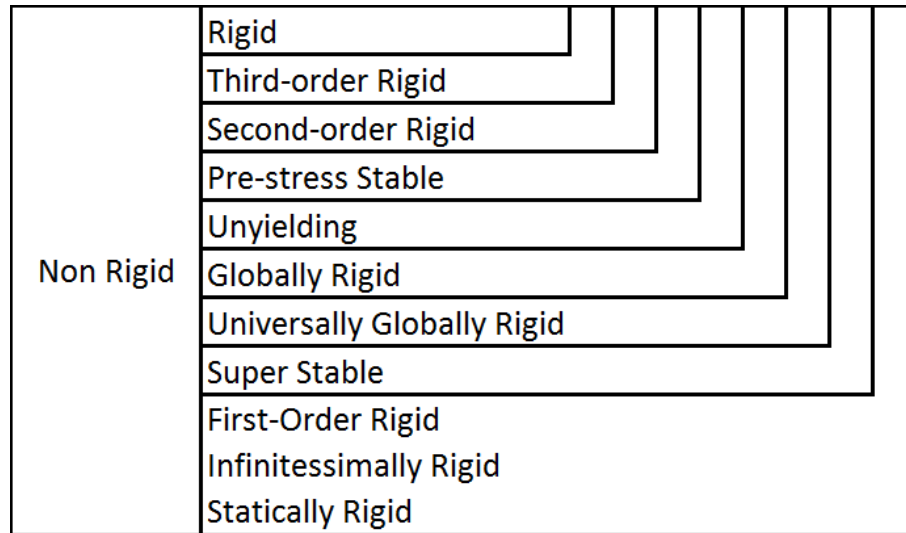


**Figure 2.12: *The Stability Hierarchy*:**The relationship between the rigidity and stability classifications with the most inclusive classifications at the bottom and the most restrictive at the top [18].

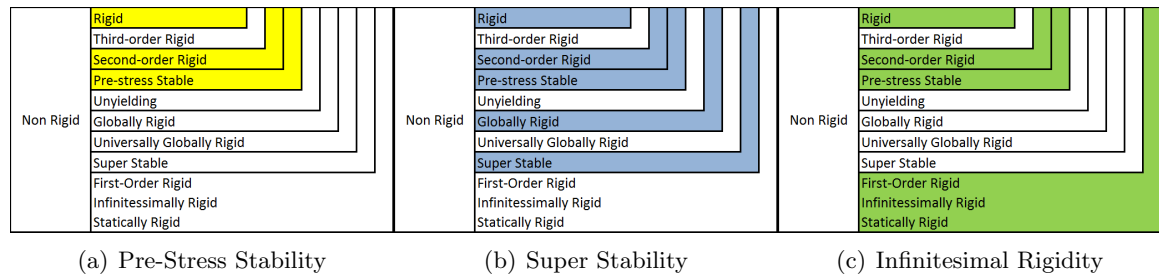


**Figure 2.13: *Rigidity Hierarchy Examples*:** (a) Pre-stress stability implies second-order rigidity and rigidity. (b) Super stability implies global rigidity and pre-stress stability. (c) Infinitesimal rigidity implies pre-stress stability [18].

Using these definitions it can be shown that prismatic tensegrity structures are never infinitesimally rigid [27], but can be pre-stress stable if the element stresses have the correct sign and magnitude. They are also super stable if these stresses are symmetric [20]. Connolly [20] proved that the only way a prismatic tensegrity structure can be rigid and stable is if it meets the super stability requirements. He went on to prove that prismatic tensegrity structures must have a specific twist angle between their upper and lower polygons in order to satisfy the super stability criterion. This twist angle will be used in the geometric intersection form finding method presented in this thesis to reduce the

solution space of the form finding problem.

The form finding problem involves both determining the location and inter-connectivity of the nodes in a tensegrity system, as well as verifying that the generated arrangement meets one or several of the rigidity and stability criteria presented in this chapter. The next chapter will give a brief description of the form finding methods that have been used to analyze and generate tensegrity systems to date.

## Chapter 3

# Literature Review of the Form Finding Problem

### 3.1 The Form Finding Problem

The early tensegrity form finding methods were based on geometry and the intuition of the designer. The goal of these methods was to calculate stable tensegrity arrangements using a set number of elements (Fuller [28] and Emmerich [29]). Initially, designers used physical models and achieved stable arrangements by adjusting the cable lengths of their tensegrity structures until all cables were in tension and all struts were in compression. The mathematical analogue of this process was eventually modelled; however some of the structures predicted by the models were unstable, which prompted the development of stability criteria [18]. Although the stability criteria allowed the designer to identify usable tensegrity configurations, the basic problem of finding the spacial arrangement of the tensegrity nodes remained. The problem of locating these nodes and determining the stability of a tensegrity system is called the form finding problem, and it stems from the fact that non-linear equations define the feasibility region of a stable tensegrity configuration.

Most tensegrity systems are underdetermined because the equilibrium equations do not have a unique solution for the location of the tensegrity nodes [3]. The equilibrium equation is [18]:

$$R(\mathbf{p})^T \frac{T_i}{d_i} = \mathbf{F}_{ext} \quad (3.1)$$

where  $i = 1 \dots \text{number of elements}$ .  $R(\mathbf{p})$  is a graph of the edge lengths of the tensegrity

system,  $d$  is an array of the edge lengths, and  $T$  is an array of the forces in each of the elements. All of these terms are dependent on both  $p_i$  and  $p_j$  (the two end points of the element), which makes Equation (3.1) non-linear. Equation (3.1) has no general solution so it is possible to generate configurations that cannot physically exist. These degenerate configurations include: trivial configurations (such as when all nodes lie on the same point) intersecting configurations, and unstable configurations (such as prismatic tensegrity structures with a non  $\theta$  angle of twist).

The form finding problem involves finding a non trivial, real, and stable tensegrity arrangement. In 2003 Tibert and Pellegrino [2] published a review of form finding methods and categorized them as either *kinematic* or *static* form finding methods. The *kinematic* form finding methods emulate the physical approach, where either the strut lengths (or cable lengths) are held constant while the cables (or struts) are shortened (or lengthened). The *static* methods use relationships between the equilibrium states of a tensegrity topology and the forces within the elements of the topology to establish the locations of the topology's nodes. Both categories of form finding methods are used to find equilibrium configurations in which the resulting tensegrity structure is in a state of prestress, which ensures the stability of the configuration. In 2007 Tur and Juan [18] expanded the catalogue of form finding methods to include more advanced *kinematic* and *static* methods as well as a new category of methods which solve for the prestress, geometry, and topology of the tensegrity structure simultaneously. One of these new *simultaneous* methods is the genetic algorithm method. Since the 2007 survey [18] the genetic algorithm method has been expanded by Rieffel [30] and a finite element method has been proposed by Pagitz [31].

The following sections give a brief description of the *kinematic*, *static*, and *simultaneous* methods along with their relative merits. This chapter concludes with a table summarizing the characteristics of the form finding methods, an explanation of the table itself, and a description of desirable characteristics a more designer friendly form finding method should have.

## 3.2 Kinematic Form Finding Methods

### 3.2.1 Analytical Method

The analytical method originally presented by Connelly and Terrell [20] and further explained in Tibert and Pellegrino [2] and Tur [18], can be used to analyze symmetric tensegrity topologies such as the three strut, nine cable Harmony tensegrity topology. Connelly and Terrell's analytical method calculates the coordinates of all the nodes in the tensegrity system based on the height, radius, and angle of twist of the system. Tibert and Pellegrino use these coordinates to create equations for the length of the elements (based on the distance between two nodes). This second approach is more desirable for the control of tensegrity mechanisms because the input variables will be the element lengths not the radius and height of the mechanism. Unfortunately this second approach will fail without warning when mathematical singularities occur. For example, the length of a strut in the harmony topology is given by the distance between its two end coordinates. The end coordinates are given by Connelly's approach as:

$$\begin{aligned} p_i &= [0, r, 0], \\ p_a &= [r \sin(\theta), r \cos(\theta), h]. \end{aligned} \tag{3.2}$$

Tibert uses the magnitude equation to determine the distance between the two end nodes:

$$l_s = \sqrt{2r^2(1 - \cos \theta) + h^2}. \tag{3.3}$$

Equation (3.3) will be imaginary when the sum of the terms under the square root become negative, resulting in degenerate configurations.

These approaches become too cumbersome to use in unsymmetric tensegrity structures because it becomes increasingly difficult to determine the geometric equations that relate the nodes. Connelly's approach will always have a real solution, but it cannot be rearranged in terms of the element lengths. Tibert's approach *is* in terms of the element lengths, but the designer can select lengths that result in non-real, or degenerate configurations. One of the most limiting aspects of the analytical method is the difficulty in solving the

form finding problem if multiple cable lengths are desired, such as in tapered prismatic tensegrity structures (where the upper and lower end cables have different lengths). Finally, the analytical method is based on vector analysis and yields little insight into the solution space of the form finding problem.

### 3.2.2 Non-Linear Constrained Minimization Method

A similar method was proposed by Pellegrino [2] and Burkhardt [32], [18], but instead of using the angle of twist and maximizing the strut length, a cable/strut length ratio (Pellegrino [2]), or target length value (Burkhardt [32]) is chosen and then optimized, for the maximum strut length. The optimization problem involves minimizing a non-linear function of multiple variables while satisfying an equivalent number of constraints, until a target range is reached. For the form finding method, the non-linear function describes the length of a single element and the constraints describe the length of every other element in the tensegrity structure [32]. This method can easily be implemented in conventional minimization algorithms found in software packages such as Mathcad.

This numerical method yields approximate results compared to the above analytical method and the more elements used to make up the structure, the greater the error between the two methods. This method requires an initial knowledge of the tensegrity topology and an initial guess at the element lengths which make up the structure. The method also requires the designer to select different length ratios between the struts (Pellegrino [2]) or strut length targets (Burkhardt [32]) in order to find the final tensegrity configuration. It is very difficult to specify multiple cable or strut lengths with this method because the problem becomes a multivariable minimization problem that will drift from the target lengths. This limits the applicability of this method, especially where tensegrity mechanisms are concerned. A preferred method would allow the designer to specify the number of elements and a constraining surface from which a family of tensegrity structures could be generated.



### 3.2.3 Dynamic Relaxation Method

The dynamic relaxation method proposed by Motro and Belkacem [2], [18] seeks to minimize the kinetic energy of a given tensegrity configuration. The elements in the structure are given constitutive relationships which relate the axial force in each element to the small axial deformation of each element. These equations are used to calculate the forces at each node. These forces are then used in the kinematic equation of the nodes to determine the acceleration of the nodes, and hence the relative unbalance between the nodes from the force distribution. The kinematic equation is then integrated to determine the location of each node. This process is repeated and the kinetic energy is monitored at every iteration. When the kinetic energy reaches a minimum the velocities are set to zero and the procedure is repeated from this configuration. This procedure is repeated until the peak kinetic energy reaches a minimum. A tensegrity topology can be evaluated by holding the length of some elements fixed and extending the rest until a pre-stress state is developed in the system. The topology can then be analyzed using the above method.

This method is best suited for topologies with fewer nodes. The method becomes more cumbersome when multiple cable/strut ratios are specified by the designer. Finally, the designer must specify these cable/strut ratios before the problem can be solved, which means that the designer must use trial and error to arrive at a configuration with the desired cable or strut length.

## 3.3 Static Form Finding Methods

### 3.3.1 Analytical Method

The first of the *static* methods was originally proposed by Connelly and Terrell [20]. It is an analytical solution that uses the force density within the tensegrity elements and equilibrium equations to determine the pre-stress stable state of rotationally symmetric tensegrities. The method yields the same equation for the optimum pre-stress angle of twist as the *kinematic* analytical method. Once the angle of twist is determined the overall

geometry can be found using the same equations outlined in *kinematic* analytical method. This method ensures the stability of the unloaded structure, but has the same drawbacks as the kinematic analytical method (Section 3.2).

### 3.3.2 Force Density Method

The force density method was originally proposed by Schek [33] and Linkwitz [34] for modeling cable net structures, but was later adapted for tensegrity structures by Vassart and Motro [35]. The stress matrix is always positive definite for cable nets and positive semi-definite for tensegrity structures [2]. This rank deficiency for tensegrity structures is the result of the struts which must have negative stress values (in cable structures all stresses must be positive, resulting in stress matrices that are always invertible, and hence positive definite). These negative force densities create null columns within the stress matrix, thereby reducing its rank. In Chapter 2 it was stated that the stability of the tensegrity arrangement was dependent on a stress matrix nullity of three and four for two and three dimensional space respectively [20]. This nullity ensures that non stable form finding solutions are eliminated by the null space of the stress matrix, leaving only stable configurations. The force density method seeks these stable solutions by solving for a set of force densities and the resulting configuration of the tensegrity. This method replaces the nonlinear node equilibrium equations (Equation (3.1)) with linear terms derived from the force densities of the elements:

$$R(\mathbf{p})\mathbf{q} = \mathbf{F}_{ext}. \quad (3.4)$$

The force densities ( $\mathbf{q}$ ) must be specified before the form finding process can begin. The force densities are combined with the connectivity matrix, to create the force density matrix. This matrix is used in the equilibrium equation to solve for the location of the topology's nodes. Generating the connectivity matrix is a non trivial exercise that can involve intuitive, iterative, or analytical methods. The intuitive method is based on the experience of the designer and is best for finding known tensegrity topologies with

relatively few elements, and a high degree of symmetry. The iterative method is a trial and error method which can be used for more complex tensegrity topologies, but takes an indeterminate amount of time to arrive at a solution. The analytical method is based on Gaussian elimination of the equilibrium matrix, which is used to determine the relationship between the force densities. Using Gaussian elimination limits the complexity of the tensegrity system because the more complex the tensegrity system the greater the number of variables that must be symbolically manipulated.

It is difficult to control the length of the elements and the overall shape of the tensegrity structure using the force density method. This is because the lengths of the tensegrity elements are embedded in the force density values and the designer can only manipulate the force densities, not the lengths directly. For example the input into the force density method is an array of force densities:

$$\mathbf{q} = \left[ \frac{T_1}{d_1}, \frac{T_2}{d_2}, \dots, \frac{T_n}{d_n} \right], \quad (3.5)$$

where  $d$  represents the element length of an element and  $T$  represents the force in an element. Only the ratio  $\frac{T}{d}$  can be specified because the length of any one element is dependent on the length of all the other elements in the system (Equation (3.4)). This difficulty also makes the force density method less desirable when creating a tensegrity system with prescribed cable or strut lengths. The only restriction on the force densities is that they must satisfy the super stability criterion from Chapter 2, which implies that they must all be non zero and negative for compression elements and positive for tension elements.

### 3.3.3 Modified Force Density Methods

#### Adapted Force Density Method

Zhang and Ohsaki [36] used an adapted numerical method in place of the analytical method proposed by Vassart and Motro [35] to find stable configurations with the force density method. Vassart and Motro's [35] analytical method used Gaussian elimination of the

equilibrium matrix to determine the relationship between the force densities that satisfies the stability conditions outlined in Connelly [20]. This method limits the complexity of the topology which can be analyzed because the force densities are analyzed in symbolic form and additional elements or elements of varying geometry increase the number of variable that must be manipulated. The adaptive force density method proposed by Zhang and Ohsaki [36] employs eigenvalue analysis and spectral decomposition to iteratively solve for stable configurations based on user defined initial guesses for the force densities. This adapted numerical method allows more complex topologies to be analyzed by manipulating the force densities, but the designer again loses direct control over the element lengths.

The force density method and the adapted method require the user to specify force densities for every sub element of the tensegrity structure; however the user is not likely to know the optimum length of these elements or the load they will experience. The initial guess at the force densities must therefore be made arbitrarily, based on the users experience, or using numerical methods. There is also little control over the geometrical and mechanical properties of the resulting tensegrity structure because of the design variables (the force densities) the user is given to manipulate. Finally the method requires several iterations to find a non degenerate configuration of the structure and becomes increasingly cumbersome as the complexity of the tensegrity system increases.

### **Adding Surface Constraints**

In [37], Masic and Skelton extend the force density method by including surface constraints with the conventional equilibrium equations to solve the form finding problem. Symmetry of tensegrity topologies is used to simplify the form finding problem wherever possible. Within the force density method, constraints can be imposed on the nodes, or the cable and strut lengths. Also a shell shape constraint can be used to force all nodes to lie on the surface of the shell. The authors used a cylinder shell as a shape constraint on a Harmony tensegrity topology as an example. They proceeded to use a tapered cylinder shell and a planar constraint surface in conjunction with the force density method to solve the form finding problem.

The examples in [37] require parameters that the designer is not likely to know beforehand, such as the height of the final structure. Even though this method provides the designer with more control over the final shape of the tensegrity system it still relies on the force density method and numerical evaluation. The numerical evaluation requires several iterations to solve even the simplest form finding problem. While this method is not computationally intensive for highly symmetric topologies, it would be challenging to implement in a real time environment, such as part of a sensor package or as part of a tensegrity mechanism control loop.

### 3.3.4 Energy Method

The Energy Method was originally proposed by Connelly in [38]. It uses stress instead of force density to linearize the equilibrium equations. An energy function is created using the stress state at each node. This energy function is then minimized to find a stable configuration. Schek [33] was able to show that the energy and force density methods are equivalent. The stress matrix is identical to the force density matrix and minimizing the energy function is equivalent to finding the positive semi-definiteness of the force density matrix [18]. The later equality amounts to determining the stability of the system, both by finding the minimum energy configuration and by finding the configuration that results in the stress matrix with the correct stresses respectively. Therefore the two methods have similar advantages and disadvantages.

### 3.3.5 Coordinate Reduction Method

The reduced coordinate method was proposed by Sultan *et al.* in 1999 [39]. In this method a set of generalized coordinates is used to describe the configuration of the structure. The number of coordinates can be reduced by exploiting symmetry. Virtual work is used to determine the forces in the cables without determining the forces in the struts. Only solutions where the cables are in tension are considered, which reduces the form finding problem to the simpler problem of determining the lengths of the cables in terms of the

generalized coordinates. The length of the cables are expressed in terms of the generalized coordinates and then these equations are differentiated to obtain a square equilibrium matrix which represents the equilibrium condition of the topology. By specifying more constraint equations, such as surface constraints, and the rank of the equilibrium matrix; the designer can create a series of simpler, lower dimensional equations that can potentially be solved analytically. These equations can then be used to determine the overall geometry of the structure.

This method requires a great deal of symbolic manipulation of the generalized coordinates in order to obtain the simplified equilibrium matrix. This requires a substantial amount of user input, or computation time depending on the complexity of the structure. This method is usually used to modify or optimize highly symmetric structures, which have previously been reduced to a few design variables using the coordinate reduction method and constraint surfaces.

## 3.4 Simultaneous Methods

### 3.4.1 Axial Force Compatibility Method

Architectural applications require the direction and location of structural elements to be specified. Engineering applications require the member forces to be controlled. A method proposed by Zhang *et al.* [3] allows the designer to control both the element locations and forces simultaneously, to varying extents. A directed graph combined with a constraint matrix and an axial force matrix is used to linearize the equilibrium equations in terms of the element force vectors. This method for generating the linear equilibrium matrix is similar to that used in the force density method.

The designer must specify the location of two or more nodes (support locations) for 2D tensegrities and three or more support nodes for 3D tensegrities. The support node locations are specified in the directed graph as imaginary fixed members that connect

each support. The fixed members turn the tensegrity structure into a self-equilibrium system. Then the designer must specify any desired symmetry constraints as well as the direction of some of the elements. The designer then uses an algorithm that searches the equilibrium modes of the constrained linearized equilibrium equations for stable tensegrity arrangements. This algorithm eventually yields the location of all nodes in the structure. Finally the fixed members are removed converting the fixed nodes back into support nodes and transforming the self-equilibrium structure into a self-stressed tensegrity structure.

The number of free variables the designer has access to are dictated by the rank of the constrained linearized equilibrium matrix. If this matrix has rank  $x$  then there are  $x$  axial forces to be defined. The rank of a slightly modified linearized equilibrium matrix dictates the number of nodes that the designer is free to manipulate in addition to the already fixed support nodes. The number of free variables can be reduced by specify more constraints.

The major advantage of this method is that it allows the designer to manipulate some of the axial forces and some of the locations of the elements simultaneously. Constraints can also be used to modify the structure. Unfortunately the algorithm used in this method computes the independent variables consecutively. This sequential computation makes it difficult to specify which members are in tension and which members are in compression, because the equilibrium state is not known until the algorithm has located all nodes. Not knowing the equilibrium state can also lead to infeasible structures such as structures with intersecting nodes or intersecting elements. Furthermore, most tensegrity structures have a large number of free variables that must be either defined or reduced by adding constraints. This may present the designer with an overly complicated or restricted solution space.

### **3.4.2 Differential Equation Method**

A more advanced kinematic form finding method was recently proposed by Micheletti and Williams [40], where a system of differential equations are used to simultaneously solve for the locations of the tensegrity elements and their stresses. For any tensegrity

structure there are a manifold of stable configurations which can be represented by a set of differential equations that relate the nodal coordinates to the lengths of the elements. This method allows the designer to modify the tensegrity structure by changing the length of one or more of its edges. When an edge length is changed the system of differential equations updates the lengths of the other elements conforming to stable paths on the tensegrity manifold. This manifold constraint ensures that the tensegrity structure remains stable while an edge length is manipulated. This kinematic stability allows the designer to create stable, collapsible or foldable tensegrity structures.

This method could be improved by adding geometric constraints to aid the designer in achieving a specific final configuration. This method is limited to structures with one instance of self stress. This limitation allows only one edge length to be modified at a time and restricts the possible stable paths the edge can take from one configuration to another. While this method gives more control over an element length and more insight into the form finding process, the characterization of the stability manifold can be quite involved especially for larger structures with many elements.

### 3.4.3 Genetic Algorithm Methods

Paul *et al.* [41] and Rieffel *et al.* [30] used genetic algorithms to generate stable tensegrities without specifying a base topology. They created a seed tensegrity structure that adhered to the definition of a tensegrity structure; namely that every node must have at least three cables and that no two struts share a common node. The Paul *et al.* genetic algorithm was programmed to vary the element to element connections in steps creating a series of new topologies, while the Rieffel *et al.* genetic algorithm used Lindenmeyer System (L-system) evolution rules. The residual forces in the elements were then computed to determine how close the configuration was to an equilibrium state. The nodes were then perturbed slightly until the residual forces were lower than a pre-set threshold. This relaxation algorithm sometimes caused the topologies to collapse. Collapsed structures were then removed



from the gene pool. At this point a random search for stable tensegrities could be conducted. A more focused search was performed by selecting a fitness criteria. The authors chose to use the maximum volume enclosed by the struts as their fitness criterion. This criterion allowed the authors to perform an evolutionary search for optimum configurations.

The strengths of these methods are that no topology is specified before the form finding process begins, allowing the computer to create completely new topologies independent of human bias. Also, the more elements the seed structure has the easier it is to find stable configurations, and irregular tensegrity configurations can be found more quickly than conventional methods. The weaknesses of this method are that for seed structures with fewer struts it becomes difficult to find optimum solutions using an evolutionary search due to the restricted solution space. Under these conditions it becomes necessary to revert to the random search method. Also, the designer has no direct control over the shape of the structure. The designer can only indirectly control the shape of the structure by specifying evolutionary criteria.

#### 3.4.4 Sequential Quadratic Programming Method

This method was proposed by Masic *et al.* [42] and uses non-linear, sequential quadratic programming to calculate an optimum equilibrium state under external loading conditions (including the case where there are no external loads), and designer imposed constraints. Unlike the force density method, which linearizes the equilibrium equations using the force densities, this method works with the non-linear equilibrium equations (along with several constraints) to arrive at stable tensegrity arrangements. The method begins by selecting a base topology that is optimized by altering the node locations and element connectivity. The optimum topology is found for a given set of external loads using structural strength constraints, constraint surfaces, and buckling constraints.

This method differs from most historical form finding methods because it uses external

loads, and because it solves the non-linear equilibrium problem directly using a numerical optimization method. The result is a tensegrity configuration that conforms to the designer's constraints, and is optimized to carry the desired external load without yielding or buckling. Unfortunately this method is computationally intensive, and the designer does not have direct control over the topology. This method may also calculate a local optimum solution instead of the global optimum solution. This possibility forces the designer to try different input configurations or constraints to determine if the calculated solution is the global optimum within the solution space of the form finding problem.

### 3.4.5 Iterative Numerical Method

This numerical method was proposed by Estrada *et al.* [43] and it iteratively calculates the force densities and equilibrium geometry once the designer specifies the connectivity of the nodes, and which members are in tension and which members are in compression. The seed coordinates of the nodes are calculated from the Schur decomposition of the force density matrix. The decomposition of the equilibrium matrix and the seed coordinates are used to generate the initial tension coefficients. The tension coefficients and seed coordinates are used to calculate the state of stress within the structure. This process repeats until a state of one self stress is achieved and the potential energy and element lengths are minimized. While the calculated geometry satisfies the stability criteria, the solution is one of many possible stable configurations for the structure.

This method can rapidly calculate stable tensegrity configurations without requiring the designer to predefine symmetry constraints, element lengths, or force densities. It also seeks out the configuration with the lowest potential energy, which corresponds to an optimum stable configuration. However, the lack of constraints and designer input also make the process difficult to control. It is possible, but not stated, that the element lengths and constraints could be imposed on this method to guide the form finding process. Finally, the numerical nature of this method requires several iterations to arrive at a stable configuration.

### 3.4.6 Finite Element Method

The finite element method was proposed by Pagitz and Tur [31] and it models the struts and cables of a tensegrity structure as two-node bar finite elements. The designer must specify the topology, the undeformed bar lengths and stiffnesses, the total length of all cables, and the cable prestresses before the form finding process can begin. The finite element method assumes that the largest amount of potential energy within the tensegrity structure is developed by the change in length of the strut elements. This assumption allows the method to maintain the total cable length, while the cable length ratios and the strut lengths are changed by a preset constant length increment and the finite difference method. This process continues until the potential energy of the system reaches a minimum.

This method can simultaneously calculate the force densities and configuration of the tensegrity structure. However, it requires the designer to specify many aspects of the tensegrity structure before the form finding process can begin. The method can also fail if the change in length of the elements is too great between iterations. The method requires a number of iterations to arrive at an optimum configuration, and this configuration is often identical to the symmetric configuration for the specified topology.

### 3.5 Form Finding Method Summary

The characteristics of the above methods are outlined in Table 3.1, which is explained in the following sections.

Method	Ref.	Class	Type	Element Length Control	Uses Symmetry	Constraint Surfaces	Comp. Complexity
Analytical	Connelly [20]	Kinematic	Analytical	Limited	Yes	No	Low
Non-Linear Constrained Minimization	Pellegrino [2], Burkhardt [32]	Kinematic	Numerical	Limited	No	No	Low
Dynamic Relaxation	Motro and Belkacem [2] [18]	Kinematic	Numerical	Limited	No	No	Mod.
Analytical	Connelly and Terrell [20]	Static	Analytical Iterative Intuitive	Limited	Yes	No	Low
Force Density	Schek <i>et al.</i> [33] [34] [35]	Static	Analytical	No	Yes	No	Mod.
Adaptive Force Density	Zhang and Ohsaki [3]	Static	Numerical	No	No	No	Mod.
Surface Constraints	Masic and Skelton [37]	Static	Numerical	No	Yes	Yes	Mod.
Energy	Connelly [38]	Static	Numerical	No	No	No	Mod.
Coordinate Reduction	Sultan <i>et al.</i> [39]	Static	Analytical	Limited	Yes	Yes	High
Axial Force Compatibility	Zhang <i>et al.</i> [36]	Simultaneous	Numerical	fill in	No	No	High
Differential Equation	Micheletti and Williams [40]	Simultaneous	Numerical	fill in	No	No	Mod.
Genetic Algorithm	Paul <i>et al.</i> [41] and Rieffel <i>et al.</i> [30]	Simultaneous	Numerical	No	No	No	High
Sequential Quadratic Programming	Masic <i>et al.</i> [42]	Simultaneous	Numerical	No	No	Yes	High
Iterative Numerical	Estrada <i>et al.</i> [43]	Simultaneous	Numerical	No	No	No	Mod.
Finite Element	Pagitz and Tur [31]	Simultaneous	Numerical	Some	No	No	High

**Table 3.1: Summary:** Characteristics of historical form finding methods.

#### 3.5.1 Class

The *kinematic*, *static*, and *simultaneous* methods tend to have separate benefits and drawbacks. The *kinematic* methods mimic the physical tensegrity building process with

analytic and numeric analogues. Some element lengths are held constant while the rest are lengthened or shortened until a geometric constraint is satisfied. None of these methods use constraint surfaces to simplify the design process. These methods have largely been replaced by the *static* methods because the *static* methods can solve the form finding problem of more complex structures [18].

The *static* methods use the forces, the stresses, or the energy within the tensegrity elements to linearize the non-linear equilibrium equations for the tensegrity structure. The strength of these methods is that they can analyze more complex structures with more elements and less symmetry than the *kinematic* methods. Unfortunately this increased applicability comes at the cost of having direct control over the tensegrity element lengths, and increased programming complexity.

The *simultaneous* methods solve for the prestress, geometry, and topology of the tensegrity structure simultaneously. They include methods based on genetic algorithms, finite element analysis and other iterative methods. None of these methods require the tensegrity structure to be symmetric, but few employ constraint surfaces, and most restrict the control the designer has over the element lengths and the shape of the final structure. The major advantage of these methods is that most do not require an initial tensegrity topology. This means that new topologies can be generated based on the designer's selection constraints instead of the designers intuition or previous experience.

### 3.5.2 Type

Most of the form finding methods are numerical methods due to the indeterminate nature of the form finding problem. Numerical methods are also better suited to tensegrity structures that have many elements and little symmetry. For simpler structures with a high degree of symmetry and fewer elements, the analytical methods are preferred because they provide exact solutions. The analytical methods require extensive matrix manipulation to determine the relationship between elements in the equilibrium equations. The matrix

manipulation becomes much more difficult and time consuming for more complex tensegrity arrangements. However, analytical methods can be significantly faster than numerical methods if the designer wishes to modify an existing configuration.

### **3.5.3 Element Length Control**

The ability to control the element lengths directly is a highly desirable aspect of any form finding method, especially in the absence of constraint surfaces. This control is necessary in real world applications where attachment points must be selected and the volume the structure occupies is limited. Length control is also necessary to predict how a tensegrity mechanism will deform as element lengths are varied.

In Table 3.1, when a variety of cable and strut lengths are selectable (unsymmetrical tensegrities) within a form finding method, the ‘Element Length Control’ category receives the ‘Several’ designation. When a group of element lengths are controllable, such as all struts have one common length and all cables have another common length, this category receives a ‘Limited’ designation. When the length of the tensegrity elements are not directly controllable, such as in the dynamic relaxation and force density methods, this category receives a ‘No’ designation.

### **3.5.4 Employs Symmetry**

Symmetry in the context of tensegrity systems generally refers to rotational symmetry. Rotational symmetry allows the designer to determine the location of a few nodes in the structure and then extrapolate the location of the rest of the nodes using the symmetry planes of the structure. Highly symmetric tensegrity arrangements allow the designer to create tensegrity structures with almost any number of elements and are much more common in real world applications. Analytical methods often use symmetry to reduce the number of variables within the solution space, while most numerical methods exploit symmetry when necessary, but can also analyze unsymmetrical structures. The ability to analyze unsymmetrical structures usually comes at the price of computational time and

implementation complexity.

In Table 3.1, a form finding method receives a ‘Yes’ designation when the method requires symmetry to solve most practical applications. When a form finding method can be used to analyze both symmetric and unsymmetric tensegrity arrangements it receives a ‘No’ designation.

### 3.5.5 Constraint Surfaces

Constraint surfaces allow the designer to control the overall shape of the tensegrity structure at a higher, more intuitive level. Only a few methods were able to incorporate constraint surfaces and they were all fairly simple, regular surfaces such as planes, spherical shells, or cylindrical shells. The three methods which use constraint surfaces tended to be more computationally complex than the rest.

In Table 3.1, a form finding method receives a ‘Yes’ designation when the method explicitly uses constraint surfaces. When a form finding method does not use constraint surfaces it receives a ‘No’ designation.

### 3.5.6 Comp. Complexity

Computational complexity refers to the complexity of the form finding method algorithm. Form finding methods received a ‘Low’ ranking when the method could be reduced to a few analytical equations. Methods received a ‘Mod.’ or moderate ranking when their algorithms required multiple iterations (less than twenty iterations for methods in this category), or two to three sequential steps to arrive at a solution. Finally, methods received a ‘High’ ranking if they required several iterations (greater than twenty), and required multiple sequential steps to arrive at a solution. It should be noted that only the more computationally complex methods (Mod. to High) were capable of analyzing non-symmetric systems, and the low complexity methods were limited to highly symmetric systems.

### 3.5.7 Form Finding Insight

A method provides form finding insight when it predicts non valid geometric arrangements or provides an intuitive or visual depiction of the solution space of the form finding problem. While the stability criteria in most of the form finding methods will predict some degenerate configurations, this criteria is mainly used to determine the stability of the configuration and provides little insight into why a configuration is degenerate. None of the form finding methods provide a clear geometric or visual representation of the form finding process; however the *kinematic* methods do mimic the way tensegrity structures are built, making these methods a bit more intuitive.

## 3.6 Discussion

Of the fifteen form finding methods analyzed only a few were computationally simple. Very few allowed the designer to directly control the lengths of the tensegrity structure elements. Only a few of the methods exploited constraint surfaces, which would make the design process much more intuitive, controllable, and efficient. Many of the newer methods are computationally intensive and some, like the genetic algorithm, do not produce symmetric structures that are common in real world applications. None of the form finding methods provided much insight into the form finding solution space or process, although the *kinematic* methods replicate the techniques used to build real world tensegrity structures.

The body of literature evidently lacks a form finding method that simplifies the design process by incorporating constraint surfaces, and direct element length control. It would also be beneficial if a method could be devised that is computationally simple, and provided some insight into the form finding problem. Such a method would have applications in many real world design projects where tensegrity structures could be parameterized with intuitive variables, such as height and radius, instead of strut lengths and cable angles. The novel geometric intersection method presented in this thesis addresses some of the deficiencies identified in the previous body of knowledge.



## Chapter 4

# Geometric Intersection Method

The form finding methods identified in Chapter 3 all have various advantages and disadvantages, but none of these methods employ a geometric approach to make the form finding process more intuitive. A geometric form finding process is more intuitive because trivial, intersecting, or unstable configurations can be identified and interpreted more quickly visually. A geometry based method also simplifies the understanding of the control system for tensegrity mechanisms, because the response of the mechanism can be directly visualized. This visualization is extremely difficult with conventional methods because of their numeric or pure algebraic nature. Other possible ways to improve the intuitive nature of the form finding process include using constraint surfaces, and parameterizing the form finding problem in terms of the controlled inputs and global outputs. For example, it is preferable from a mechanism control perspective, if the inputs to the form finding problem are the controlled lengths of the elements, and the outputs are the global height and radius of the prismatic tensegrity system.

With these criteria in mind, a novel geometric method was developed based in part on the kinematic analytical method developed by Connelly in [20] (See Chapter 3). The geometric intersection method presented in this chapter retains all the benefits of Connelly's method, but with the added advantage of making the form finding process more intuitive. This improvement is achieved by using a geometric representation of the form finding problem, by using input and output parameters that are better suited to controlling

tensegrity mechanisms, and by employing geometric constraint surfaces. Unfortunately the geometric intersection method also retains some of the disadvantages of Connelly's method, most notably both are limited to the analysis of prismatic, symmetric tensegrity systems. This deficiency is not overly limiting due to the wide use of symmetric tensegrity structures and the inherent stability of the prismatic tensegrity topology.

The next section lists the assumptions used in both the geometric intersection and kinematic analytical methods, then the geometric intersection method will be presented. Tibert's interpretation of Connelly's kinematic analytical method will then be derived from the geometric intersection method to prove their analytical equivalence. Finally, this chapter will conclude with a discussion of the implementation of the geometric method in a hybrid Mathcad-ProEngineer model.

## 4.1 Assumptions

The following assumptions are used in both the kinematic analytical and geometric intersection methods:

1. only symmetric prismatic tensegrity systems are considered;
2. the number of struts is known;
3. the connectivity of the elements is known;
4. all nodes are modelled as spherical joints;
5. cables and struts maintain their lengths for each value of the input parameters (ie. they will not deform under load);
6. no external forces act on the structure, including body forces;
7. the structure is free standing, without any supports.

The first assumption is the primary limitation of both the geometric intersection and kinematic analytical methods. Both methods can only be used to analyze symmetric tensegrity structures such as the Harmony tensegrity structure in Figure 4.1. This assumption limits the ability of these methods to adequately model tensegrity mechanisms because real world tensegrity mechanism will have positioning errors, and consequently will not be exactly symmetric. The elements of a prismatic tensegrity system are grouped into

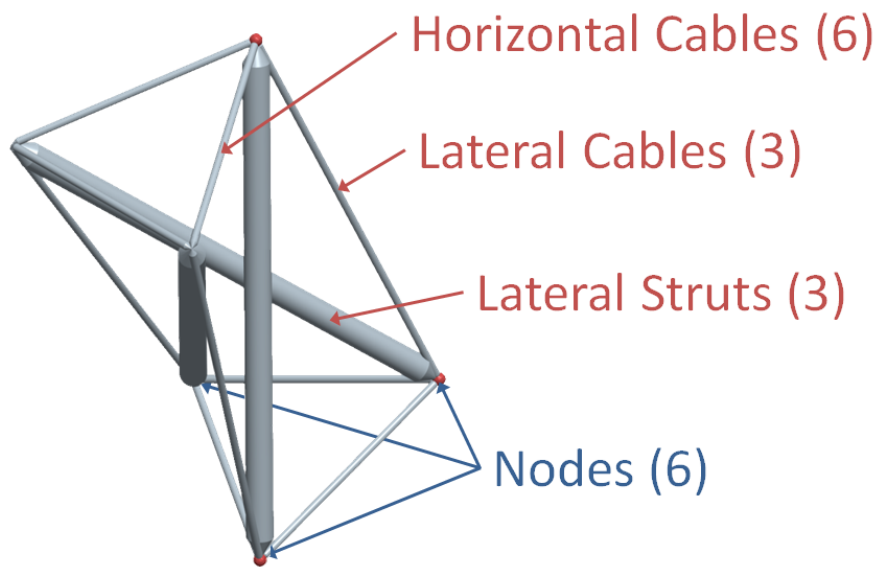


**Figure 4.1: Prismatic Tensegrity System Elements:** Prismatic tensegrity systems are characterized by their symmetry, and connectivity. Their symmetry results in three separate element categories: lateral cables, lateral struts, and horizontal or end cables. All elements in a category have the same length.

three categories (Connelly called them transitive element classes [20]): horizontal cables; lateral cables; and lateral struts. Assumptions two and three yield the parameters needed to define a unique topology as was discussed in Chapter 2. For example the Harmony tensegrity arrangement shown in Figure 4.1 has three struts ( $n_s = 3$ ), and has connectivity terms  $j = 1$  and  $k = 1$ . These parameters can be used to define the prismatic tensegrity graph of the structure ( $P_{n_s}(j, k) \rightarrow P_3(1, 1)$ ).

Assumption four is the result of the incompressibility of the cable elements. The cables are rigidly connected to the struts, but their incompressibility results in a large number of degrees of freedom, which can be modelled with spherical joints. This element of the models, as well as the length constraint in assumption five are only used in the stability analysis of the structure (see Chapter 2).

Assumptions six and seven simplify the analysis of the models by eliminating all external forces from the nodal equilibrium equations. This simplification has consequences for the stability of the structure, but is beyond the scope of the methods compared in this chapter. Assumptions five, six, and seven further limit the applicability of these methods to tensegrity mechanisms, and must be addressed before the dynamic motion of a tensegrity system can be modeled. While the above assumptions limit the applicability of the kinematic methods and the geometric intersection method, this first development can be used for the initial design of many tensegrity systems. Some proposals for removing some of these assumptions are discussed in Chapter 6.

## 4.2 Geometric Intersection Method Premise

The premise of the geometric intersection method is that any three prismatic tensegrity parameters can be calculated from the remaining parameters by finding the intersection points between two spheres and a circular cylinder. The cylinder has radius  $r$  and all tensegrity nodes lie on its surface. These nodes are divided into two groups. The upper nodes define the upper node plane, and the lower nodes define the lower node plane. The two node planes are parallel and the perpendicular distance between them is the height  $h$  of the tensegrity system (Figure 4.2). The nodes of the prismatic tensegrity system are labeled following the convention established by Connelly in [20]; however the coordinate system is selected to simplify the derivation of the geometric intersection method. Due to the symmetry of prismatic tensegrity systems, only the connections to one node  $p_i$  must be analyzed. The nodes are labeled in the following way, and are illustrated in Figure 4.3:

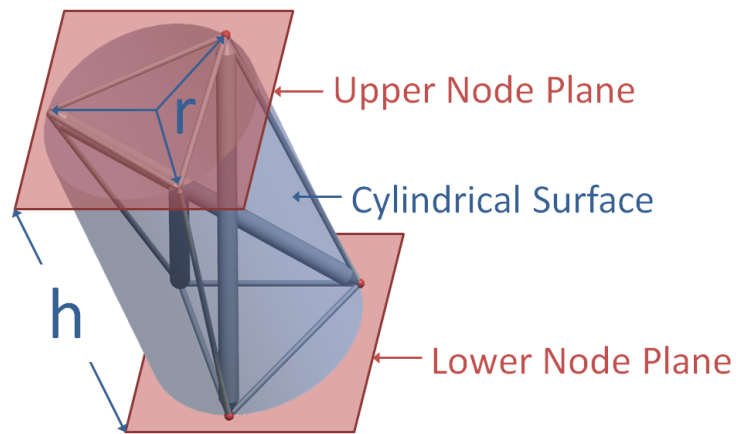


**Figure 4.2: Geometric Method Cylinder:** All the nodes of a prismatic tensegrity system lie on a circular cylinder of radius  $r$  and of height  $h$ . These nodes also make up the upper and lower node planes.

- the lateral strut, of length  $l_s$ , will connect nodes  $p_i$  and  $p_a$ ;
- the lateral cable, of length  $l_c$ , will connect nodes  $p_a$  and  $p_d$  (this is a slight departure from Tibert's notation [2] because he uses the equivalent length  $p_i$  to  $p_b$ );
- the horizontal cables, of length  $l_e$ , will connect nodes  $p_i$  and  $p_c$  (clockwise) and  $p_i$  and  $p_d$  (counterclockwise).

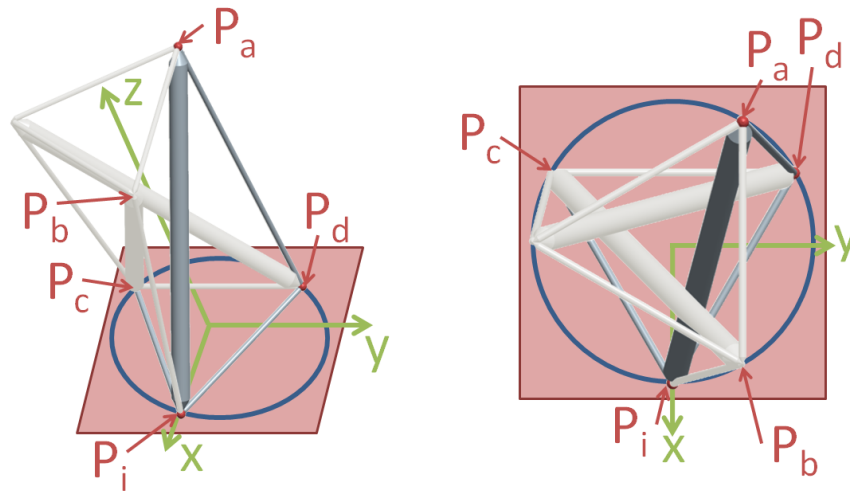


**Figure 4.3: Geometric Method Points and Coordinates:** The node labels and coordinate system are similar to those used in Connelly’s method [20], except that the lateral cable has been defined from  $p_a$  to  $p_d$  instead of from  $p_i$  to  $p_b$ , and the coordinate system has been shifted to the lower node plane from the upper node plane.

The coordinate system is located and oriented as follows:

- the x axis will be positive in the direction from the center of the cylinder through the  $p_i$  node, and shall lie in the lower node plane;
- the y axis will be positive in the direction normal to the x axis and lie in the lower node plane;
- the z axis will pass through the central rotation axis, and complete a right hand coordinate system.

The first sphere has a radius equal to the lateral strut length  $l_s$ , and its center is located at node  $p_i$ . The second sphere has a radius equal to the lateral cable length  $l_c$ , and its center is located at node  $p_d$ . The intersection between the two spheres and the cylinder surface yields the location of node  $p_a$  (Figure 4.4).

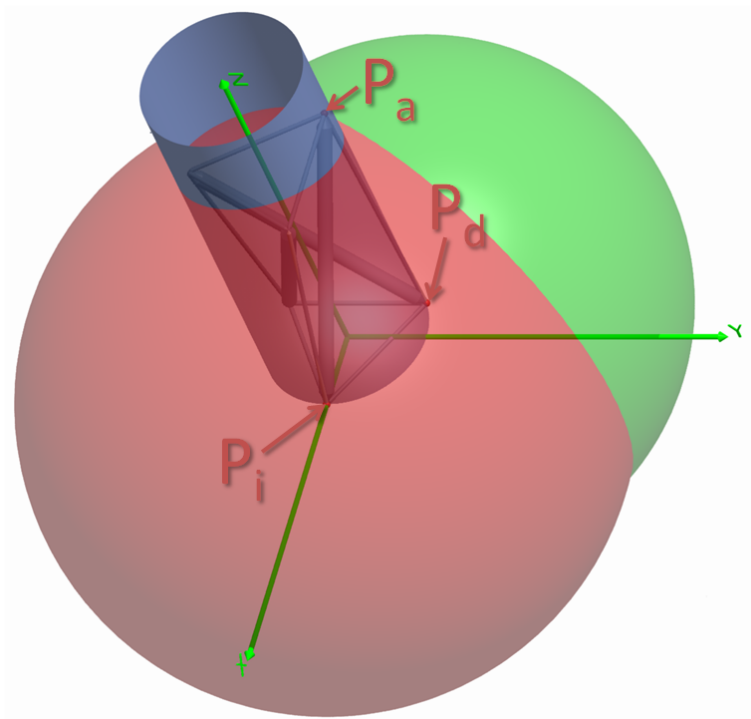


**Figure 4.4: Geometric Method Surfaces:** The two spherical surfaces intersect in a circle. This circle intersects with the cylindrical surface in a unique point  $p_a$ , in the positive  $z$  plane.

### 4.3 Symmetry in the Geometric Intersection Method

Prismatic tensegrity systems are well suited to the application of group theory due to their regular polygonal shapes [36]. Let  $H$  be the group of isometries that preserve the Euclidian distance between the nodes in a prismatic tensegrity system (alternatively,  $H$  is the group of isometries that make the coordinates of the nodes of  $P_{n_s}(j, k)$  invariant [20]). This definition means that group  $H$  contains reflections and rotations about the symmetry axes of the prismatic tensegrity system. In prismatic tensegrity systems the rotation axis is taken to be the vertical  $z$  axis and there are  $n_s$  reflection mirror lines to the rotation axis. This symmetry allows us to consider only one collection of transitive element classes (end cables, longitudinal cables, and longitudinal struts [20]) to completely define the geometry of the prismatic tensegrity system. The geometry definition is accomplished by determining the coordinates of the nodes that make up one collection of transitive elements and then

reflecting this collection about the  $n_s$  mirror lines to represent the tensegrity system in its entirety.

#### 4.4 Geometric Intersection Method

The coordinates of the nodes in a prismatic tensegrity have historically been calculated using the angle of twist  $\theta$  (which is unique for a set number of struts  $n_s$  and connectivity terms  $j$ ), and by specifying the desired height and radius of the cylinder that is bounded by these nodes. This is the method presented by Connelly in [20]. This method was adapted slightly by Tibert in [2], in which he used the magnitude of the distance between two nodes to calculate the element length between the two nodes. Both of these approaches are difficult to visualize and the adaptation presented by Tibert [2] has the additional disadvantage of failing without warning when a combination of element lengths result in an impossible kinematic geometry (a configuration that cannot be physically assembled). While it is desirable to express the overall prismatic tensegrity system in terms of its connectivity parameters, radius, and height; from a control perspective, it is more advantageous to control the cable and strut lengths directly. The geometric intersection method presented here allows the end cable and strut lengths, or end cable and lateral cable lengths to be specified. The missing cable or strut length, as well as the radius and height of the prismatic tensegrity system can then be computed. First, the radius is determined using the coordinate system illustrated in Figure 4.3.

The radius of the cylinder is a function of the connectivity term  $k$ , the number of struts  $n_s$ , and the end cable length  $l_e$ :

$$r = \frac{l_e}{2 \sin\left(\frac{\beta}{2}\right)}, \quad (4.1)$$

where  $\beta$  is:

$$\beta = \frac{2\pi k}{n_s}. \quad (4.2)$$

The relations in Equations (4.1) and (4.2) can be derived from Figure 4.5. The radius forms



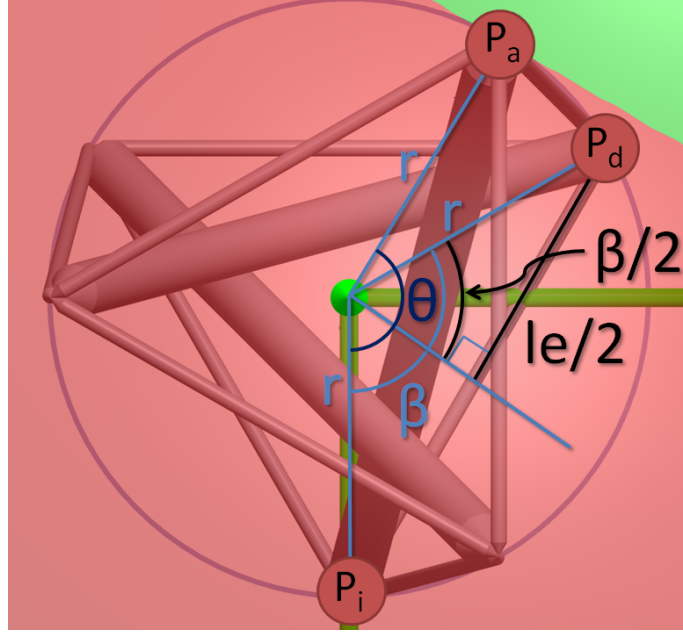


**Figure 4.5: Geometric Method Angles:**  $\beta$  is the angle between two adjacent nodes in the lower node plane.  $\theta$  is the angle between the nodes at the end of a strut, projected into either the upper or lower node plane.

the hypotenuse of a right angle triangle. This triangle is created by bisecting the end cable  $l_e$ . The length of  $l_e$  is known, and  $\beta$  can be calculated from Equation (4.2) as long as the number of struts ( $n_s$ ) is known. The radius can be calculated using  $\frac{\beta}{2}$ ,  $\frac{l_e}{2}$ , and Figure 4.5:

$$\sin\left(\frac{\beta}{2}\right) = \frac{l_e}{2} \cdot \frac{1}{r}. \quad (4.3)$$

Equation (4.3) can then be solved for  $r$ , yielding Equation (4.1). Calculating  $h$  is slightly more involved. The process begins by determining the angle of twist for the desired configuration.

The angle of twist  $\theta$  for any prismatic tensegrity configuration  $P_{n_s}(j, k)$  is known to be (see Connolly [20]):

$$\theta = \pi \cdot \left(\frac{1}{2} + \frac{j}{n_s}\right). \quad (4.4)$$

Equation (4.4) is a necessary and sufficient condition to guarantee the stability of the prismatic tensegrity structure [20]. Next the locations of the sphere centers are determined.

The center of the sphere with radius  $l_s$  is located at node  $p_i$ , and the center of the sphere with radius  $l_c$  is located at node  $p_d$ . The coordinates of these nodes are expressed by:

$$p_i = \begin{pmatrix} r \\ 0 \\ 0 \end{pmatrix}, \quad (4.5)$$

and

$$p_d = \begin{pmatrix} r \cos(\beta) \\ r \sin(\beta) \\ 0 \end{pmatrix}. \quad (4.6)$$

The Cartesian equation for a sphere offset from the origin is given by:

$$(x - x_i)^2 + (y - y_i)^2 + (z - z_i)^2 = r^2, \quad (4.7)$$

where  $(x_i, y_i, z_i)$  are the coordinates for the center of the sphere. The equations for the two spheres are then:

$$(x - p_{i_0})^2 + (y - p_{i_1})^2 + (z - p_{i_2})^2 = l_s^2, \quad (4.8)$$

and

$$(x - p_{d_0})^2 + (y - p_{d_1})^2 + (z - p_{d_2})^2 = l_c^2. \quad (4.9)$$

The axis of the cylinder contains the origin and is coincident with the  $z$  axis. The cross section of the cylinder is:

$$x^2 + y^2 = r^2. \quad (4.10)$$

Equations (4.8), (4.9), and (4.10) can be solved simultaneously for the missing strut or cable length, and  $h$ . These equations can have four real solutions, however only one solution can have the correct angle of twist and be in the positive  $z$  plane. The four possible solutions are illustrated in Figure 4.6 (only the two intersection points above the  $z = 0$  plane are visible in Figure 4.6, but all four can be seen in Figure 4.7). When the solutions are not constrained by the correct angle of twist (the angle of twist that ensures stability), the circle of intersection points between the two spheres can intersect the cylinder in four points (Figure 4.7). The

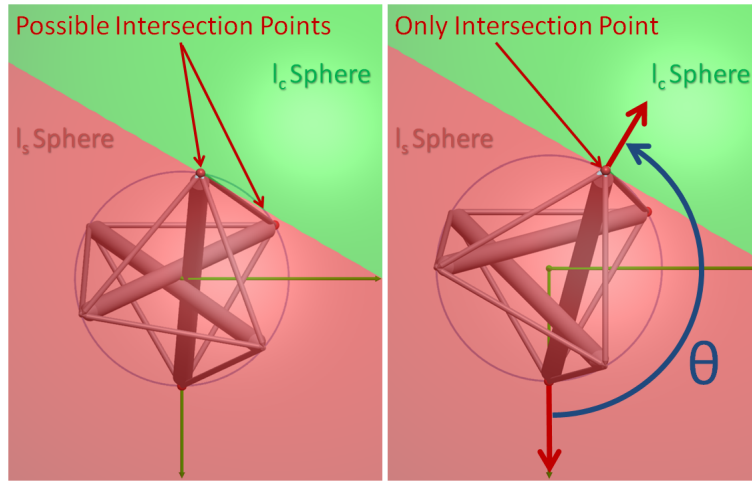


**Figure 4.6: Geometric Method Solutions:** if the solution is not constrained by the proper angle of twist then there can be at most four solutions, or intersection points. When the solutions are constrained by the correct angle of twist there can be only one intersection point above the  $z = 0$  plane.

correct angle of twist forces the plane containing the circle of intersection points to be tangent to the surface of the cylinder. This tangency reduces the possible solutions from four to two. Of these two solutions, only one has a positive  $z$  coordinate. The negative  $z$  solution is a valid solution, and results in a reflection of the tensegrity topology using the  $z = 0$  plane as a mirror line.

#### 4.4.1 Analytical Method and Derivation of the Analytic Kinematic Method From the Geometric Intersection Method

The analytical form of the geometric intersection method can be derived by rearranging Equations (4.8), (4.9), and (4.10) in terms of the desired output parameters. Let  $y$ ,  $z$ , and  $l_c$  or  $l_s$  be the desired parameters. The analytical equation for  $y$  is given by:

$$y = \pm \sqrt{r^2 - x^2}, \quad (4.11)$$

where

$$x = r \cos(\theta). \quad (4.12)$$

According to Equation (4.11)  $y$  can either be positive or negative, but Figure 4.8 can be used to show that only the  $y = +r^2 \sqrt{1 - \cos^2(\theta)}$  equation results in the correct angle of

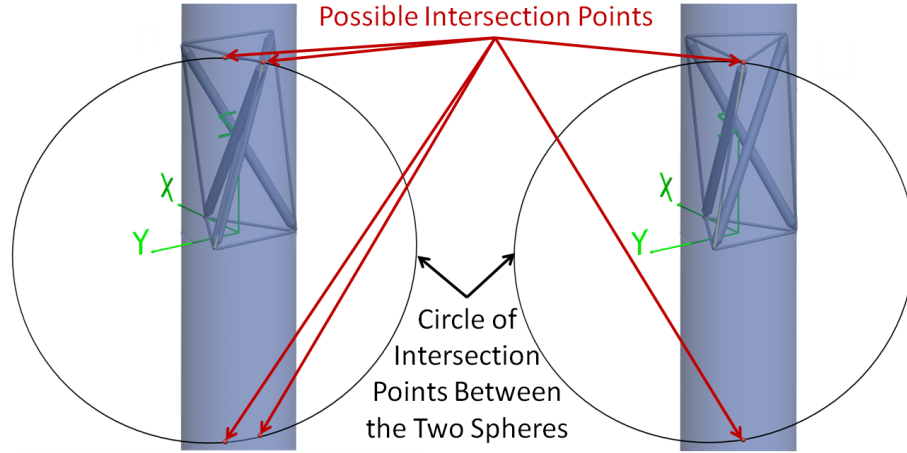


**Figure 4.7: Geometric Method Solutions:** the two spheres intersect in a circle, and this circle intersects the cylinder in four locations defining four intersection points. When the correct angle of twist is used the four possible intersection points are reduced to two, because the circle of intersection points becomes tangent to the cylinder.

twist.  $y = -r^2\sqrt{1 - \cos^2(\theta)}$  is equivalent to  $y = -r^2 \sin \theta$ , which in turn is equivalent to  $y = +r^2 \sin(-\theta)$ . This equation gives the  $y$  coordinate for an imaginary point (point  $p'_a$  from Figure 4.8), which has no physical significance for the form finding problem.

$z$  and  $l_c$  or  $l_s$  can be determined by rearranging Equations (4.8), and (4.9) in terms of  $z$ ,  $\theta$ , and  $r$ . This process begins by substituting both Equations (4.12) and (4.11) into Equations (4.8) and (4.9):

$$l_s^2 = [r \cos(\theta) - p_{i_0}]^2 + \left[ \sqrt{r^2 - (r \cos(\theta))^2} - p_{i_1} \right]^2 + (z - p_{i_2})^2, \quad (4.13)$$

and

$$l_c^2 = [r \cos(\theta) - p_{d_0}]^2 + \left[ \sqrt{r^2 - (r \cos(\theta))^2} - p_{d_1} \right]^2 + (z - p_{d_2})^2. \quad (4.14)$$

Equation (4.13) can be simplified by substituting the coordinates for the center of the  $l_s$  sphere, which are in terms of  $r$  and  $\theta$ :

$$\begin{aligned} l_s^2 &= [r \cos \theta - r]^2 + \left[ \sqrt{r^2 - (r \cos \theta)^2} - 0 \right]^2 + (z - 0)^2, \\ l_s^2 &= r^2 (\cos \theta - 1)^2 + r^2 - r^2 \cos^2 \theta + z^2, \\ l_s^2 &= r^2 (\cos^2 \theta - 2 \cos \theta + 1 + 1 - \cos^2 \theta) + z^2, \\ l_s^2 &= r^2 (2 - 2 \cos \theta) + z^2, \\ l_s^2 &= 2r^2 (1 - \cos \theta) + z^2. \end{aligned} \quad (4.15)$$

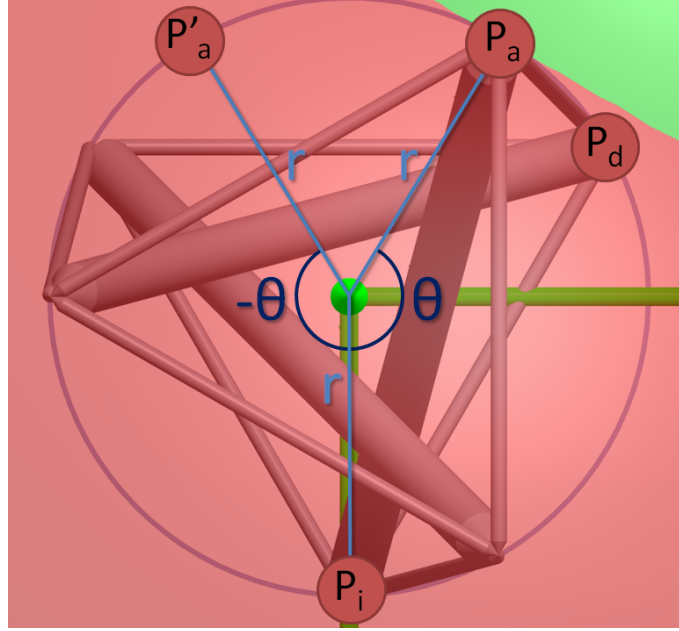


**Figure 4.8: Correct  $y$  Value:** The positive value for the angle of twist ( $\theta$ ) can be used to determine the correct coordinates for  $p_a$ . Coordinates calculated using the negative value for  $\theta$  would give the location of point  $p'_a$ , which has no physical meaning in the context of the geometric form finding method.

Equation (4.15) is the same equation Tibert derived in [2] from Connolly's coordinates in [20] (Tibert used a different coordinate system so his equation for the cable length is equal to the above equation for the strut length). A similar method can be used to simplify Equation (4.14):

$$\begin{aligned} l_c^2 &= [r \cos \theta - r \cos \beta]^2 + \left[ \sqrt{r^2 - (r \cos \theta)^2} - r \sin \beta \right]^2 + (z - 0)^2, \\ l_c^2 &= r^2 (\cos \theta - \cos \beta)^2 + \left[ r \sqrt{1 - \cos^2 \theta} - r \sin \beta \right]^2 + z^2. \end{aligned} \quad (4.16)$$

Using the following trigonometric identities:

$$\begin{aligned} \cos a - \cos b &= -2 \sin \left( \frac{a+b}{2} \right) \sin \left( \frac{a-b}{2} \right), \\ \sin^2 a &= 1 - \cos^2 a, \end{aligned} \quad (4.17)$$

Equation (4.16) becomes:

$$\begin{aligned} l_c^2 &= r^2 \left[ -2 \sin \left( \frac{\theta+\beta}{2} \right) \sin \left( \frac{\theta-\beta}{2} \right) \right]^2 + \left[ r \sqrt{\sin^2 \theta} - r \sin \beta \right]^2 + z^2, \\ l_c^2 &= r^2 \left[ 4 \sin^2 \left( \frac{\theta+\beta}{2} \right) \sin^2 \left( \frac{\theta-\beta}{2} \right) + (\sin \theta - \sin \beta)^2 \right] + z^2. \end{aligned} \quad (4.18)$$

Using the following trigonometric identity:

$$\sin a - \sin b = 2 \cos \left( \frac{a+b}{2} \right) \sin \left( \frac{a-b}{2} \right), \quad (4.19)$$

Equation (4.18) becomes:

$$\begin{aligned} l_c^2 &= r^2 \left[ 4 \sin^2 \left( \frac{\theta+\beta}{2} \right) \sin^2 \left( \frac{\theta-\beta}{2} \right) + 4 \cos^2 \left( \frac{\theta+\beta}{2} \right) \sin^2 \left( \frac{\theta-\beta}{2} \right) \right] + z^2, \\ l_c^2 &= 4r^2 \left[ \sin^2 \left( \frac{\theta-\beta}{2} \right) \left[ \sin^2 \left( \frac{\theta+\beta}{2} \right) + \cos^2 \left( \frac{\theta+\beta}{2} \right) \right] \right] + z^2, \\ l_c^2 &= 4r^2 \sin^2 \left( \frac{\theta-\beta}{2} \right) + z^2. \end{aligned} \quad (4.20)$$

Finally, the following relation can be used to obtain the cable length equation found in Tibert [2]:

$$\sin^2 a = \frac{1}{2} (1 - \cos(2a)). \quad (4.21)$$

Equation (4.21) becomes:

$$l_c^2 = 2r^2 [1 - \cos(\theta - \beta)] + z^2. \quad (4.22)$$

The height of the prismatic tensegrity ( $z$  or  $h$ ) can be calculated by rearranging either Equation (4.15) or Equation (4.22) as follows:

$$\begin{aligned} l_s^2 &= 2r^2 (1 - \cos \theta) + z^2, \\ z^2 &= l_s^2 - 2r^2 (1 - \cos \theta), \end{aligned} \quad (4.23)$$

or,

$$\begin{aligned} l_c^2 &= 2r^2 [1 - \cos(\theta - \beta)] + z^2, \\ z^2 &= l_c^2 - 2r^2 [1 - \cos(\theta - \beta)]. \end{aligned} \quad (4.24)$$

Equations (4.15) and (4.22) prove that the geometric intersection method will always yield equivalent results to both Connelly's method [20] and Tibert's interpretation of Connelly's method [2], because one can be derived from the other. However, the geometric method is based on a physical interpretation of the solution space, where Connelly's method is based on trigonometry. This geometric basis has distinct advantages that will be illustrated in Chapter 5. The next section will discuss how the geometric intersection method was implemented in Mathcad and ProEngineer to generate the examples in Chapter 5.

## 4.5 Mathcad/ProEngineer Implementation

A parametric ProEngineer 3D model of a generic prismatic tensegrity system was created to allow the user to input desired element lengths, connectivity, and number of struts. These values were then analyzed in an integrated Mathcad worksheet feature to determine the height and angle of twist of the resulting prismatic tensegrity system. These values were used to update the old generic ProEngineer parameters, creating a visualization of the new geometry. This implementation allowed several prismatic tensegrity systems to be analyzed visually, under a wide variety of element lengths and number of struts. A transcript of the Mathcad code can be found in Appendix A.

### 4.5.1 Computational Complexity

The computational complexity of the implementation of the geometric intersection algorithm was low when compared to the form finding methods in Chapter 3, Table 3.1. This is to be expected because the geometric intersection method arrives at the same analytical equations as Connelly's and Tibert's methods [20], [2]. An alternate implementation is documented in Appendix A where the constraint surface equations are used directly, and solved numerically to arrive at a solution. This particular implementation is particularly useful because it allows the constraint surfaces to be changed without re-derive the analytical equations. Also the input variables can be changed and the numerical solver will automatically calculate the missing parameters as long as enough input variables have been specified. By contrast, if different input or output variables are desired then Connelly's and Tibert's equations must be rearranged in terms of the desired variables. While this equation manipulation is not particularly difficult, it does add an additional step to the form finding algorithm that the numerical implementation of the geometric intersection method avoids.

## Chapter 5

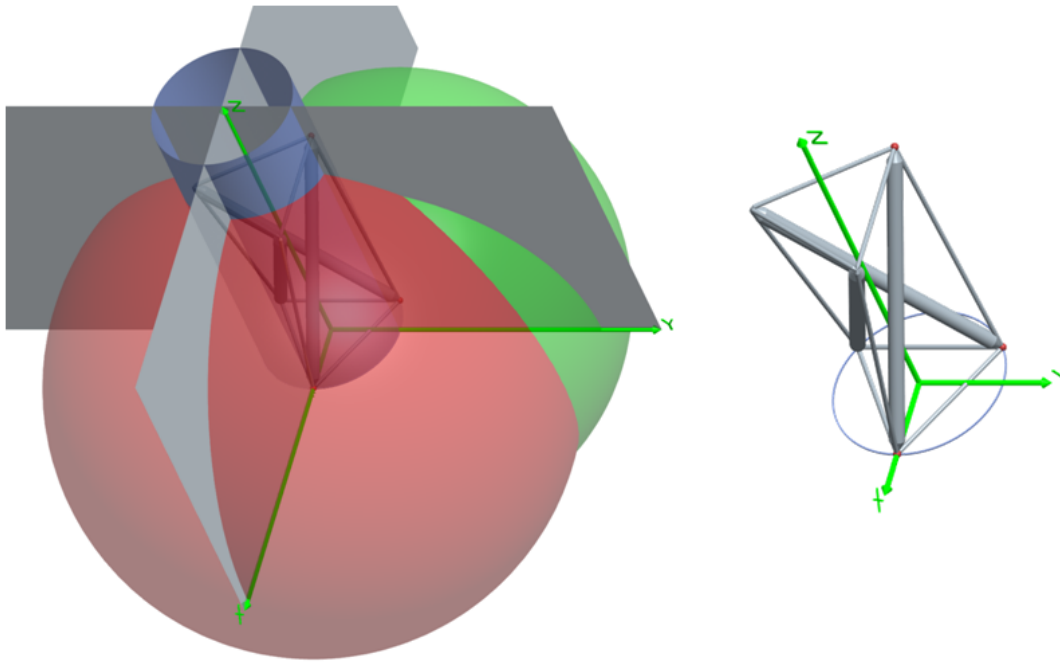
### Examples

The examples in this chapter will serve four purposes. First, they will illustrate one potential implementation of the geometric intersection method and how it can be used to help design and control prismatic tensegrity systems. Second, they will demonstrate the mathematical equivalence between the geometric intersection method and Connelly's method [20]. Third, they will illustrate how the geometric intersection method can be used to visually identify the boundaries of the form finding solution space (ie. when a set of parameters will result in a degenerate tensegrity system that has no real physical representation). Finally, they will illustrate how other surfaces can be substituted for the cylinder surface to determine stable configurations of a wider variety of tensegrity topologies.

#### 5.1 Implementation of the Geometric Intersection Method

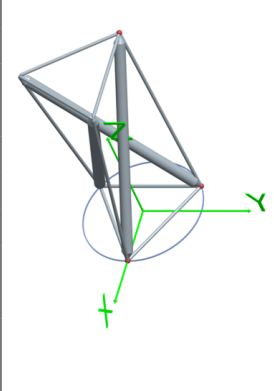
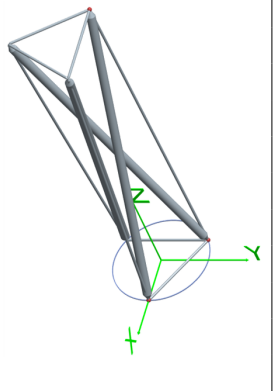
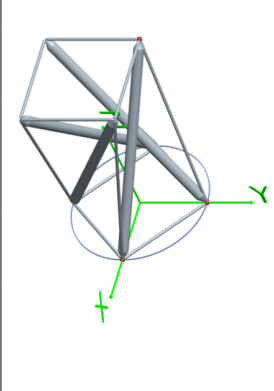
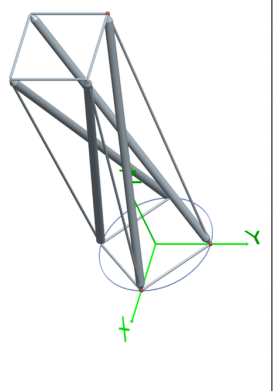
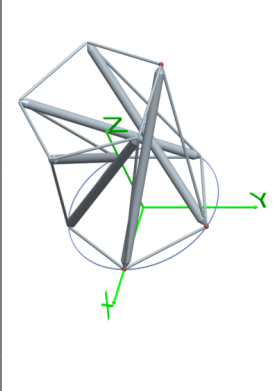
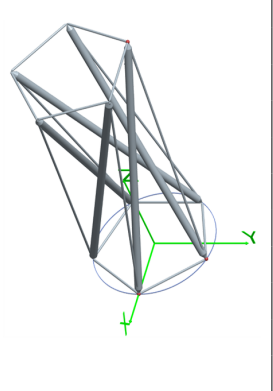
The following examples were implemented using ProEngineer with an embedded Mathcad worksheet feature, as discussed at the end of Chapter 4. The form finding process begins by starting from a known configuration and altering the connectivity, number of struts, or element lengths (Figure 5.1).



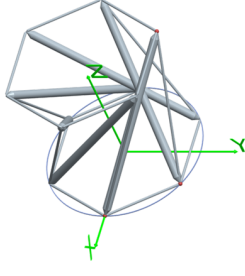
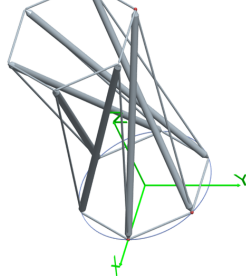
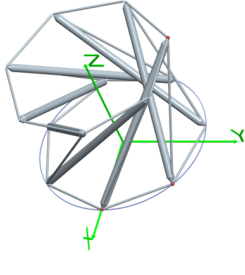
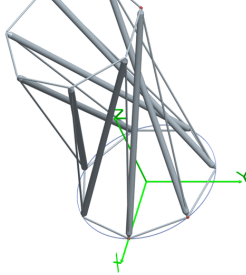
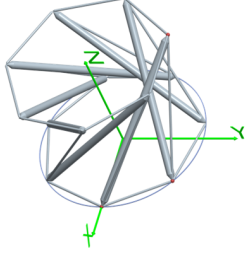
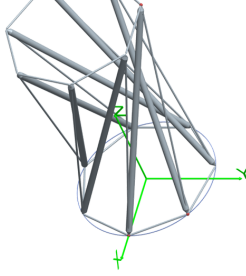


**Figure 5.1: *Generic Model Configuration:*** The spheres and cylinder used to generate the generic prismatic tensegrity arrangement are shown on the left. This same generic configuration is more easily seen when these surfaces are hidden (the image on the right).

If the kinematic geometry of the tensegrity system has variable radius, and lateral cable lengths, then Table 5.1 and 5.2 illustrate the end poses of the tensegrity system, assuming a constant lateral strut length for each pose.

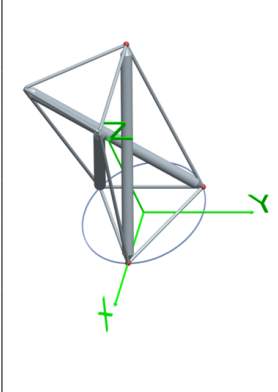
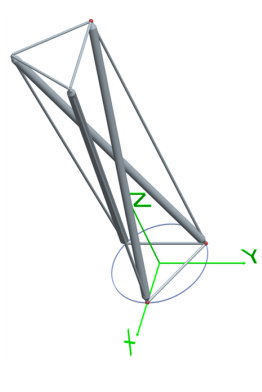
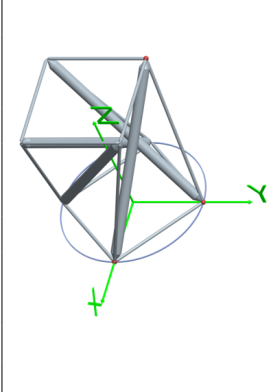
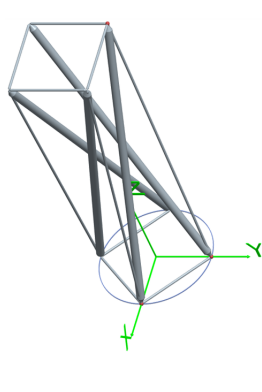
Initial	Parameters	$l_c = 2.0$	$l_c = 2.5$	$l_c = 3.0$	$l_c = 3.5$	$l_c = 4.0$	Final
	$j$	1	1	1	1	1	
	$k$	1	1	1	1	1	
	$n_s$	3	3	3	3	3	
	$\theta$	150°	150°	150°	150°	150°	
	$r$	0.57735	0.57735	0.57735	0.57735	0.57735	
	Geo.	$\begin{bmatrix} h \\ l_s \\ l_e \end{bmatrix}$	$\begin{bmatrix} 1.97754 \\ 2.27040 \\ 1.00000 \end{bmatrix}$	$\begin{bmatrix} 2.36291 \\ 2.61292 \\ 1.00000 \end{bmatrix}$	$\begin{bmatrix} 2.88675 \\ 3.09473 \\ 1.00000 \end{bmatrix}$	$\begin{bmatrix} 3.40343 \\ 3.58153 \\ 1.00000 \end{bmatrix}$	
Con.	$\begin{bmatrix} h \\ l_s \\ l_e \end{bmatrix}$	$\begin{bmatrix} 1.97754 \\ 2.27040 \\ 1.00000 \end{bmatrix}$	$\begin{bmatrix} 2.36291 \\ 2.61292 \\ 1.00000 \end{bmatrix}$	$\begin{bmatrix} 2.88675 \\ 3.09473 \\ 1.00000 \end{bmatrix}$	$\begin{bmatrix} 3.40343 \\ 3.58153 \\ 1.00000 \end{bmatrix}$	$\begin{bmatrix} 3.91578 \\ 4.07153 \\ 1.00000 \end{bmatrix}$	
	$j$	1	1	1	1	1	
	$k$	1	1	1	1	1	
	$n_s$	4	4	4	4	4	
	$\theta$	135°	135°	135°	135°	135°	
	$r$	0.70711	0.70711	0.70711	0.70711	0.70711	
	Geo.	$\begin{bmatrix} h \\ l_s \\ l_e \end{bmatrix}$	$\begin{bmatrix} 1.92538 \\ 2.32685 \\ 1.00000 \end{bmatrix}$	$\begin{bmatrix} 2.44072 \\ 2.76843 \\ 1.00000 \end{bmatrix}$	$\begin{bmatrix} 2.70054 \\ 3.00000 \\ 1.00000 \end{bmatrix}$	$\begin{bmatrix} 3.24698 \\ 3.50000 \\ 1.00000 \end{bmatrix}$	
Con.	$\begin{bmatrix} h \\ l_s \\ l_e \end{bmatrix}$	$\begin{bmatrix} 1.92538 \\ 2.32685 \\ 1.00000 \end{bmatrix}$	$\begin{bmatrix} 2.44072 \\ 2.76843 \\ 1.00000 \end{bmatrix}$	$\begin{bmatrix} 2.70054 \\ 3.00000 \\ 1.00000 \end{bmatrix}$	$\begin{bmatrix} 3.24698 \\ 3.50000 \\ 1.00000 \end{bmatrix}$	$\begin{bmatrix} 3.78059 \\ 4.00000 \\ 1.00000 \end{bmatrix}$	
	$j$	1	1	1	1	1	
	$k$	1	1	1	1	1	
	$n_s$	5	5	5	5	5	
	$\theta$	126°	126°	126°	126°	126°	
	$r$	0.85065	0.85065	0.85065	0.85065	0.85065	
	Geo.	$\begin{bmatrix} h \\ l_s \\ l_e \end{bmatrix}$	$\begin{bmatrix} 1.84484 \\ 2.38774 \\ 1.00000 \end{bmatrix}$	$\begin{bmatrix} 2.37770 \\ 2.81981 \\ 1.00000 \end{bmatrix}$	$\begin{bmatrix} 2.48524 \\ 2.91106 \\ 1.00000 \end{bmatrix}$	$\begin{bmatrix} 3.07025 \\ 3.42407 \\ 1.00000 \end{bmatrix}$	
Con.	$\begin{bmatrix} h \\ l_s \\ l_e \end{bmatrix}$	$\begin{bmatrix} 1.84484 \\ 2.38774 \\ 1.00000 \end{bmatrix}$	$\begin{bmatrix} 2.37770 \\ 2.81981 \\ 1.00000 \end{bmatrix}$	$\begin{bmatrix} 2.48524 \\ 2.91106 \\ 1.00000 \end{bmatrix}$	$\begin{bmatrix} 3.07025 \\ 3.42407 \\ 1.00000 \end{bmatrix}$	$\begin{bmatrix} 3.62993 \\ 3.93373 \\ 1.00000 \end{bmatrix}$	

**Table 5.1:  $l_c$  Variable 1:** In these examples the connectivity terms  $j$  and  $k$  are constant, as are the number of struts ( $n_s$ ), and the end cable length ( $l_e$ ). The output variables height ( $h$ ), and strut length ( $l_s$ ), are calculated using both the geometric method (Geo.) and Connelley’s method (Con.) [20]. Images of the configurations corresponding to  $l_c = 2.0$  are shown on the left and configurations corresponding to  $l_c = 4.0$  are shown on the right.

Initial	Parameters	$l_c = 2.0$	$l_c = 2.5$	$l_c = 3.0$	$l_c = 3.5$	$l_c = 4.0$	Final	
	$j$	1	1	1	1	1		
	$k$	1	1	1	1	1		
	$n_s$	6	6	6	6	6		
	$\theta$	120°	120°	120°	120°	120°		
	$r$	1.00000	1.00000	1.00000	1.00000	1.00000		
	Geo.	$h$	1.73205	2.29129	2.82843	2.87228		3.46410
		$l_s$	2.44949	2.87228	3.31662	3.35410		3.87298
		$l_e$	1.00000	1.00000	1.00000	1.00000		1.00000
	Con.	$h$	1.73205	2.29129	2.82843	2.87228		3.46410
		$l_s$	2.44949	2.87228	3.31662	3.35410		3.87298
$l_e$		1.00000	1.00000	1.00000	1.00000	1.00000		
	$j$	1	1	1	1	1		
	$k$	1	1	1	1	1		
	$n_s$	7	7	7	7	7		
	$\theta$	115.714°	115.714°	115.714°	115.714°	115.714°		
	$r$	1.15238	1.15238	1.15238	1.15238	1.15238		
	Geo.	$h$	1.58000	2.17863	2.73796	3.27817		3.80742
		$l_s$	2.51093	2.92485	3.36226	3.81507		4.27841
		$l_e$	1.00000	1.00000	1.00000	1.00000		1.00000
	Con.	$h$	1.58000	2.17863	2.73796	3.27817		3.80742
		$l_s$	2.51093	2.92485	3.36226	3.81507		4.27841
$l_e$		1.00000	1.00000	1.00000	1.00000	1.00000		
	$j$	1	1	1	1	1		
	$k$	1	1	1	1	1		
	$n_s$	8	8	8	8	8		
	$\theta$	112.5°	112.5°	112.5°	112.5°	112.5°		
	$r$	1.30656	1.30656	1.30656	1.30656	1.30656		
	Geo.	$h$	1.37563	2.03528	2.62533	3.18471		3.72724
		$l_s$	2.57160	2.97710	3.40780	3.85527		4.31429
		$l_e$	1.00000	1.00000	1.00000	1.00000		1.00000
	Con.	$h$	1.37563	2.03528	2.62533	3.18471		3.72724
		$l_s$	2.57160	2.97710	3.40780	3.85527		4.31429
$l_e$		1.00000	1.00000	1.00000	1.00000	1.00000		

**Table 5.2:  $l_c$  Variable 2:** This is a continuation of Table 5.1, where  $l_c$  is the variable and the output parameters are  $l_s$  and  $h$ .

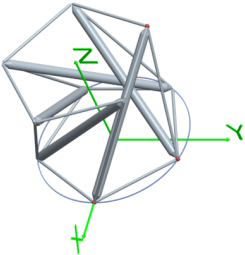
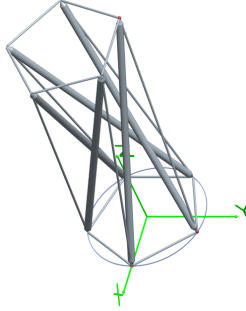
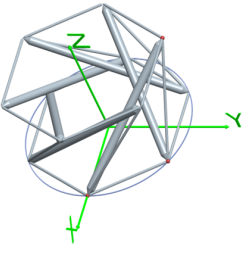
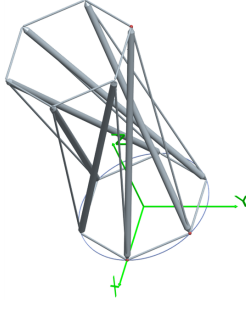
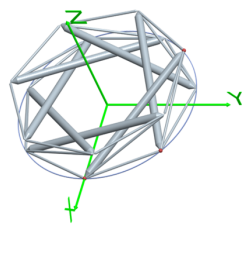
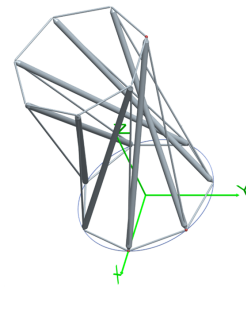
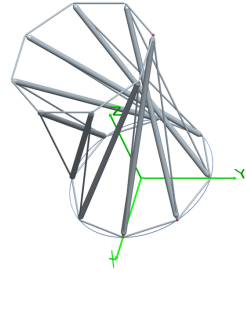
Similarly, Table 5.3 and 5.4 illustrate the beginning and end geometry if the user decides to control the end cable and strut lengths instead of the end cable and lateral cable lengths.

Initial	Parameters	$l_s = 2.0$	$l_s = 2.5$	$l_s = 3.0$	$l_s = 3.5$	$l_s = 4.0$	Final
	$j$	1	1	1	1	1	
	$k$	1	1	1	1	1	
	$n_s$	3	3	3	3	3	
	$\theta$	150°	150°	150°	150°	150°	
	$r$	0.57735	0.57735	0.57735	0.57735	0.57735	
	Geo.	$\begin{bmatrix} h \\ l_c \\ l_e \end{bmatrix}$	$\begin{bmatrix} 1.66012 \\ 1.68680 \\ 1.00000 \end{bmatrix}$	$\begin{bmatrix} 2.23741 \\ 2.25728 \\ 1.00000 \end{bmatrix}$	$\begin{bmatrix} 2.78496 \\ 2.80095 \\ 1.00000 \end{bmatrix}$	$\begin{bmatrix} 3.31753 \\ 3.33096 \\ 1.00000 \end{bmatrix}$	
Con.	$\begin{bmatrix} h \\ l_c \\ l_e \end{bmatrix}$	$\begin{bmatrix} 1.66012 \\ 1.68680 \\ 1.00000 \end{bmatrix}$	$\begin{bmatrix} 2.23741 \\ 2.25728 \\ 1.00000 \end{bmatrix}$	$\begin{bmatrix} 2.78496 \\ 2.80095 \\ 1.00000 \end{bmatrix}$	$\begin{bmatrix} 3.31753 \\ 3.33096 \\ 1.00000 \end{bmatrix}$	$\begin{bmatrix} 3.84135 \\ 3.85296 \\ 1.00000 \end{bmatrix}$	
	$j$	1	1	1	1	1	
	$k$	1	1	1	1	1	
	$n_s$	4	4	4	4	4	
	$\theta$	135°	135°	135°	135°	135°	
	$r$	0.70711	0.70711	0.70711	0.70711	0.70711	
	Geo.	$\begin{bmatrix} h \\ l_c \\ l_e \end{bmatrix}$	$\begin{bmatrix} 1.51423 \\ 1.60804 \\ 1.00000 \end{bmatrix}$	$\begin{bmatrix} 2.13141 \\ 2.19904 \\ 1.00000 \end{bmatrix}$	$\begin{bmatrix} 2.70054 \\ 2.75423 \\ 1.00000 \end{bmatrix}$	$\begin{bmatrix} 3.24698 \\ 3.29178 \\ 1.00000 \end{bmatrix}$	
Con.	$\begin{bmatrix} h \\ l_c \\ l_e \end{bmatrix}$	$\begin{bmatrix} 1.51423 \\ 1.60804 \\ 1.00000 \end{bmatrix}$	$\begin{bmatrix} 2.13141 \\ 2.19904 \\ 1.00000 \end{bmatrix}$	$\begin{bmatrix} 2.70054 \\ 2.75423 \\ 1.00000 \end{bmatrix}$	$\begin{bmatrix} 3.24698 \\ 3.29178 \\ 1.00000 \end{bmatrix}$	$\begin{bmatrix} 3.78059 \\ 3.81913 \\ 1.00000 \end{bmatrix}$	

**Table 5.3:  $l_s$  Variable 1:** In these examples  $j$ ,  $k$ ,  $n_s$ , and  $l_e$  are constant. The output variables  $h$ , and  $l_c$  are calculated using both the geometric method (Geo.) and Connelly's method (Con.) [20]. The images correspond to the extreme configurations ( $l_s = 2.0$  and 4.0).

## 5.2 Equivalence of the Geometric Form Finding Method to Connelly's Method

Tables 5.1, 5.2, 5.3, and 5.4 empirically show that the geometric intersection method is mathematically equivalent to Connelly's method [20] as expected. This equivalence occurs

Initial	Parameters	$l_s = 2.0$	$l_s = 2.5$	$l_s = 3.0$	$l_s = 3.5$	$l_s = 4.0$	Final
	$j$	1	1	1	1	1	
	$k$	1	1	1	1	1	
	$n_s$	5	5	5	5	5	
	$\theta$	126°	126°	126°	126°	126°	
	$r$	0.85065	0.85065	0.85065	0.85065	0.85065	
	Geo. $\begin{bmatrix} h \\ l_c \\ l_e \end{bmatrix}$	$\begin{bmatrix} h \\ l_c \\ l_e \end{bmatrix}$	$\begin{bmatrix} 1.30466 \\ 1.51615 \\ 1.00000 \end{bmatrix}$	$\begin{bmatrix} 1.98800 \\ 2.13277 \\ 1.00000 \end{bmatrix}$	$\begin{bmatrix} 2.58885 \\ 2.70161 \\ 1.00000 \end{bmatrix}$	$\begin{bmatrix} 3.15470 \\ 3.24788 \\ 1.00000 \end{bmatrix}$	
Con. $\begin{bmatrix} h \\ l_c \\ l_e \end{bmatrix}$	$\begin{bmatrix} h \\ l_c \\ l_e \end{bmatrix}$	$\begin{bmatrix} 1.30466 \\ 1.51615 \\ 1.00000 \end{bmatrix}$	$\begin{bmatrix} 1.98800 \\ 2.13277 \\ 1.00000 \end{bmatrix}$	$\begin{bmatrix} 2.58885 \\ 2.70161 \\ 1.00000 \end{bmatrix}$	$\begin{bmatrix} 3.15470 \\ 3.24788 \\ 1.00000 \end{bmatrix}$	$\begin{bmatrix} 3.70164 \\ 3.78136 \\ 1.00000 \end{bmatrix}$	
	$j$	1	1	1	1	1	
	$k$	1	1	1	1	1	
	$n_s$	6	6	6	6	6	
	$\theta$	120°	120°	120°	120°	120°	
	$r$	1.00000	1.00000	1.00000	1.00000	1.00000	
	Geo. $\begin{bmatrix} h \\ l_c \\ l_e \end{bmatrix}$	$\begin{bmatrix} h \\ l_c \\ l_e \end{bmatrix}$	$\begin{bmatrix} 1.00000 \\ 1.41421 \\ 1.00000 \end{bmatrix}$	$\begin{bmatrix} 1.80278 \\ 2.06155 \\ 1.00000 \end{bmatrix}$	$\begin{bmatrix} 2.44949 \\ 2.64575 \\ 1.00000 \end{bmatrix}$	$\begin{bmatrix} 3.04138 \\ 3.20156 \\ 1.00000 \end{bmatrix}$	
Con. $\begin{bmatrix} h \\ l_c \\ l_e \end{bmatrix}$	$\begin{bmatrix} h \\ l_c \\ l_e \end{bmatrix}$	$\begin{bmatrix} 1.00000 \\ 1.41421 \\ 1.00000 \end{bmatrix}$	$\begin{bmatrix} 1.80278 \\ 2.06155 \\ 1.00000 \end{bmatrix}$	$\begin{bmatrix} 2.44949 \\ 2.64575 \\ 1.00000 \end{bmatrix}$	$\begin{bmatrix} 3.04138 \\ 3.20156 \\ 1.00000 \end{bmatrix}$	$\begin{bmatrix} 3.60555 \\ 3.74166 \\ 1.00000 \end{bmatrix}$	
	$j$	1	1	1	1	1	
	$k$	1	1	1	1	1	
	$n_s$	7	7	7	7	7	
	$\theta$	115.714°	115.714°	115.714°	115.714°	115.714°	
	$r$	1.15238	1.15238	1.15238	1.15238	1.15238	
	Geo. $\begin{bmatrix} h \\ l_c \\ l_e \end{bmatrix}$	$\begin{bmatrix} h \\ l_c \\ l_e \end{bmatrix}$	$\begin{bmatrix} 0.43778 \\ 1.30201 \\ 1.00000 \end{bmatrix}$	$\begin{bmatrix} 1.56258 \\ 1.98626 \\ 1.00000 \end{bmatrix}$	$\begin{bmatrix} 2.27852 \\ 2.58752 \\ 1.00000 \end{bmatrix}$	$\begin{bmatrix} 2.90545 \\ 3.15361 \\ 1.00000 \end{bmatrix}$	
Con. $\begin{bmatrix} h \\ l_c \\ l_e \end{bmatrix}$	$\begin{bmatrix} h \\ l_c \\ l_e \end{bmatrix}$	$\begin{bmatrix} 0.43778 \\ 1.30201 \\ 1.00000 \end{bmatrix}$	$\begin{bmatrix} 1.56258 \\ 1.98626 \\ 1.00000 \end{bmatrix}$	$\begin{bmatrix} 2.27852 \\ 2.58752 \\ 1.00000 \end{bmatrix}$	$\begin{bmatrix} 2.90545 \\ 3.15361 \\ 1.00000 \end{bmatrix}$	$\begin{bmatrix} 3.49165 \\ 3.70071 \\ 1.00000 \end{bmatrix}$	
Undefined	$j$	1	1	1	1	1	
	$k$	1	1	1	1	1	
	$n_s$	8	8	8	8	8	
	$\theta$	112.5°	112.5°	112.5°	112.5°	112.5°	
	$r$	1.30656	1.30656	1.30656	1.30656	1.30656	
	Geo. $\begin{bmatrix} h \\ l_c \\ l_e \end{bmatrix}$	$\begin{bmatrix} h \\ l_c \\ l_e \end{bmatrix}$	$\begin{bmatrix} \text{undefined} \\ \text{undefined} \\ 1.00000 \end{bmatrix}$	$\begin{bmatrix} 1.23662 \\ 1.90706 \\ 1.00000 \end{bmatrix}$	$\begin{bmatrix} 2.06863 \\ 2.52723 \\ 1.00000 \end{bmatrix}$	$\begin{bmatrix} 2.74394 \\ 3.10433 \\ 1.00000 \end{bmatrix}$	
Con. $\begin{bmatrix} h \\ l_c \\ l_e \end{bmatrix}$	$\begin{bmatrix} h \\ l_c \\ l_e \end{bmatrix}$	$\begin{bmatrix} 0.84899i \\ 1.17766 \\ 1.00000 \end{bmatrix}$	$\begin{bmatrix} 1.23662 \\ 1.90706 \\ 1.00000 \end{bmatrix}$	$\begin{bmatrix} 2.06863 \\ 2.52723 \\ 1.00000 \end{bmatrix}$	$\begin{bmatrix} 2.74394 \\ 3.10433 \\ 1.00000 \end{bmatrix}$	$\begin{bmatrix} 3.35846 \\ 3.65881 \\ 1.00000 \end{bmatrix}$	

**Table 5.4:  $l_s$  Variable 2:** This is a continuation of Table 5.3, where  $l_s$  is the variable and the output parameters are  $l_c$  and  $h$ . Note that for  $n_s = 8$  there is no geometric solution, and no real solution for Connelly's method.

because both Connelly's method and the geometric intersection method arrive at the same analytical equations, despite being derived using completely different methods (algebraic derivation vs. geometric derivation). One notable exception occurs in Table 5.4, where the output variables  $h$  and  $l_c$  are undefined for the geometric intersection method and imaginary for Connelly's method. This result occurs in Connelly's method because the left hand side of  $z^2 = l_s^2 - 2r^2(1 - \cos \theta)$  becomes negative when  $l_s^2 < 2r^2(1 - \cos \theta)$ . This inequality explains mathematically why there is no real solution for  $h$ , but it is arguably not intuitive. The differences between Connelly's and Tibert's methods and the geometric intersection method become clearer when the algorithm for each of these methods is described.

### 5.3 Form Finding Method Algorithm Comparison

All method algorithms begin by defining the topology of the tensegrity system. These definitions include specifying the number of compression elements and the  $j$  and  $k$  values that define how the tension elements connect to the compression elements. Connelly's method can then be implemented using the following algorithm:

1. Specify the radius of the topology  $r$ , and the height of the topology  $h$ .
2. Determine the angle of twist that will ensure the stability of the topology using:

$$\theta = \pi \left( \frac{1}{2} + \frac{j}{n_s} \right). \quad (5.1)$$

3. Calculate the coordinates of the nodes using the following equations:

$$\begin{aligned} p_i &= [0, r, 0], \\ p_a &= [r \sin(\theta), r \cos(\theta), h], \\ p_b &= \left[ r \sin\left(\theta + \frac{2\pi j}{n_s}\right), r \cos\left(\theta + \frac{2\pi j}{n_s}\right), h \right], \\ p_c &= \left[ r \sin\left(\frac{2\pi k}{n_s}\right), r \cos\left(\frac{2\pi k}{n_s}\right), 0 \right] \\ p_d &= \left[ -r \sin\left(\frac{2\pi k}{n_s}\right), r \cos\left(\frac{2\pi k}{n_s}\right), 0 \right]. \end{aligned} \quad (5.2)$$

4. Plot the resulting configuration.
5. Calculate the length of the elements by using the following equations:

$$\begin{aligned}
 l_s &= \sqrt{2r^2(1 - \cos \theta) + h^2}, \\
 l_c &= \sqrt{2r^2[1 - \cos(\theta - \beta)] + h^2}, \\
 l_e &= 2r \sin\left(\frac{\beta}{2}\right).
 \end{aligned} \tag{5.3}$$

6. Change the height, radius, number of elements or connectivity variables to achieve the desired element lengths.

Tibert's method can be implemented using the following algorithm:

1. Specify the input variables:
  - One input variable must be either the radius of the topology  $r$  or the length of the end cables  $l_e$ ,
  - The other input variable must be the height of the topology  $h$ , the length of the side cables  $l_c$ , or the length of the struts  $l_s$ .
  - For this example the length of the end cables and the struts will be specified.
2. Evaluate the following boundary condition to ensure the existence of a solution:

$$l_s^2 < 2r^2(1 - \cos(\theta)). \tag{5.4}$$

3. If the inequality is not satisfied alter the radius or the strut length until the inequality is satisfied.
4. Determine the angle of twist that will ensure the stability of the topology using:

$$\theta = \pi \left( \frac{1}{2} + \frac{j}{n_s} \right). \tag{5.5}$$

5. Simultaneously solve the following equations for  $h$  and  $l_c$ :

$$\begin{aligned} l_s &= \sqrt{2r^2(1 - \cos \theta) + h^2}, \\ l_c &= \sqrt{2r^2[1 - \cos(\theta - \beta)] + h^2}. \end{aligned} \tag{5.6}$$

6. Plot the resulting configuration.

The geometric intersection method can be implemented using the following algorithm:

1. Specify the input variables:

- One input variable must be either the radius of the topology  $r$  or the length of the end cables  $l_e$ ,
- The other input variable must be the height of the topology  $h$ , the length of the side cables  $l_c$ , or the length of the struts  $l_s$ .
- For this example the length of the end cables and the struts will be specified.

2. Evaluate the following boundary condition to ensure the existence of a solution:

$$l_s^2 < 2r^2(1 - \cos(\theta)). \tag{5.7}$$

3. If the inequality is not satisfied alter the radius or the strut length until the inequality is satisfied.

4. Determine the angle of twist that will ensure the stability of the topology using:

$$\theta = \pi \left( \frac{1}{2} + \frac{j}{n_s} \right). \tag{5.8}$$

5. Calculate the coordinates for the two sphere centers using the following equations:

$$p_i = \begin{pmatrix} r \\ 0 \\ 0 \end{pmatrix}, \tag{5.9}$$



and

$$p_d = \begin{pmatrix} r \cos(\beta) \\ r \sin(\beta) \\ 0 \end{pmatrix}. \quad (5.10)$$

6. Simultaneously solve the following equations for  $h$  and  $l_c$ :

$$\begin{aligned} l_s &= \sqrt{2r^2(1 - \cos \theta) + h^2}, \\ l_c &= \sqrt{2r^2[1 - \cos(\theta - \beta)] + h^2}. \end{aligned} \quad (5.11)$$

7. Plot the resulting configuration.

Connelly's method will always have a solution, but does not allow the element lengths to be directly controlled. Both Tibert's method and the geometric intersection method allow the element lengths to be controlled, but they must both evaluate a boundary condition to ensure the existence of a solution. The geometric intersection method does not offer a significant advantage over Tibert's method *for an unknown configuration*, but once the element lengths of a non degenerate configuration are known, the geometric intersection method can be used to optimize the configuration using a more intuitive process.

## 5.4 Optimization of a Known Configuration

Connelly's method can be used to optimize a known configuration using the same algorithm presented above. The optimization is conducted by altering the radius and height of the tensegrity topology until the desired element lengths are achieved (the exact element lengths may not be achievable depending on the number of struts and the connectivity terms  $j$  and  $k$ ). This method is difficult to use as part of an optimization process because it does not allow the element lengths to be optimized directly. Similarly Tibert's method can be used to optimize a known configuration using the above algorithm and altering the input variables. Difficulties arise when the specified element lengths approach the boundary condition. In Tibert's method it is not clear which element lengths must be altered in order to avoid the

boundary condition. Like Tibert's method, the geometric intersection method can optimize a known configuration using the above method and altering the input variables. Unlike Tibert's method, the geometric method provides a new boundary condition which is more intuitive.

## 5.5 Determining Boundary Conditions Geometrically

A closer examination of the geometric method reveals that the intersection point between the spheres and the cylinder is about to be lost when the cylinder does not extend below the  $xy$  plane. The loss of the intersection point corresponds to a zero or negative height, which is an  $\mathbb{E}^3$  boundary condition for this configuration. This result is immediately obvious when  $l_s$  is reduced until it becomes imaginary. This more intuitive visual approach to examining the boundary conditions of the form finding problem is illustrated in Figure 5.2.

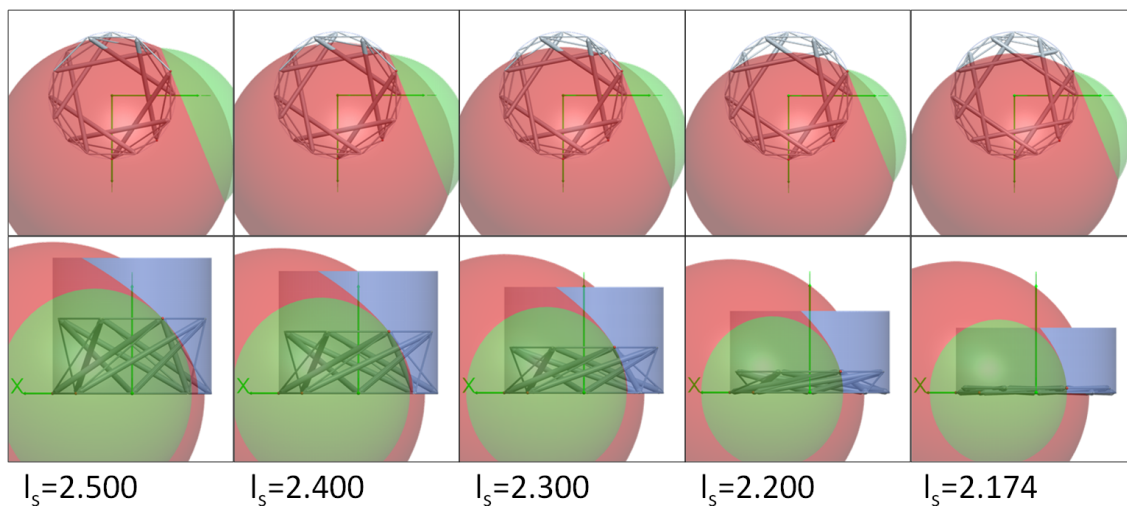


**Figure 5.2: Cylinder Boundary Evaluation:** The upper row is the top view of the 8 strut tensegrity from Table 5.2, and the lower row is a side view of the same topology. The upper row illustrates that the  $l_c$  sphere is becoming smaller relative to the  $l_s$  sphere. The lower row shows that the intersection point is rapidly approaching the  $xy$  plane, and a degenerate  $\mathbb{E}^3$  configuration.

Another indication that a boundary condition has been reached is when the  $l_c$  sphere is completely enveloped by the  $l_s$  sphere. If  $l_c$  is inside  $l_s$  then no real intersection between the three surfaces can exist. This condition can be restated mathematically as:

$$l_s \geq l_c + l_e. \quad (5.12)$$

Equation 5.12 can be derived from Figure 5.3. These two methods of visually identifying

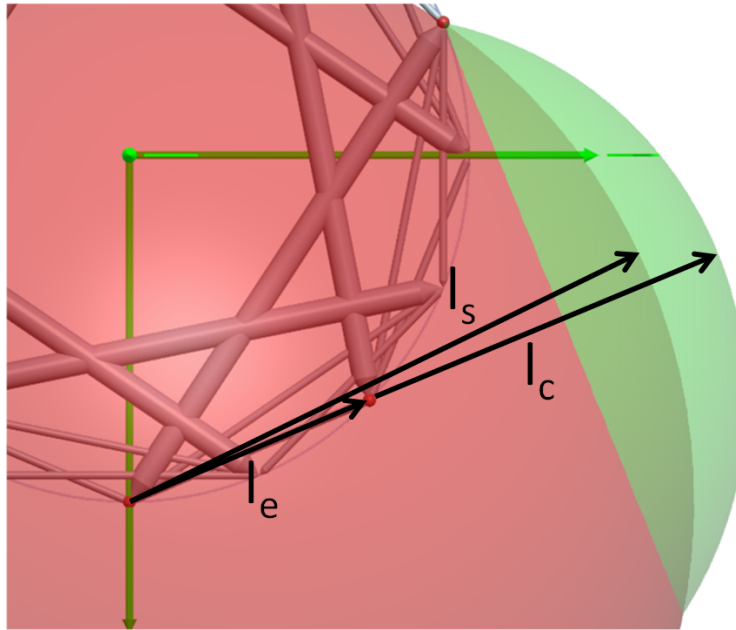


**Figure 5.3: Sphere Boundary Evaluation:** If  $l_c + l_e$  becomes less than  $l_s$  then the  $l_c$  sphere will be completely inside the  $l_s$  sphere, and no intersection between the three surfaces is possible.

the boundary conditions for the form finding process can allow the designer or the algorithm to quickly identify when a degenerate configuration will occur. The geometric intersection method also provides a new context in which to understand the nature of these boundary conditions. Using the geometric method, the boundary conditions are identified by determining when the parameters result in a cylinder and two spheres that have no intersection in common. When this situation occurs there can be no real representation of the tensegrity configuration in the workspace. Furthermore, since each constraint surface is directly linked to the length of the elements, the designer can immediately identify which element lengths should be altered to avoid approaching a boundary condition. This visual

feedback is in contrast to Connolly's method where the designer must interpret the output configuration alone, without the aid of the constraint surfaces.

Figure 5.4 illustrates this advantage. The geometric intersection method clearly shows that the length of the cable (represented by the green sphere) should be increased to prevent the red sphere (which represents the strut length) from enveloping the green sphere. If the one sphere is enveloped by the other then the intersection point will be lost, and there will be no solution to the form finding problem. Connolly's method is shown on the right and it is not immediately obvious which element lengths need to be changed in order to move away from the boundary condition. This visual feedback is one of the greatest advantages of the geometric intersection method because it is the only method that provides this information.

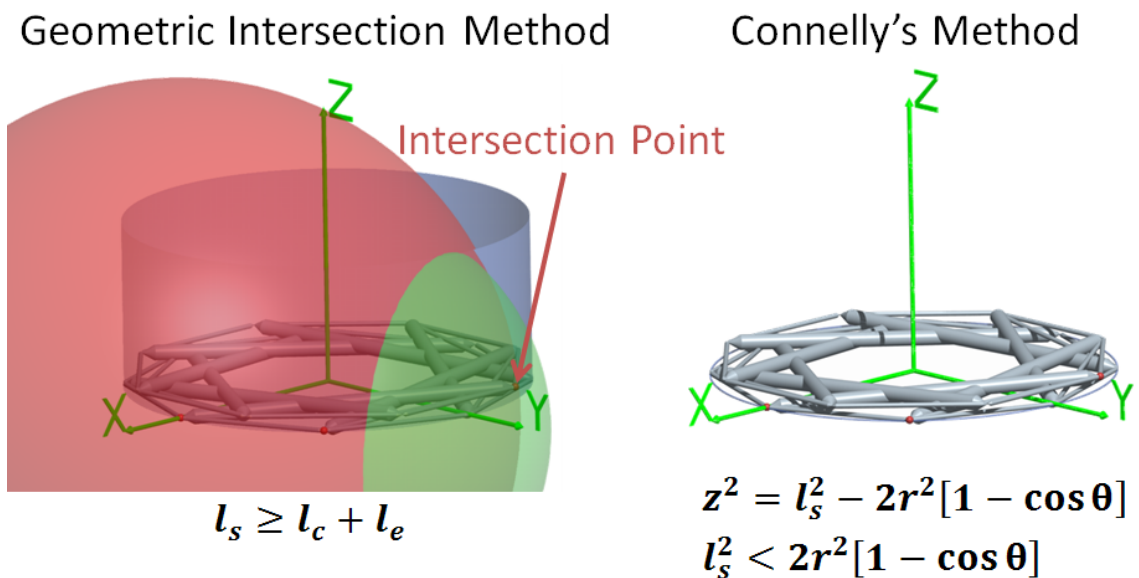


**Figure 5.4: Boundary Condition Evaluation:** The geometric intersection method output is shown on the left along with its boundary condition, and the output from Connolly's method is shown on the right along with its boundary condition. Without the constraint surfaces it is difficult to determine which element lengths should be changed to ensure that Connolly's boundary condition is satisfied. The geometric intersection method clearly shows that the cable length must be increased to ensure that the strut sphere (red) does not envelope the cable sphere (green).

## 5.6 Using Alternate Control Surfaces

Alternate geometric surfaces can be used in place of the cylinder as long as some degree of symmetry is maintained. One of the most practical surfaces after the cylinder is the cone. A conical prismatic tensegrity topology finds use in a variety of real world applications, including intermediate poses of tensegrity mechanisms. The Cartesian equation for a cone is:

$$(x^2 + y^2) \left( \frac{h_{\text{cone}}}{r_{\text{cone}}} \right)^2 = (z - h_{\text{cone}})^2, \quad (5.13)$$

where  $h_{\text{cone}}$  is the height of the cone and  $r_{\text{cone}}$  is the radius of the base. Equation 5.13 can be rearranged in terms of the prismatic tensegrity parameters by letting  $r_{\text{cone}} = r_1$ , and specifying a new radius  $r_2$  at  $h$  as shown in Figure 5.5. Figure 5.5 can also be used to derive

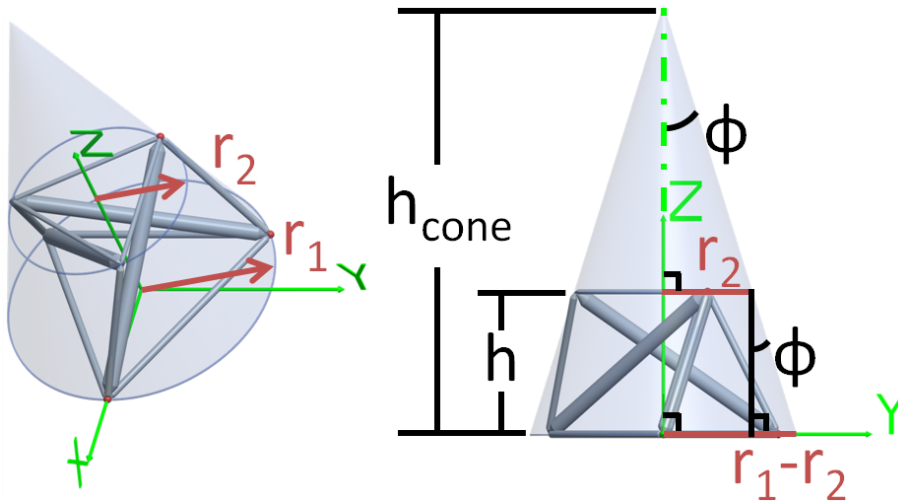


**Figure 5.5: Cone Surface Parameters:** A truncated cone can be parameterized by the radius of two circles dividing a cone into two sections. One of these circles is in the base plane ( $z = 0$ ), and the other is in a parallel plane that is also occupied by the upper tensegrity nodes ( $z = h$ ).

the relationship between  $h_{\text{cone}}$  and  $h$  as follows:

$$\begin{aligned} \tan(\phi) &= \frac{r_1}{h_{\text{cone}}}, \\ \tan(\phi) &= \frac{r_1 - r_2}{h}, \\ \frac{r_1}{h_{\text{cone}}} &= \frac{r_1 - r_2}{h}, \\ h_{\text{cone}} &= \frac{r_1 h}{r_1 - r_2}. \end{aligned} \quad (5.14)$$

In terms of these new variables, Equation 5.13 becomes:

$$(x^2 + y^2) \left( \frac{h}{r_1 - r_2} \right)^2 = z - h \left( \frac{r_1}{r_1 - r_2} \right)^2. \quad (5.15)$$

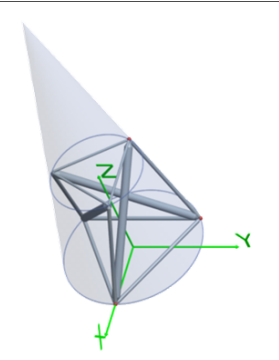
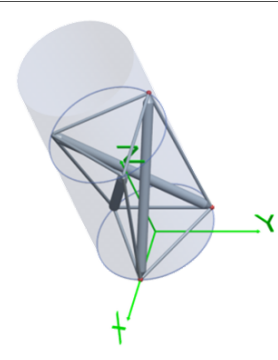
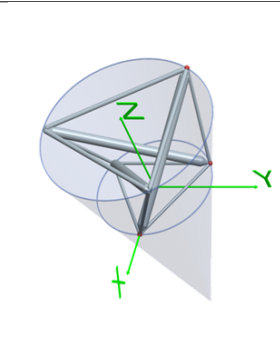
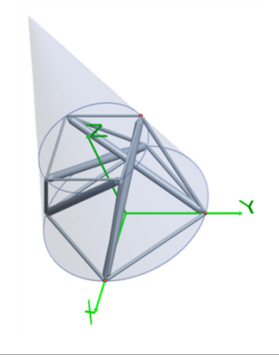
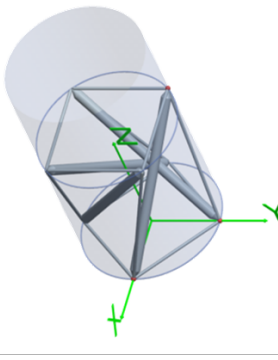
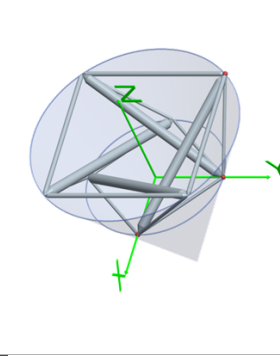
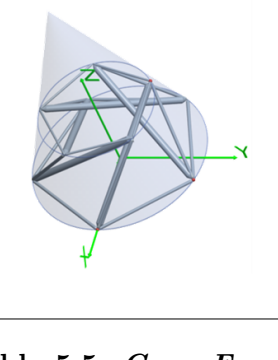
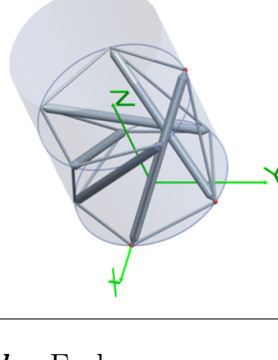
Equation 5.15 can be further simplified because the  $z$  coordinate of the intersection point is equal to  $h$ :

$$\begin{aligned} (x^2 + y^2) z^2 \left( \frac{1}{r_1 - r_2} \right)^2 &= z^2 \left[ 1 - \left( \frac{r_1}{r_1 - r_2} \right) \right]^2, \\ (x^2 + y^2) &= r_2^2 \frac{(r_1 - r_2)^2}{(r_1 - r_2)^2}, \\ x^2 + y^2 &= r_2^2. \end{aligned} \quad (5.16)$$

Equation 5.16 can now be used with the two sphere equations to determine the desired parameters of the prismatic tensegrity structure. An additional parameter is required to account for the different end cable lengths between the upper nodes. This new parameter can be either  $r_2$  or  $l_t$ , where  $l_t$  is the upper end cable length. The relationship between  $r_2$  and  $l_t$  is given by:

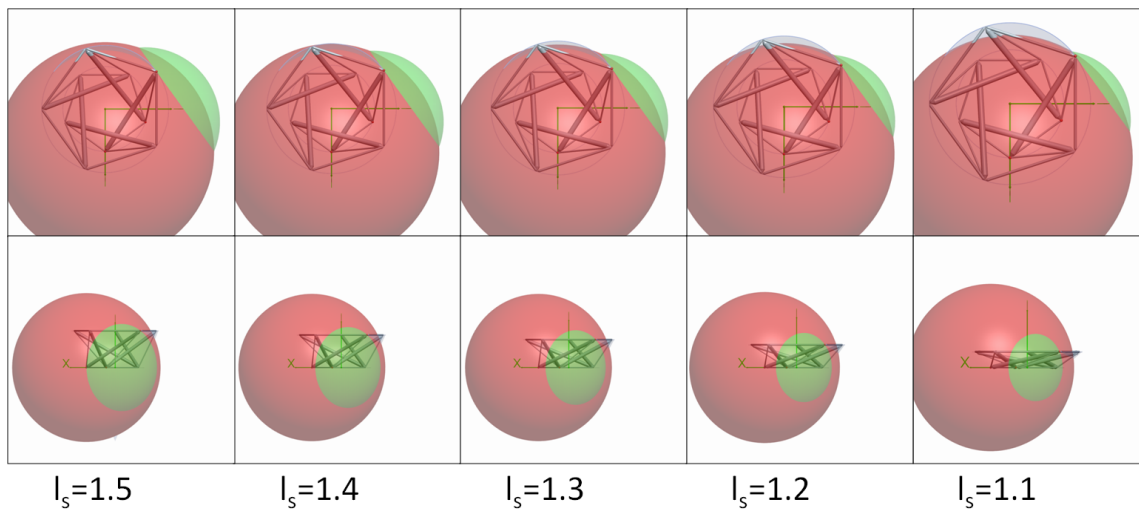
$$r_2 = \frac{l_t}{2 \sin \left( \frac{\beta}{2} \right)}. \quad (5.17)$$

Table 5.5 contains a series of prismatic tensegrities where the ratio between  $l_e$  and  $l_t$  is altered while the rest of the geometric and connectivity parameters remain constant.

$\frac{l_t}{l_e} = \frac{2}{3}$	$\frac{l_t}{l_e} = 1$	$\frac{l_t}{l_e} = \frac{3}{2}$
		
		
		Undefined

**Table 5.5: Cone Example:** Each row corresponds to an increased number of struts (3, 4, and 5 struts). The side wall of the cone will slope outwards if  $\frac{l_t}{l_e} > 1$  and slope inwards if  $\frac{l_t}{l_e} < 1$ . The cone becomes a cylinder when  $\frac{l_t}{l_e} = 1$ .

The need to define an additional parameter for cone prismatic tensegrities is offset by the larger subset of tensegrity topologies that can be modelled. Connelly's method can also be adapted to model different topologies, but it is much easier to think of these changes in terms of selecting a new constraint surface than it is to derive the new relationships between the parameters algebraically. Table 5.5 again illustrates a case where an infeasible geometry is reached. This configuration can be further analyzed by examining the configurations leading up to the infeasible geometry (Figure 5.6).



**Figure 5.6: Cone Boundary Evaluation:** As  $l_s$  is reduced the intersection point between the three surfaces is lost. This occurs because the  $l_s$  sphere envelops the  $l_c$  sphere. Also the height of the cone is approaching zero as can be seen in the lower series of images.



The preceding examples have demonstrated the suitability of the geometric intersection method for solving the form finding problem of prismatic tensegrity systems. They have also demonstrated the mathematical equivalence of the geometric intersection method and Connelly's method (Tables 5.1, 5.2, 5.3, and 5.4). Figures 5.2 and 5.6 have illustrated a new rationale for the occurrence of degenerate configurations, which is completely unique to the geometric intersection method. It is clear that degenerate configurations will occur if a combination of parameter values results in a loss of intersection between one or more of the three geometric surfaces. This rationale is very intuitive, and can warn the designer when a given configuration becomes infeasible. This aspect of the geometric intersection method would be particularly useful for determining the reachable workspace of a prismatic tensegrity mechanism. Finally, the geometric intersection method can easily be reformulated to accept other geometric shapes as constraint surfaces. A truncated cone is an especially important surface because of its applicability to the deployment and actuation of tensegrity structures and mechanisms.

## Chapter 6

### Conclusions

The current literature suggests that there is an absence of form finding methods that can provide insight into the form finding process, make the form finding process more intuitive for those wishing to exploit the benefits of tensegrity systems, and which can be more easily implemented in a tensegrity mechanism control loop. The geometric intersection method presented in this thesis addresses these shortcomings by providing a more visual interpretation of the solution space, and by being easier to adapt to more complex tensegrity topologies. These advantages are achieved due to the novel derivation of the geometric intersection method.

The geometric intersection method is derived in a completely different way than conventional form finding methods. While most conventional form finding methods are derived using vector analysis, the geometric form finding method is derived using geometric analysis, making it arguably much easier to use and interpret. Part of its usefulness comes from its simplicity. The geometric intersection method determines the location of the nodes in a tensegrity system by finding the intersection points between two spheres and a circular cylinder. Each sphere is defined by its radius and the coordinates of its center. The radius is given by either the lateral strut or cable length, and its center location is defined by the coordinates of the end cable nodes. The cylinder is defined by its radius and central axis. The radius of this cylinder is defined by the end cable length and the number of struts, while the central axis is coincident with the z axis of the coordinate system.

These simple geometric shapes give an immediate visual impression of how the parameters of the tensegrity system influence the final shape of the tensegrity system. Furthermore, these shapes are parameterized in terms of the element lengths ( $l_s$ ,  $l_c$ , and  $l_e$ ), which are most likely to be controlled in a tensegrity mechanism. This formulation makes the geometric intersection method better suited to tensegrity mechanism control than conventional form finding methods because it is much easier to understand the relationship between the element lengths and the final shape of the tensegrity system. Once the end cable length and either the lateral cable length or the strut length are defined, the length of the missing lateral element is calculated, as well as the global parameters (the radius and height) of the resulting tensegrity system.

Both Connelly's [20] and Tibert's [2] methods can be derived from the geometric intersection method, which guarantees their algebraic equivalence. This equivalence is especially clear when comparing Tibert's method to the geometric intersection method. Tibert's method is based on calculating the length of a vector between the tensegrity system's nodes (the coordinates of the nodes being calculated first using Connelly's method) to determine the length of the end cables, lateral cables, and lateral struts. This method is based on vector algebra and does not immediately give a sense of the resulting tensegrity system, or when this system is approaching a boundary condition and a degenerate configuration. The geometric method provides the exact same solution, but with the added benefit of clearly establishing the relationships between the input parameters and the output parameters. The geometric intersection method also provides immediate visual feedback when a combination of parameters is about to result in a degenerate configuration.

The geometric intersection method was implemented in a ProEngineer-Mathcad model so that it could be compared with a similar model of Connelly's kinematic analytical method. It was demonstrated in Chapter 4 that the geometric intersection method can be used to derive Connelly's method, and the examples generated from the ProEngineer-Mathcad model confirm the algebraic equivalence of the two methods. The

major advantage of the geometric intersection method is the clear way the element lengths affect the final geometry of the tensegrity system. This relationship is best illustrated when a combination of element lengths are selected, which result in a degenerate, non-real configuration.

When a degenerate configuration occurs, both the geometric intersection method and Connelly's method will provide an imaginary solution that has no physical significance. The geometric intersection method reveals that the degenerate configuration is due to the loss of intersection between the three constraint surfaces, while the relationships in Connelly's method result in a negative term under a square root; giving no clear indication of which parameters have caused the degenerate configuration. The geometric intersection method can quickly identify which parameters should be altered to restore the tensegrity system, because each of the constraint surfaces in the geometric intersection method correspond to an element length (the radius of the cylinder is given by the end cable length, and the radii of the spheres are given by the lateral element lengths). This direct relationship helps make the geometric intersection method more intuitive than other methods.

Another aspect of the geometric intersection method that makes it more intuitive and useful for designers than other methods, is that it can quickly be adapted to solve the form finding problem for other symmetric tensegrity systems. These modifications can be accomplished by replacing the circular cylinder with another geometric shape, such as an elliptical cylinder, another sphere, or a cone. The cone is a particularly useful surface because conic tensegrity systems are found in many real world applications, and they can represent the intermediate poses of some tensegrity mechanisms ( [13], [4], [5] ). Implementing the cone surface in the geometric intersection method involves replacing the circular cylinder equation with the equation for a cone. This substitution requires an additional parameter to be selected (either the new upper radius, or upper end cable length). By contrast, Connelly's method would require redefining the node coordinate equations algebraically, which is arguably less intuitive than substituting constraint surface equations. The versatility

and visual nature of the geometric intersection method should allow it to find applications in a wide variety of tensegrity systems, especially in the design and control of tensegrity mechanisms.

## 6.1 Contributions

The primary contribution of this thesis is the introduction of the geometric intersection method, which is a better optimization and interpretation tool for designing tensegrity systems. Additionally the literature review presented in Chapter 3 is more up to date than Tibert's review [2] and Tur's review [18]. The updated, and in some cases, more in depth literature review should be a valuable resource to anyone seeking an updated introduction to tensegrity form finding methods.

## 6.2 Future Work

The geometric intersection method should be further developed to solve the form finding problem for a wider range of tensegrity topologies. It should also be adapted to include the deformation of the elements, and the response of a tensegrity system to external loads. The current geometric intersection method can be used to control tensegrity mechanisms, but these mechanisms must maintain their symmetry throughout their actuation. If more irregular topologies could be analyzed then the geometric intersection method could model tensegrity mechanisms with irregular deployment or actuation schemes. The following assumptions were made in Chapter 5 to reduce the complexity of developing the geometric form finding method:

1. only symmetric prismatic tensegrity systems are considered;
2. the number of struts is known;
3. the connectivity of the elements is known;
4. all nodes are modelled as spherical joints;

5. cables and struts maintain their lengths for each value of the input parameters (ie. they will not deform under load);
6. no external forces act on the structure, including body forces;
7. the structure is free standing, without any supports.

The above assumptions create restrictions on the symmetry, element material properties, and loading environment of the tensegrity systems that can be analyzed by the geometric intersection method.

Currently the geometric intersection method is limited to symmetric prismatic tensegrity structures. While different constraint surfaces can be substituted for the circular cylinder surface, the new topologies must still have a large degree of symmetry. More irregular tensegrity topologies could be modelled if the length of each element were represented by its own sphere. The intersection points between these spheres and a control surface could then be calculated to determine the coordinates of the nodes. The stability of these new topologies would then need to be evaluated. Once more irregular tensegrity topologies can be analyzed, the mass properties of the tensegrity elements could be used in conjunction with the generally unsymmetric element displacements to evaluate the transient dynamics of a tensegrity mechanisms.

## Chapter 7

### Glossary

**Affine Transformation** affine transformations preserve the distance, but not necessarily orientation between objects. For example two points will always remain the same distance apart when an affine transformation is applied to them, but their location and orientation in space may be altered. The group of affine transformations include: rotations, translations, reflections, and glides (reflection then translation or vice versa).

**Bars** connect two nodes, and can never change in length. They can be in tension or compression.

**Cables** connect two nodes, and can only increase in length. They are only stable in tension.

**Compression** a force that tends to decrease the length of an object.

**Congruence** two sets of points are called congruent if one can be transformed into the other by an isometry, i.e., a combination of translations, rotations, glides, and reflections. Less formally, two figures are congruent if they have the same shape and size, but are in different positions (for instance a set of points may be rotated, flipped, or moved, but their relative distance must be maintained).

**Eigenvalues** are scaling factors for eigenvectors. If they are negative they flip the direction of the eigenvector.

**Eigenvectors** Are vectors that maintain their direction, but not necessarily their magnitude when multiplied by a matrix:  $\mathbf{A}x = xl$ , where  $l$  is the eigenvalue scalar.

**Force density** the amount of force per unit length in a tensegrity element.

**Form finding** refers to the process of determining the stable geometry of a tensegrity system.

**Framework** a framework is any point cloud, where every point is connected to at least two other points by a structural element. These elements can be bars, struts, or cables.

**Isometry** a group theory concept that includes all transformations that preserve distance (for instance the distance between two points).

**Mirror Line** a mirror line is the line or plane about which an object is reflected.

**Nullity, Null space, Kernel** In a system of equations in matrix form, the null space is the number of equations that cause the variables to equal zero. For instance the null space is equal to the number of vectors  $x$  that cause  $\mathbf{A}x = 0$ , where  $\mathbf{A}$  is the matrix.

**Positive Definite Matrix** a positive definite matrix has all positive eigenvalues.

**Proper Self Stress** a tensegrity system is in a proper stress state when all cables have a positive self stress, and all struts have a negative self stress.

**Rank** the column rank of a matrix is equal to the number of linearly independent columns in the matrix.

**Strict Proper Self Stress** a tensegrity system is in a strict proper stress state when all cables have a positive self stress, all struts have a negative self stress, and no struts or cables have a self stress equal to zero.

**Struts** connect two nodes, and can only decrease in length. They are only stable in compression.



**Tensegrity** a term developed by Richard Buckminster Fuller to describe systems composed of compression element kept in static equilibrium by a network of tension elements.

**Tensegrity configuration** a specific instance of a tensegrity topology. All elements have a specified length, all nodes have fixed coordinates, and all elements are connected by a unique set of connections.

**Tensegrity mechanism** a tensegrity topology whose element lengths can be changed to produce a desired motion or transformation of energy.

**Tensegrity structure** a tensegrity topology in static equilibrium.

**Tensegrity system** a tensegrity that can either be a static structure, or an actuated mechanism.

**Tensegrity topology** refers to a unique set of connections between the elements in a tensegrity structure or mechanism (It encompasses all possible lengths and nodal placements of the tensegrity elements using this unique set of connections).

**Tension** a force that tends to increase the length of an object.

**Topology** A specific arrangement or set of connections between elements. A given topology includes all element lengths that are achievable, with a single set of element connections.

**Transitive Element Classes** this nomenclature was used by Connelly [20] to describe the elements in a prismatic tensegrity system that share the same length. The three transitive element classes are: lateral struts, lateral cables, and end cables.

**Trivial** In this thesis, trivial parameters are parameters that are equal to zero.

## List of References

- [1] R. Motro, *Tensegrity: structural systems for the future*. 120 Pentonville Road London N1 9JN UK: Kogan Page Science, 2003.
- [2] A. Tibert and S. Pellegrino, *Review of Form-Finding Methods for Tensegrity Structures*. Department of Structural Engineering, Royal Institute of Technology, 2003.
- [3] J. Zhang and M. Ohsaki, “Adaptive force density method for form-finding problem of tensegrity structures,” *International Journal of Solids and Structures*, vol. 43, pp. 5658 – 5673, February 2006.
- [4] C. Paul, J. Roberts, H. Lipson, and F. Cuevas, “Gait production in a tensegrity based robot,” *Proceedings of the International Conference on Advanced Robotics*, 2005.
- [5] C. Paul, F. J. Valero-Cuevas, and H. Lipson, “Design and control of tensegrity robots for locomotion,” *IEEE Transactions on Robotics*, vol. 22, pp. 944–957, October 2006.
- [6] D. Ingber, “Tensegrity-based mechanosensing from macro to micro,” *Progress in Biophysics & Molecular Biology*, vol. 97, pp. 163–179, February 2008.
- [7] J. M. Tur and S. H. Juan, “Tensegrity frameworks: Dynamic analysis review and open problems,” *Mechanism and Machine Theory*, vol. 44, pp. 1–18, June 2008.
- [8] Kacey, “Biosphere built by us for expo ’67.” Available at: <http://picasaweb.google.com/lh/photo/107A5TrUyc-BDKJrnAtW1A>, September 2007.
- [9] ucumari, “Georgia dome.” Available at: <http://www.flickr.com/photos/ucumari/481430551/>, May 2007.
- [10] C. R. Architects, “Tank street bridge or kurilpa bridge.” Available at: <http://www.greenlaunches.com/2009/10/06/Kurilpa-Solar-Powered-Bridge-1.jpg>, November 2009.
- [11] D. Ingber, R. Groleau, C. Lowe, S. Patel, and D. Bulli, “Tensegrity in a cell.” Available at: [http://www.childrenshospital.org/research/cell\\_tensegrity/index.html](http://www.childrenshospital.org/research/cell_tensegrity/index.html), 2005.

- [12] K. Kassolik, A. Jaskolska, K. Kisiel-Sajewicz, J. Marusiak, A. Kawczynski, and A. Jaskolski, “Tensegrity principle in massage demonstrated by electro- and mechanomyography,” *Journal of Bodywork and Movement Therapies*, vol. 13, pp. 164–170, November 2007.
- [13] G. Tibert, *Deployable Tensegrity Structures for Space Applications*. Doctoral thesis, Royal Institute of Technology: Department of Mechanics, SE-100 44 Stockholm, Sweden, July 2002.
- [14] A. G. Tibert and S. Pellegrino, “Deployable tensegrity reflectors for small satellites,” *Journal of Spacecraft and Rockets*, vol. 39, pp. 701–709, September–October 2002.
- [15] C. Sultan, M. Corless, and R. E. Skelton, “Peak to peak control of an adaptive tensegrity space telescope,” *SPIE Conference on Mathematical and Control of Smart Structures*, vol. 3667, pp. 190–201, March 1999.
- [16] C. Sultan and R. E. Skelton, “Force and torque smart tensegrity sensor,” *SPIE Conference on Mathematical and Control of Smart Structures*, vol. 3323, pp. 357–368, March 1998.
- [17] M. Masic and R. E. Skelton, “Open-loop control of class-2 tensegrity towers,” *SPIE Conference on Modeling, Signal Processing, and Control*, vol. 5383, pp. 298–308, March 2004.
- [18] J. M. Tur and S. H. Juan, “Tensegrity frameworks: Static analysis review,” *Mechanism and Machine Theory*, vol. 43, pp. 859–881, June 2007.
- [19] R. Connelly, *Tensegrities and Global Rigidity*. Department of Mathematics, Cornell University, Ithica, NY 14853: Self Published, may 2009. Available online.
- [20] R. Connelly and M. Terrell, “Globally rigid symmetric tensegrities,” *Structural Topology*, vol. 21, pp. 59–79, 1995.
- [21] B. Roth and W. Whiteley, “Tensegrity frameworks,” *American Mathematical Society*, vol. 265, no. 2, pp. 419–446, 1981.
- [22] B. Roth, “Rigid and flexible frameworks,” *The American Mathematical Monthly*, vol. 88, pp. 6–21, January 1981.
- [23] B. Roth, *Unfinished*. draft 1 ed., April 1987.
- [24] S. Guest, “The stiffness of prestressed frameworks: A unifying approach,” *International Journal of Solids and Structures*, vol. 43, pp. 842–854, 2006.
- [25] R. Connelly and W. Whiteley, “Second-order rigidity and pre-stress stability for tensegrity frameworks,” *Discrete Mathematics*, vol. 9, no. 3, pp. 453–491, 1996.

- [26] R. Connelly, *Basic Concepts of Infinitesimal Rigidity*. Department of Mathematics, Cornell University, Ithica, NY 14853: Self Published, 1987. Available online.
- [27] R. Connelly and A. Back, “Mathematics and tensegrity,” *American Scientist*, vol. 86, pp. 142–151, March-April 1998.
- [28] R. B. Fuller, *Synergetics: Explorations in the Geometry of Thinking*. Macmillan Publishing co. Inc., 1979 ed., 1975.
- [29] D. G. Emmerich, *Structures Tendues et Autotendantes*. 1988.
- [30] J. Rieffel, F. Valero-Cuevas, and H. Lipson, “Automated discovery and optimization of large irregular tensegrity structures,” *Computers and Structures*, vol. 87, pp. 368–379, 2009.
- [31] M. Pagitz and J. M. Tur, “Finite element based form-finding algorithm for tensegrity structures,” *International Journal of Solids and Structures*, vol. 46, pp. 3235–3240, 2009.
- [32] R. Burkhardt, “The application of nonlinear programming to the design and validation of tensegrity structures with special attention to skew prisms,” *Journal of the International Association for Shell and Spatial Structures*, vol. 47, no. 1, pp. 3–15, 2006.
- [33] H. Schek, “The force density method for form finding and computation of general networks,” *Computer Methods in Applied Mechanics and Engineering*, vol. 3, pp. 115–134, July 1974.
- [34] K. Linkwitz, “Formfinding by the direct approach and pertinent strategies for the conceptual design of prestressed and hanging structures,” *International Journal of Space Structures*, vol. 14, pp. 73–87, April 1999.
- [35] N. Vassart and R. Motro, “Multiparametered formfinding method: Application to tensegrity systems,” *International Journal of Space Structures*, vol. 14, pp. 147–154, April 1999.
- [36] J. Zhang, M. Ohsaki, and Y. Kanno, “A direct approach to design of geometry and forces of tensegrity systems,” *International Journal of Solids and Structures*, vol. 43, pp. 2260 – 2278, July 2006.
- [37] M. Masic, R. E. Skelton, and P. E. Gill, “Algebraic tensegrity form-finding,” *International Journal of Solids and Structures*, vol. 42, pp. 4833–4858, January 2005.
- [38] R. Connelly, *Handbook of Convex Geometry*, ch. Rigidity, pp. 223–271. Elsevier Publishers Ltd, 1993.

- [39] C. Sultan, M. Corless, and R. E. Skelton, “The prestressability problem of tensegrity structures: Some analytical solutions,” *International Journal of Solids and Structures*, vol. 38, pp. 5223–5252, 2001.
- [40] A. Micheletti and W. Williams, “A marching procedure for form-finding for tensegrity structures,” *Journal Of Mechanics Of Materials And Structures*, vol. 2, no. 5, pp. 2–27, 2007.
- [41] C. Paul, H. Lipson, and F. V. Cuevas, “Evolutionary form-finding of tensegrity structures,” 12, (Washington D.C., USA), Genetic and Evolutionary Computation Conference, June 2005.
- [42] M. Masic, R. E. Skelton, and P. E. Gill, “Optimization of tensegrity structures,” *International Journal of Solids and Structures*, vol. 43, pp. 4687–4703, 2006.
- [43] G. G. Estrada, H.-J. Bungartz, and C. Mohrdieck, “Numerical form-finding of tensegrity structures,” *International Journal of Solids and Structures*, vol. 43, pp. 6855–6868, 2006.

## Appendix A

### Mathcad Transcript

The following transcript corresponds to version 10 of the Mathcad worksheet relations10.xmcd, which is current as of October 2009.

Calculates the overall height (H) of the tensegrity cell given a side element ratio L/l:

Variables from Proe to Mathcad:

```

j := 1.0000000000    k := 1.0000000000
number_of_struts := 3.0000000000
strut_length := 2.1000000000
side_cable_length := 2.0000000000
end_cable_length := 1.0000000000
height := 1

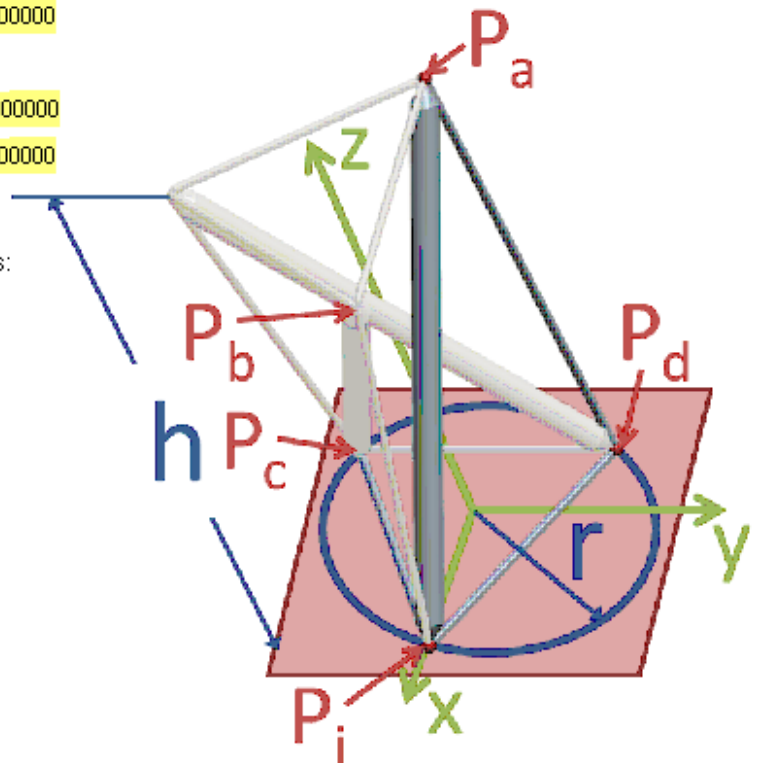
```

Transform into mathcad variables:

```

j_w := j = 1
k_w := k = 1
H_w := height = 1
l_s := strut_length
l_c := side_cable_length
l_e := end_cable_length
n_s := number_of_struts

```



Angle of twist:

$$\theta := \pi \cdot \left( \frac{1}{2} + \frac{j}{n_s} \right) = 150 \cdot \text{deg}$$

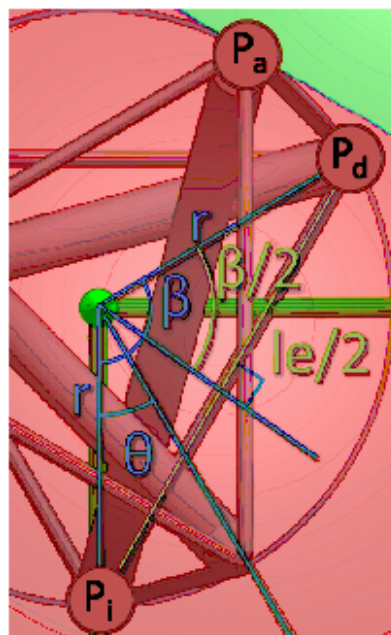
Polygon angles:

$$\alpha := \frac{2 \cdot \pi \cdot j}{n_s} = 120 \cdot \text{deg}$$

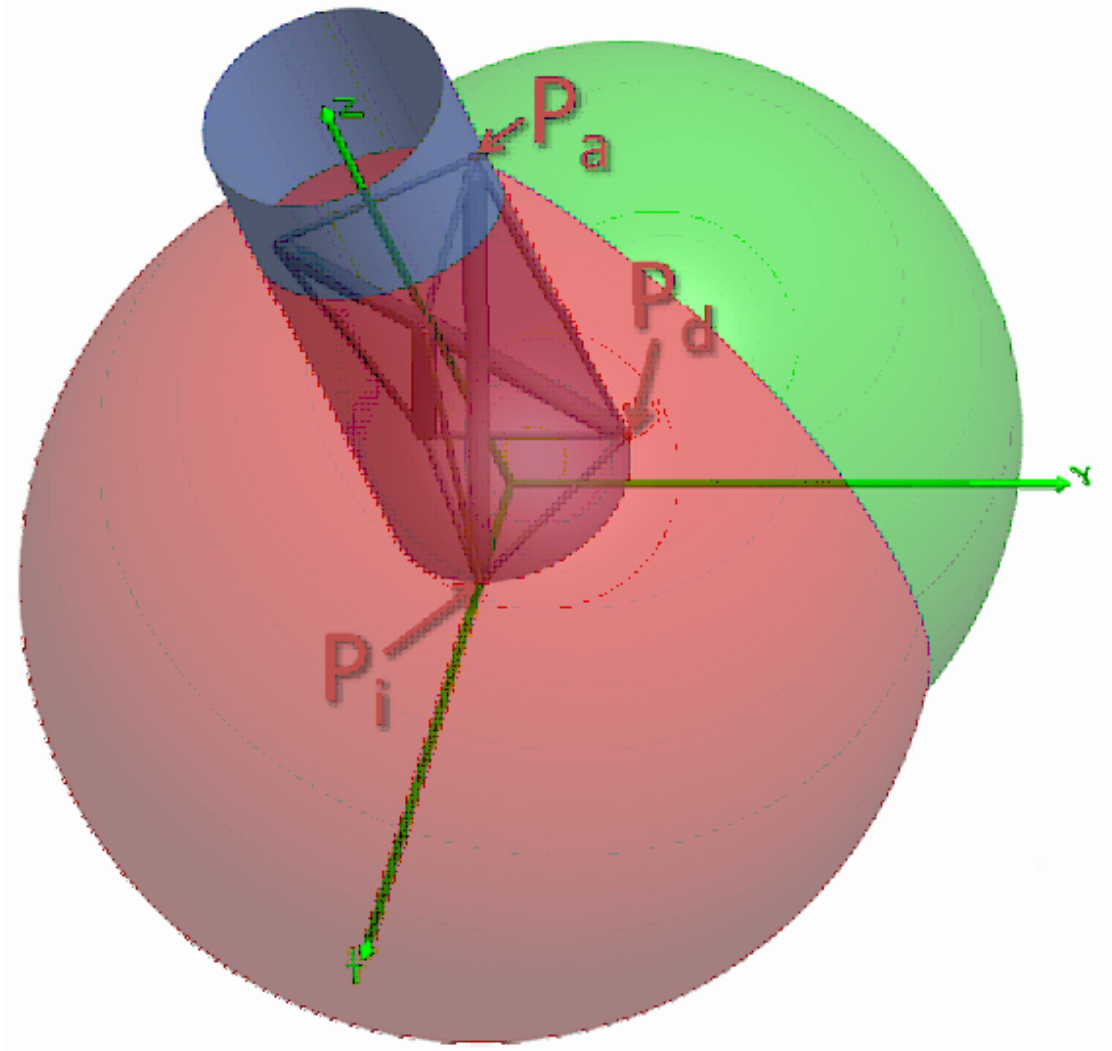
$$\beta := \frac{2 \cdot \pi \cdot k}{n_s} = 120 \cdot \text{deg}$$

The radius of the cylinder is purely a function of the end cable length:

$$r := \frac{l_e}{2 \cdot \sin\left(\frac{\beta}{2}\right)} = 0.577$$



The height of the circumscribed cylinder section is given by the intersection of the two spheres with centers at each end of the base cable 'le' and radii equal to the strut length 'ls' and side cable length 'lc' and the cylinder itself assumed to have infinite height:



First find the centers for the two spheres ( $P_i$  and  $P_d$  above):

$p_i$  has coordinates:

$$p_i := \begin{pmatrix} r \\ 0 \\ 0 \end{pmatrix} = \begin{pmatrix} 0.577 \\ 0 \\ 0 \end{pmatrix}$$

$p_d$  has coordinates:

$$p_d := \begin{pmatrix} r \cdot \cos(\beta) \\ r \cdot \sin(\beta) \\ 0 \end{pmatrix} = \begin{pmatrix} -0.289 \\ 0.5 \\ 0 \end{pmatrix}$$



Next determine the coordinates for vertex pa:

First guess:

$$x := r \cdot \cos(\theta) = -0.5 \quad y := r \cdot \sin(\theta) = 0.289$$

$$z := \text{height}$$

$$l_s = 2.1 \quad l_c = 2$$

$$\sqrt{x^2 + y^2} = 0.577 \quad r = 0.577$$

<--x will always be negative or 0 if  $j = 1$

because:

$\theta$  will always be greater than or equal to 90 so use a negative number for its initial guess

<--should match

Given

$$(x - p_{d0})^2 + (y - p_{d1})^2 + (z - p_{d2})^2 = l_c^2$$

$$(x - p_{i0})^2 + (y - p_{i1})^2 + (z - p_{i2})^2 = l_s^2$$

$$x^2 + y^2 = r^2$$

$$\text{parameters} := \text{Find}(l_c, y, z) = \begin{pmatrix} 1.80424 \\ 0.28868 \\ 1.77932 \end{pmatrix}$$

<-- Note: for this sheet indexes start at 0

$$p_i = \begin{pmatrix} 0.577 \\ 0 \\ 0 \end{pmatrix}$$

$$p_d = \begin{pmatrix} -0.289 \\ 0.5 \\ 0 \end{pmatrix}$$

$$H := \text{parameters}_2 = 1.779$$

$$\theta = 150 \cdot \text{deg}$$

$$l_c := \text{parameters}_0 = 1.804$$

$$\text{ratio} := \frac{l_s}{l_c} = 1.164$$

$$(l_c + l_e) - l_s = 0.704$$

$$l_s = 2.1$$

Check cylinder condition:

$$x^2 + (\text{parameters}_1)^2 = 0.333 \quad r^2 = 0.333$$

<--should match

I will use Connelly's method from connelly95 and tibert2003 to check the above:

$$cl_s := l_s = 2.1$$

$$cl_c := \sqrt{\left[ cl_s^2 - 4r^2 \left( \sin\left(\frac{2\theta - \beta}{2}\right) \cdot \sin\left(\frac{\beta}{2}\right) \right) \right]} = 1.80424$$

$$c_{\text{height}} := \sqrt{cl_c^2 - 2r^2(1 - \cos(\theta - \alpha))} = 1.77932$$

$$cl_{s'} := \sqrt{2r^2(1 - \cos(\theta)) + (c_{\text{height}})^2} = 2.1$$

$$cl_{c'} := \sqrt{2r^2(1 - \cos(\theta - \beta)) + (c_{\text{height}})^2} = 1.80424$$

$$cl_{c''} := \sqrt{4r^2 \sin\left(\frac{\theta - \beta}{2}\right)^2 + c_{\text{height}}^2} = 1.80424$$

There is a limit on the maximum ratio between the lateral cable and strut. If one sphere is completely inside the other sphere then no intersection is possible. This corresponds to the condition where:

$$l_s \geq l_e + l_c$$

Rearranging the above in terms of the strut/cable ratio:

$$\text{ratio\_limit} := \frac{l_e}{cl_c} + 1 = 1.554$$

or:

$$\text{ratio\_limit} := \frac{2 \cdot r \cdot \sin\left(\frac{\beta}{2}\right)}{\sqrt{2 \cdot r^2 (1 - \cos(\theta - \beta)) + (c_{\text{height}})^2}} + 1 = 1.554$$

The current ratio is:

$$\text{ratio} := \frac{cl_s}{cl_c} = 1.164$$

$$\text{ratio\_limit} - \text{ratio} = 0.39$$

Which must be less than ratio\_limit in order for this method to work.

The analytical solution will be derived next  
Reset the variables:

$$x := x \quad y := y \quad z := z$$

First rearrange the lc sphere equation for z:

$$z = \sqrt{l_c^2 - (x - p_{d0})^2 - (y - p_{d1})^2} + p_{d2}$$

Using the equations for x and the cylinder:

$$x = r \cdot \sin(\theta)$$

$$x^2 + y^2 = r^2 \quad y = -\sqrt{r^2 - x^2} \quad \leftarrow y \text{ will always be negative or } 0 \text{ because } \theta \text{ will always be greater than or equal to } 90^\circ$$

z becomes:

$$z := \sqrt{l_c^2 - (r \cdot \sin(\theta) - p_{d0})^2 - \left[-\sqrt{r^2 - (r \cdot \sin(\theta))^2} - p_{d1}\right]^2} + p_{d2} = 1.386$$

Which reduces to:

$\leftarrow$  see journal entry 2009\_10\_12

$$z := \sqrt{l_c^2 - 2 \cdot r^2 \cdot (1 - \cos(\theta - \beta))} + p_{d2} = 1.779$$

Which is another way of proving Connelly's method.

Output the parameters back to Proe:

<u>height</u> := H	theta := 0	<u>side_cable_length</u> := l <sub>c</sub>
height = 1.779	theta = 2.618	side_cable_length = 1.804